

AD-A051 454

UTAH STATE UNIV LOGAN ELECTRO-DYNAMICS LAB
AIRCRAFT BORNE MEASUREMENTS OF INFRARED ENHANCEMENTS DURING ICE--ETC(U)
SEP 77 R J HUPPI, J W REED

F/G 4/1

F19628-74-C-0190

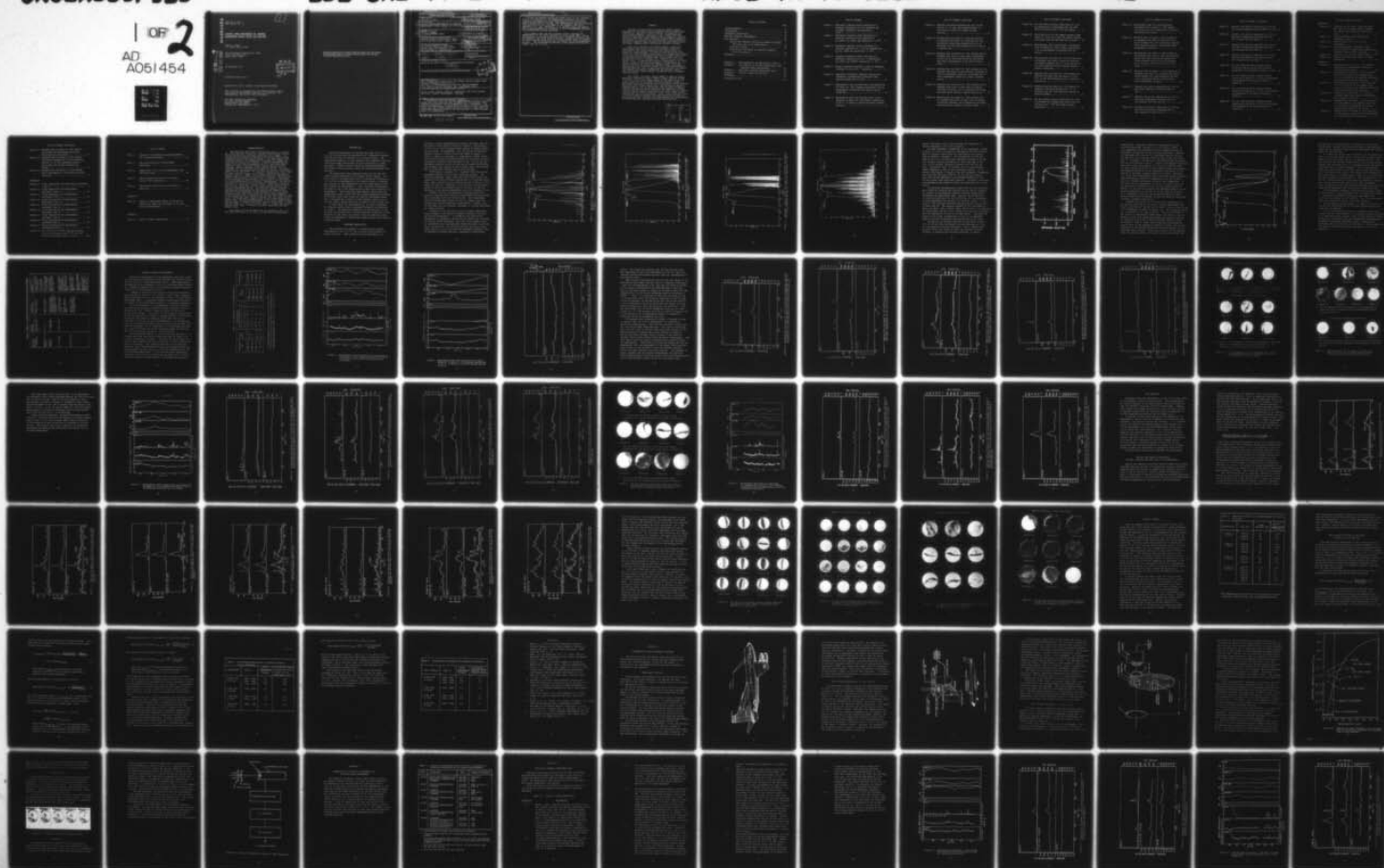
UNCLASSIFIED

EDL-SRL-77-2

AFGL-TR-77-0232

NL

1 OF 2
AD
A051454



AD A051454

AFGL-TR-77-0232
HAES Report No. 68

AIRCRAFT BORNE MEASUREMENTS OF INFRARED
ENHANCEMENTS DURING ICECAP 1975 AND 1976

Ronald J. Huppi
J.W. Reed, Major, USAF

Electro-Dynamics Laboratories (SRL)
Utah State University
Logan, Utah 84322

28 September 1977

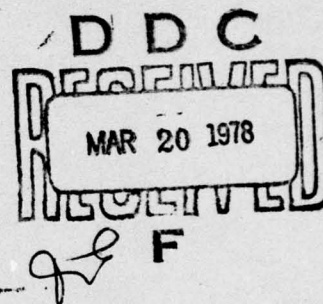
Scientific Report No. 3

Approved for public release; distribution unlimited

This research was sponsored by the Defense Nuclear Agency
under Subtask S99QAXHI004, Work Unit 11, entitled: IR
Phenomenology and Optical Code Development

AIR FORCE GEOPHYSICS LABORATORY
AIR FORCE SYSTEMS COMMAND
UNITED STATES AIR FORCE
HANSCOM AFB, MASSACHUSETTS 01731

AD No. _____
DDC FILE COPY



Qualified requestors may obtain additional copies from the Defense Documentation Center. All others should apply to the National Technical Information Service.

UNCLASSIFIED

SECURITY CLASSIFICATION OF THIS PAGE (When Data Entered)

REPORT DOCUMENTATION PAGE		READ INSTRUCTIONS BEFORE COMPLETING FORM
1. REPORT NUMBER AFGL-TR-77-0232 ✓	2. GOVT ACCESSION NO. (14) EDL-SRL-77-2 ✓	3. RECIPIENT'S CATALOG NUMBER
4. TITLE (and Subtitle) AIRCRAFT BORNE MEASUREMENTS OF INFRARED ENHANCEMENTS DURING ICECAP 1975 AND 1976		5. TYPE OF REPORT & PERIOD COVERED Scientific Report No. 3 ✓
7. AUTHOR(s) (10) Ronald J. Huppi J.W. Reed, Major, USAF *		6. PERFORMING ORG. REPORT NUMBER HAES Report No. 68
9. PERFORMING ORGANIZATION NAME AND ADDRESS Electro-Dynamics Laboratories (SRL), Utah State University, Logan, Utah		8. CONTRACT OR GRANT NUMBER(s) (15) F19628-74-C-0190
11. CONTROLLING OFFICE NAME AND ADDRESS Air Force Geophysics Laboratory Hanscom AFB, Massachusetts 01731 Monitor/Brian P. Sandford/OPR		10. PROGRAM ELEMENT, PROJECT, TASK AREA & WORK UNIT NUMBERS (17) P.E. 62704H, Proj S99QAXH H1004, Work Unit: 11 CDNA-00-04
14. MONITORING AGENCY NAME & ADDRESS (if different from Controlling Office) (18) AFGL, DNA		12. REPORT DATE (11) 28 Sep 77
(19) TR-77-0232, HAES-68		13. NUMBER OF PAGES 128
16. DISTRIBUTION STATEMENT (of this Report) Approved for public release, distribution unlimited (12) 129p.		15. SECURITY CLASS. (of this report) UNCLASSIFIED
17. DISTRIBUTION STATEMENT (of the abstract entered in Block 20, if different from Report)		15a. DECLASSIFICATION/DOWNGRADING SCHEDULE
18. SUPPLEMENTARY NOTES This research was sponsored by the Defense Nuclear Agency under Subtask S99QSHI004, Work Unit 11 Entitled: IR Phenomenology and Optical Code Development *J.W. Reed is now at Visidyne, Inc., Burlington, Mass.		
19. KEY WORDS (Continue on reverse side if necessary and identify by block number) Nitric oxide, aurora, hydroxyl, radiometer, NKC-135A aircraft, emissions, auroral enhancement, infrared.		
20. ABSTRACT (Continue on reverse side if necessary and identify by block number) Significant infrared emission enhancements in the 2.75-3.04 μ m region have been measured from the AFGL NKC-135A aircraft while viewing an aurorally excited atmosphere with a radiometer. The measured enhancements occurred while viewing all types of auroral forms, and they became significant with respect to the night sky background emissions whenever the N_2^+ emissions at 3914A exceeded about 20 kiloRayleighs. → next page N2(+)		

DD FORM 1 JAN 73 1473

EDITION OF 1 NOV 65 IS OBSOLETE

UNCLASSIFIED

SECURITY CLASSIFICATION OF THIS PAGE (When Data Entered)

123 870

AB

DDC
MAR 20 1978
RECEIVED
F

UNCLASSIFIED

SECURITY CLASSIFICATION OF THIS PAGE(When Data Entered)

micrometers
N₂(+)
Delta

Within the angular resolution capabilities of the instrumentation, the measured 2.8 μm enhancements appeared to co-vary spatially and temporally with enhancements in the ionization-prompt fluorescence of the N₂. The enhancements did not correlate with emissions of the (5,3) band of the hydroxyl (OH) $\Delta V=2$ sequence at 1.7 μm . Therefore, it is unlikely that the enhancements were the result of increases in the OH fundamental sequence due to perturbed airglow processes.

It appears that the most probable source creating the enhancements is the first overtone of nitric oxide (NO). Using the measured 2.8 μm and 3914A data and a synthetic NO model, the percentage of the total auroral electron energy which is radiated as first overtone NO photons was calculated for seven enhancement periods. The calculated percentage, photo-energy efficiencies, ranged from .4% to 1.0%.

micrometers

UNCLASSIFIED

SECURITY CLASSIFICATION OF THIS PAGE(When Data Entered)

PREFACE

The High Altitude Effects Simulation (HAES) Program sponsored by the Defense Nuclear Agency since the early 1970 time period, comprises several groupings of separate, but interrelated technical activities, e.g., ICECAP (Infrared Chemistry Experiments--Coordinated Auroral Program). Each of the latter have the common objective of providing information ascertained as essential for the development and validation of predictive computer codes designed for use with high priority DOD radar, communications, and optical defensive systems.

Since the inception of the HAES Program, significant achievements and results have been described in reports published by DNA, participating service laboratories, and supportive organizations. In order to provide greater visibility for such information and enhance its timely applications, significant reports published since early calendar 1974 shall be identified with an assigned HAES serial number and the appropriate activity acronym (e.g., ICECAP) as part of the report title. A complete and current bibliography of all HAES reports issued prior to and subsequent to HAES Report No. 1, dated 5 February 1974 entitled, "Rocket Launch of an SWIR Spectrometer into an Aurora (ICECAP 72)", AFCRL Environmental Research Paper No. 466, is maintained and available on request from DASIAC, DOD Nuclear Information and Analysis Center, 816 State Street, Santa Barbara, California 93102, Telephone (805) 965-0551.

This report, Scientific Report Number 3 under Air Force Geophysics Laboratory (AFGL, formerly AFCRL) contract F19628-74-C-0190 is the sixty eighth report in the HAES series, and covers a portion of the ICECAP airborne technical efforts performed by the AFGL Infrared Flying Laboratory during February-March 1975 and February-March 1976. The purpose of the work reported herein was to investigate high altitude atmospheric infrared emissions from the spatially and temporally varying locations of the NKC-135A platform at the same times as intense auroral sampling efforts from ground and rocket-borne ICECAP experiments were being performed. Thus, a cost effective state of the art probe of selected infrared radiations was made to provide bench mark radiance level measurements for determination of future spectral scanning instrument specifications.

1. <input checked="" type="checkbox"/> WFO Section 2. <input type="checkbox"/> WFO Section 3. <input type="checkbox"/> WFO Section 4. <input type="checkbox"/> WFO Section 5. <input type="checkbox"/> WFO Section 6. <input type="checkbox"/> WFO Section 7. <input type="checkbox"/> WFO Section 8. <input type="checkbox"/> WFO Section 9. <input type="checkbox"/> WFO Section 10. <input type="checkbox"/> WFO Section 11. <input type="checkbox"/> WFO Section 12. <input type="checkbox"/> WFO Section 13. <input type="checkbox"/> WFO Section 14. <input type="checkbox"/> WFO Section 15. <input type="checkbox"/> WFO Section 16. <input type="checkbox"/> WFO Section 17. <input type="checkbox"/> WFO Section 18. <input type="checkbox"/> WFO Section 19. <input type="checkbox"/> WFO Section 20. <input type="checkbox"/> WFO Section 21. <input type="checkbox"/> WFO Section 22. <input type="checkbox"/> WFO Section 23. <input type="checkbox"/> WFO Section 24. <input type="checkbox"/> WFO Section 25. <input type="checkbox"/> WFO Section 26. <input type="checkbox"/> WFO Section 27. <input type="checkbox"/> WFO Section 28. <input type="checkbox"/> WFO Section 29. <input type="checkbox"/> WFO Section 30. <input type="checkbox"/> WFO Section 31. <input type="checkbox"/> WFO Section 32. <input type="checkbox"/> WFO Section 33. <input type="checkbox"/> WFO Section 34. <input type="checkbox"/> WFO Section 35. <input type="checkbox"/> WFO Section 36. <input type="checkbox"/> WFO Section 37. <input type="checkbox"/> WFO Section 38. <input type="checkbox"/> WFO Section 39. <input type="checkbox"/> WFO Section 40. <input type="checkbox"/> WFO Section 41. <input type="checkbox"/> WFO Section 42. <input type="checkbox"/> WFO Section 43. <input type="checkbox"/> WFO Section 44. <input type="checkbox"/> WFO Section 45. <input type="checkbox"/> WFO Section 46. <input type="checkbox"/> WFO Section 47. <input type="checkbox"/> WFO Section 48. <input type="checkbox"/> WFO Section 49. <input type="checkbox"/> WFO Section 50. <input type="checkbox"/> WFO Section 51. <input type="checkbox"/> WFO Section 52. <input type="checkbox"/> WFO Section 53. <input type="checkbox"/> WFO Section 54. <input type="checkbox"/> WFO Section 55. <input type="checkbox"/> WFO Section 56. <input type="checkbox"/> WFO Section 57. <input type="checkbox"/> WFO Section 58. <input type="checkbox"/> WFO Section 59. <input type="checkbox"/> WFO Section 60. <input type="checkbox"/> WFO Section 61. <input type="checkbox"/> WFO Section 62. <input type="checkbox"/> WFO Section 63. <input type="checkbox"/> WFO Section 64. <input type="checkbox"/> WFO Section 65. <input type="checkbox"/> WFO Section 66. <input type="checkbox"/> WFO Section 67. <input type="checkbox"/> WFO Section 68. <input type="checkbox"/> WFO Section 69. <input type="checkbox"/> WFO Section 70. <input type="checkbox"/> WFO Section 71. <input type="checkbox"/> WFO Section 72. <input type="checkbox"/> WFO Section 73. <input type="checkbox"/> WFO Section 74. <input type="checkbox"/> WFO Section 75. <input type="checkbox"/> WFO Section 76. <input type="checkbox"/> WFO Section 77. <input type="checkbox"/> WFO Section 78. <input type="checkbox"/> WFO Section 79. <input type="checkbox"/> WFO Section 80. <input type="checkbox"/> WFO Section 81. <input type="checkbox"/> WFO Section 82. <input type="checkbox"/> WFO Section 83. <input type="checkbox"/> WFO Section 84. <input type="checkbox"/> WFO Section 85. <input type="checkbox"/> WFO Section 86. <input type="checkbox"/> WFO Section 87. <input type="checkbox"/> WFO Section 88. <input type="checkbox"/> WFO Section 89. <input type="checkbox"/> WFO Section 90. <input type="checkbox"/> WFO Section 91. <input type="checkbox"/> WFO Section 92. <input type="checkbox"/> WFO Section 93. <input type="checkbox"/> WFO Section 94. <input type="checkbox"/> WFO Section 95. <input type="checkbox"/> WFO Section 96. <input type="checkbox"/> WFO Section 97. <input type="checkbox"/> WFO Section 98. <input type="checkbox"/> WFO Section 99. <input type="checkbox"/> WFO Section 100. <input type="checkbox"/> WFO Section 101. <input type="checkbox"/> WFO Section 102. <input type="checkbox"/> WFO Section 103. <input type="checkbox"/> WFO Section 104. <input type="checkbox"/> WFO Section 105. <input type="checkbox"/> WFO Section 106. <input type="checkbox"/> WFO Section 107. <input type="checkbox"/> WFO Section 108. <input type="checkbox"/> WFO Section 109. <input type="checkbox"/> WFO Section 110. <input type="checkbox"/> WFO Section 111. <input type="checkbox"/> WFO Section 112. <input type="checkbox"/> WFO Section 113. <input type="checkbox"/> WFO Section 114. <input type="checkbox"/> WFO Section 115. <input type="checkbox"/> WFO Section 116. <input type="checkbox"/> WFO Section 117. <input type="checkbox"/> WFO Section 118. <input type="checkbox"/> WFO Section 119. <input type="checkbox"/> WFO Section 120. <input type="checkbox"/> WFO Section 121. <input type="checkbox"/> WFO Section 122. <input type="checkbox"/> WFO Section 123. <input type="checkbox"/> WFO Section 124. <input type="checkbox"/> WFO Section 125. <input type="checkbox"/> WFO Section 126. <input type="checkbox"/> WFO Section 127. <input type="checkbox"/> WFO Section 128. <input type="checkbox"/> WFO Section 129. <input type="checkbox"/> WFO Section 130. <input type="checkbox"/> WFO Section 131. <input type="checkbox"/> WFO Section 132. <input type="checkbox"/> WFO Section 133. <input type="checkbox"/> WFO Section 134. <input type="checkbox"/> WFO Section 135. <input type="checkbox"/> WFO Section 136. <input type="checkbox"/> WFO Section 137. <input type="checkbox"/> WFO Section 138. <input type="checkbox"/> WFO Section 139. <input type="checkbox"/> WFO Section 140. <input type="checkbox"/> WFO Section 141. <input type="checkbox"/> WFO Section 142. <input type="checkbox"/> WFO Section 143. <input type="checkbox"/> WFO Section 144. <input type="checkbox"/> WFO Section 145. <input type="checkbox"/> WFO Section 146. <input type="checkbox"/> WFO Section 147. <input type="checkbox"/> WFO Section 148. <input type="checkbox"/> WFO Section 149. <input type="checkbox"/> WFO Section 150. <input type="checkbox"/> WFO Section 151. <input type="checkbox"/> WFO Section 152. <input type="checkbox"/> WFO Section 153. <input type="checkbox"/> WFO Section 154. <input type="checkbox"/> WFO Section 155. <input type="checkbox"/> WFO Section 156. <input type="checkbox"/> WFO Section 157. <input type="checkbox"/> WFO Section 158. <input type="checkbox"/> WFO Section 159. <input type="checkbox"/> WFO Section 160. <input type="checkbox"/> WFO Section 161. <input type="checkbox"/> WFO Section 162. <input type="checkbox"/> WFO Section 163. <input type="checkbox"/> WFO Section 164. <input type="checkbox"/> WFO Section 165. <input type="checkbox"/> WFO Section 166. <input type="checkbox"/> WFO Section 167. <input type="checkbox"/> WFO Section 168. <input type="checkbox"/> WFO Section 169. <input type="checkbox"/> WFO Section 170. <input type="checkbox"/> WFO Section 171. <input type="checkbox"/> WFO Section 172. <input type="checkbox"/> WFO Section 173. <input type="checkbox"/> WFO Section 174. <input type="checkbox"/> WFO Section 175. <input type="checkbox"/> WFO Section 176. <input type="checkbox"/> WFO Section 177. <input type="checkbox"/> WFO Section 178. <input type="checkbox"/> WFO Section 179. <input type="checkbox"/> WFO Section 180. <input type="checkbox"/> WFO Section 181. <input type="checkbox"/> WFO Section 182. <input type="checkbox"/> WFO Section 183. <input type="checkbox"/> WFO Section 184. <input type="checkbox"/> WFO Section 185. <input type="checkbox"/> WFO Section 186. <input type="checkbox"/> WFO Section 187. <input type="checkbox"/> WFO Section 188. <input type="checkbox"/> WFO Section 189. <input type="checkbox"/> WFO Section 190. <input type="checkbox"/> WFO Section 191. <input type="checkbox"/> WFO Section 192. <input type="checkbox"/> WFO Section 193. <input type="checkbox"/> WFO Section 194. <input type="checkbox"/> WFO Section 195. <input type="checkbox"/> WFO Section 196. <input type="checkbox"/> WFO Section 197. <input type="checkbox"/> WFO Section 198. <input type="checkbox"/> WFO Section 199. <input type="checkbox"/> WFO Section 200. <input type="checkbox"/> WFO Section 201. <input type="checkbox"/> WFO Section 202. <input type="checkbox"/> WFO Section 203. <input type="checkbox"/> WFO Section 204. <input type="checkbox"/> WFO Section 205. <input type="checkbox"/> WFO Section 206. <input type="checkbox"/> WFO Section 207. <input type="checkbox"/> WFO Section 208. <input type="checkbox"/> WFO Section 209. <input type="checkbox"/> WFO Section 210. <input type="checkbox"/> WFO Section 211. <input type="checkbox"/> WFO Section 212. <input type="checkbox"/> WFO Section 213. <input type="checkbox"/> WFO Section 214. <input type="checkbox"/> WFO Section 215. <input type="checkbox"/> WFO Section 216. <input type="checkbox"/> WFO Section 217. <input type="checkbox"/> WFO Section 218. <input type="checkbox"/> WFO Section 219. <input type="checkbox"/> WFO Section 220. <input type="checkbox"/> WFO Section 221. <input type="checkbox"/> WFO Section 222. <input type="checkbox"/> WFO Section 223. <input type="checkbox"/> WFO Section 224. <input type="checkbox"/> WFO Section 225. <input type="checkbox"/> WFO Section 226. <input type="checkbox"/> WFO Section 227. <input type="checkbox"/> WFO Section 228. <input type="checkbox"/> WFO Section 229. <input type="checkbox"/> WFO Section 230. <input type="checkbox"/> WFO Section 231. <input type="checkbox"/> WFO Section 232. <input type="checkbox"/> WFO Section 233. <input type="checkbox"/> WFO Section 234. <input type="checkbox"/> WFO Section 235. <input type="checkbox"/> WFO Section 236. <input type="checkbox"/> WFO Section 237. <input type="checkbox"/> WFO Section 238. <input type="checkbox"/> WFO Section 239. <input type="checkbox"/> WFO Section 240. <input type="checkbox"/> WFO Section 241. <input type="checkbox"/> WFO Section 242. <input type="checkbox"/> WFO Section 243. <input type="checkbox"/> WFO Section 244. <input type="checkbox"/> WFO Section 245. <input type="checkbox"/> WFO Section 246. <input type="checkbox"/> WFO Section 247. <input type="checkbox"/> WFO Section 248. <input type="checkbox"/> WFO Section 249. <input type="checkbox"/> WFO Section 250. <input type="checkbox"/> WFO Section 251. <input type="checkbox"/> WFO Section 252. <input type="checkbox"/> WFO Section 253. <input type="checkbox"/> WFO Section 254. <input type="checkbox"/> WFO Section 255. <input type="checkbox"/> WFO Section 256. <input type="checkbox"/> WFO Section 257. <input type="checkbox"/> WFO Section 258. <input type="checkbox"/> WFO Section 259. <input type="checkbox"/> WFO Section 260. <input type="checkbox"/> WFO Section 261. <input type="checkbox"/> WFO Section 262. <input type="checkbox"/> WFO Section 263. <input type="checkbox"/> WFO Section 264. <input type="checkbox"/> WFO Section 265. <input type="checkbox"/> WFO Section 266. <input type="checkbox"/> WFO Section 267. <input type="checkbox"/> WFO Section 268. <input type="checkbox"/> WFO Section 269. <input type="checkbox"/> WFO Section 270. <input type="checkbox"/> WFO Section 271. <input type="checkbox"/> WFO Section 272. <input type="checkbox"/> WFO Section 273. <input type="checkbox"/> WFO Section 274. <input type="checkbox"/> WFO Section 275. <input type="checkbox"/> WFO Section 276. <input type="checkbox"/> WFO Section 277. <input type="checkbox"/> WFO Section 278. <input type="checkbox"/> WFO Section 279. <input type="checkbox"/> WFO Section 280. <input type="checkbox"/> WFO Section 281. <input type="checkbox"/> WFO Section 282. <input type="checkbox"/> WFO Section 283. <input type="checkbox"/> WFO Section 284. <input type="checkbox"/> WFO Section 285. <input type="checkbox"/> WFO Section 286. <input type="checkbox"/> WFO Section 287. <input type="checkbox"/> WFO Section 288. <input type="checkbox"/> WFO Section 289. <input type="checkbox"/> WFO Section 290. <input type="checkbox"/> WFO Section 291. <input type="checkbox"/> WFO Section 292. <input type="checkbox"/> WFO Section 293. <input type="checkbox"/> WFO Section 294. <input type="checkbox"/> WFO Section 295. <input type="checkbox"/> WFO Section 296. <input type="checkbox"/> WFO Section 297. <input type="checkbox"/> WFO Section 298. <input type="checkbox"/> WFO Section 299. <input type="checkbox"/> WFO Section 300. <input type="checkbox"/> WFO Section 301. <input type="checkbox"/> WFO Section 302. <input type="checkbox"/> WFO Section 303. <input type="checkbox"/> WFO Section 304. <input type="checkbox"/> WFO Section 305. <input type="checkbox"/> WFO Section 306. <input type="checkbox"/> WFO Section 307. <input type="checkbox"/> WFO Section 308. <input type="checkbox"/> WFO Section 309. <input type="checkbox"/> WFO Section 310. <input type="checkbox"/> WFO Section 311. <input type="checkbox"/> WFO Section 312. <input type="checkbox"/> WFO Section 313. <input type="checkbox"/> WFO Section 314. <input type="checkbox"/> WFO Section 315. <input type="checkbox"/> WFO Section 316. <input type="checkbox"/> WFO Section 317. <input type="checkbox"/> WFO Section 318. <input type="checkbox"/> WFO Section 319. <input type="checkbox"/> WFO Section 320. <input type="checkbox"/> WFO Section 321. <input type="checkbox"/> WFO Section 322. <input type="checkbox"/> WFO Section 323. <input type="checkbox"/> WFO Section 324. <input type="checkbox"/> WFO Section 325. <input type="checkbox"/> WFO Section 326. <input type="checkbox"/> WFO Section 327. <input type="checkbox"/> WFO Section 328. <input type="checkbox"/> WFO Section 329. <input type="checkbox"/> WFO Section 330. <input type="checkbox"/> WFO Section 331. <input type="checkbox"/> WFO Section 332. <input type="checkbox"/> WFO Section 333. <input type="checkbox"/> WFO Section 334. <input type="checkbox"/> WFO Section 335. <input type="checkbox"/> WFO Section 336. <input type="checkbox"/> WFO Section 337. <input type="checkbox"/> WFO Section 338. <input type="checkbox"/> WFO Section 339. <input type="checkbox"/> WFO Section 340. <input type="checkbox"/> WFO Section 341. <input type="checkbox"/> WFO Section 342. <input type="checkbox"/> WFO Section 343. <input type="checkbox"/> WFO Section 344. <input type="checkbox"/> WFO Section 345. <input type="checkbox"/> WFO Section 346. <input type="checkbox"/> WFO Section 347. <input type="checkbox"/> WFO Section 348. <input type="checkbox"/> WFO Section 349. <input type="checkbox"/> WFO Section 350. <input type="checkbox"/> WFO Section 351. <input type="checkbox"/> WFO Section 352. <input type="checkbox"/> WFO Section 353. <input type="checkbox"/> WFO Section 354. <input type="checkbox"/> WFO Section 355. <input type="checkbox"/> WFO Section 356. <input type="checkbox"/> WFO Section 357. <input type="checkbox"/> WFO Section 358. <input type="checkbox"/> WFO Section 359. <input type="checkbox"/> WFO Section 360. <input type="checkbox"/> WFO Section 361. <input type="checkbox"/> WFO Section 362. <input type="checkbox"/> WFO Section 363. <input type="checkbox"/> WFO Section 364. <input type="checkbox"/> WFO Section 365. <input type="checkbox"/> WFO Section 366. <input type="checkbox"/> WFO Section 367. <input type="checkbox"/> WFO Section 368. <input type="checkbox"/> WFO Section 369. <input type="checkbox"/> WFO Section 370. <input type="checkbox"/> WFO Section 371. <input type="checkbox"/> WFO Section 372. <input type="checkbox"/> WFO Section 373. <input type="checkbox"/> WFO Section 374. <input type="checkbox"/> WFO Section 375. <input type="checkbox"/> WFO Section 376. <input type="checkbox"/> WFO Section 377. <input type="checkbox"/> WFO Section 378. <input type="checkbox"/> WFO Section 379. <input type="checkbox"/> WFO Section 380. <input type="checkbox"/> WFO Section 381. <input type="checkbox"/> WFO Section 382. <input type="checkbox"/> WFO Section 383. <input type="checkbox"/> WFO Section 384. <input type="checkbox"/> WFO Section 385. <input type="checkbox"/> WFO Section 386. <input type="checkbox"/> WFO Section 387. <input type="checkbox"/> WFO Section 388. <input type="checkbox"/> WFO Section 389. <input type="checkbox"/> WFO Section 390. <input type="checkbox"/> WFO Section 391. <input type="checkbox"/> WFO Section 392. <input type="checkbox"/> WFO Section 393. <input type="checkbox"/> WFO Section 394. <input type="checkbox"/> WFO Section 395. <input type="checkbox"/> WFO Section 396. <input type="checkbox"/> WFO Section 397. <input type="checkbox"/> WFO Section 398. <input type="checkbox"/> WFO Section 399. <input type="checkbox"/> WFO Section 400. <input type="checkbox"/> WFO Section 401. <input type="checkbox"/> WFO Section 402. <input type="checkbox"/> WFO Section 403. <input type="checkbox"/> WFO Section 404. <input type="checkbox"/> WFO Section 405. <input type="checkbox"/> WFO Section 406. <input type="checkbox"/> WFO Section 407. <input type="checkbox"/> WFO Section 408. <input type="checkbox"/> WFO Section 409. <input type="checkbox"/> WFO Section 410. <input type="checkbox"/> WFO Section 411. <input type="checkbox"/> WFO Section 412. <input type="checkbox"/> WFO Section 413. <input type="checkbox"/> WFO Section 414. <input type="checkbox"/> WFO Section 415. <input type="checkbox"/> WFO Section 416. <input type="checkbox"/> WFO Section 417. <input type="checkbox"/> WFO Section 418. <input type="checkbox"/> WFO Section 419. <input type="checkbox"/> WFO Section 420. <input type="checkbox"/> WFO Section 421. <input type="checkbox"/> WFO Section 422. <input type="checkbox"/> WFO Section 423. <input type="checkbox"/> WFO Section 424. <input type="checkbox"/> WFO Section 425. <input type="checkbox"/> WFO Section 426. <input type="checkbox"/> WFO Section 427. <input type="checkbox"/> WFO Section 428. <input type="checkbox"/> WFO Section 429. <input type="checkbox"/> WFO Section 430. <input type="checkbox"/> WFO Section 431. <input type="checkbox"/> WFO Section 432. <input type="checkbox"/> WFO Section 433. <input type="checkbox"/> WFO Section 434. <input type="checkbox"/> WFO Section 435. <input type="checkbox"/> WFO Section 436. <input type="checkbox"/> WFO Section 437. <input type="checkbox"/> WFO Section 438. <input type="checkbox"/> WFO Section 439. <input type="checkbox"/> WFO Section 440. <input type="checkbox"/> WFO Section 441. <input type="checkbox"/> WFO Section 442. <input type="checkbox"/> WFO Section 443. <input type="checkbox"/> WFO Section 444. <input type="checkbox"/> WFO Section 445. <input type="checkbox"/> WFO Section 446. <input type="checkbox"/> WFO Section 447. <input type="checkbox"/> WFO Section 448. <input type="checkbox"/> WFO Section 449. <input type="checkbox"/> WFO Section 450. <input type="checkbox"/> WFO Section 451. <input type="checkbox"/> WFO Section 452. <input type="checkbox"/> WFO Section 453. <input type="checkbox"/> WFO Section 454. <input type="checkbox"/> WFO Section 455. <input type="checkbox"/> WFO Section 456. <input type="checkbox"/> WFO Section 457. <input type="checkbox"/> WFO Section 458. <input type="checkbox"/> WFO Section 459. <input type="checkbox"/> WFO Section 460. <input type="checkbox"/> WFO Section 461. <input type="checkbox"/> WFO Section 462. <input type="checkbox"/> WFO Section 463. <input type="checkbox"/> WFO Section 464. <input type="checkbox"/> WFO Section 465. <input type="checkbox"/> WFO Section 466. <input type="checkbox"/> WFO Section 467. <input type="checkbox"/> WFO Section 468. <input type="checkbox"/> WFO Section 469. <input type="checkbox"/> WFO Section 470. <input type="checkbox"/> WFO Section 471. <input type="checkbox"/> WFO Section 472. <input type="checkbox"/> WFO Section 473. <input type="checkbox"/> WFO Section 474. <input type="checkbox"/> WFO Section 475. <input type="checkbox"/> WFO Section 476. <input type="checkbox"/> WFO Section 477. <input type="checkbox"/> WFO Section 478. <input type="checkbox"/> WFO Section 479. <input type="checkbox"/> WFO Section 480. <input type="checkbox"/> WFO Section 481. <input type="checkbox"/> WFO Section 482. <input type="checkbox"/> WFO Section 483. <input type="checkbox"/> WFO Section 484. <input type="checkbox"/> WFO Section 485. <input type="checkbox"/> WFO Section 486. <input type="checkbox"/> WFO Section 487. <input type="checkbox"/> WFO Section 488. <input type="checkbox"/> WFO Section 489. <input type="checkbox"/> WFO Section

TABLE OF CONTENTS

	Page
ACKNOWLEDGEMENTS.....	13
INTRODUCTION.....	14
EXPERIMENT DESCRIPTION.....	14
MEASURED INFRARED ENHANCEMENTS.....	26
DATA ANALYSIS.....	49
Spatial and Temporal Correlation Between 3914A(N ₂ ⁺)	
Emissions and 2.8 μm Enhancements.....	49
Linearity Studies.....	63
Photo-Energy Efficiency of Aurorally Enhanced	
2.94 μm Emissions.....	65
REFERENCES.....	71
APPENDIX A -- Instrumentation and Measurement Platform.	72
APPENDIX B -- Coordination of Aircraft Measurements and	
Chatanika Radar Measurements.....	83
APPENDIX C -- Additional Infrared Enhancement Data.....	85
APPENDIX D -- Aircraft Flight Description.....	98
REFERENCES.....	109
DISTRIBUTION LIST.....	110

LIST OF FIGURES

- Figure 1. Radiometer response curves overlayed on a synthetic spectrum of OH $\Delta V=1$ computed for $T_R=220^{\circ}\text{K}$, $T_V=5000^{\circ}\text{K}$, and resolution = 1 cm^{-1} 16
- Figure 2. Radiometer response curves overlayed on a synthetic spectrum of H_2O computed for $T_R= 220^{\circ}\text{K}$, $T_V= 220^{\circ}\text{K}$ and resolution = 1 cm^{-1} .. 17
- Figure 3. Radiometer response curves overlayed on a synthetic spectrum of $2.7\text{ }\mu\text{m CO}_2$ computed for $T_R= T_V= 220^{\circ}\text{K}$ and resolution = 1 cm^{-1} 18
- Figure 4. Radiometer response curves overlayed on a synthetic spectrum of NO $\Delta V = 2$ computed for $T_R= 220^{\circ}\text{K}$, $T_V= 5000^{\circ}\text{K}$, resolution = 1 cm^{-1} 19
- Figure 5. Relative spectral response of the OH radiometer overlayed on an OH $\Delta V = 2$ spectrum..... 21
- Figure 6. Radiometer instrument responses overlayed on atmospheric transmittance calculated from Lowtran program for 10.5 km..... 23
- Figure 7. Measurements from aircraft-borne instrumentation for March 10, 1975, showing significant $2.83\text{ }\mu\text{m}$ enhancements correlated with various auroral formations..... 28
- Figure 8. Measurements made from aircraft borne instrumentation on March 15, 1975 showing correlation of OH $\Delta V = 2$ during a period of minimal auroral activity..... 29

LIST OF FIGURES (Continued)

- Figure 9. Measured correlation between the 2.83 μm data and the 1.7 μm (OH) data measured March 15, 1975 during a period of minimal auroral activity..... 30
- Figure 10. Measured data for March 10, 1975 plotted with an expanded time scale to illustrate the time and spatial correlation between the 2.83 μm emissions and the 3914A emissions while viewing an auroral arc..... 32
- Figure 11. Measured data for March 10, 1975 plotted with an expanded time scale to show small enhancements of the 2.83 μm emissions which are correlated with small enhancements of the 3914A fluorescence..... 33
- Figure 12. Measured data for March 10, 1975 plotted with an expanded time scale to show detailed structure of 2.83 μm enhancement which are correlated with a 3914A enhancement caused by a broad, diffused aurora..... 34
- Figure 13. Measured data for March 10, 1975 plotted with an expanded time scale to show time and spatial correlation between 2.83 μm emissions and 3914A emissions while viewing a narrow auroral arc.... 35
- Figure 14. Measured data for March 10, 1975 plotted with an expanded time scale to show time and spatial correlation between 2.83 μm emissions and 3914A emissions while viewing an auroral patch..... 36

LIST OF FIGURES (Continued)

- Figure 15. All sky camera pictures taken March 10, 1975 by Photometrics Incorporated from the AFGL NKC-135 aircraft with a 160° FOV camera..... 37
- Figure 16. Continuation of all sky camera pictures taken March 10, 1975 with a 160° FOV camera viewing vertically from the AFGL NKC-135 aircraft.... 38
- Figure 17. Measurements from aircraft-borne instrumentation for March 26, 1976, showing significant 2.94 μm enhancements correlated with the aurora..... 40
- Figure 18. Measured data for March 26, 1976 plotted with an expanded time scale to show the detailed correlation between the 2.94 μm emissions and the 3914A emissions during rapidly varying auroral conditions..... 41
- Figure 19. Measured data for March 26, 1976 showing the detailed structure and correlation of the 2.94 μm and 3914A emissions while viewing an auroral arc..... 42
- Figure 20. Measured data for March 26, 1976 showing the detailed correlation between the 2.94 μm emissions and the 3914A emissions during an auroral breakup..... 43
- Figure 21. All sky camera pictures taken March 26, 1976 by Photometrics Incorporated from the KC-135 aircraft with a 160° FOV camera viewing vertically..... 44

LIST OF FIGURES (Continued)

- Figure 22. Measurements made with aircraft-borne instrumentation on March 7, 1976 showing significant infrared enhancements which are correlated with aurora..... 45
- Figure 23. Measured data for March 7, 1976 plotted on an expanded time scale to show the correlation between the 2.94 μm emissions and the 3914A emissions during a period when small enhancements occurred..... 46
- Figure 24. Measured data for March 7, 1976 plotted on an expanded time scale to show the excellent spatial and time correlation between the 3914A emissions and the 2.94 μm emissions during rapidly fluctuating auroral conditions..... 47
- Figure 25. Measured data for March 7, 1976 plotted on an expanded time scale to illustrate the correlation between the 3914A emissions and the 2.94 μm emissions during a period when a large enhancement occurred..... 48
- Figure 26. Temporal and spatial comparisons of 2.94 μm and 3914A enhancements measured March 3, 1976..... 51
- Figure 27. Temporal and spatial comparisons of 2.94 μm and 3914A enhancements measured March 3, 1976 between 1000 and 1030 UT..... 52
- Figure 28. Temporal and spatial comparisons of 2.94 μm and 3914A enhancements measured March 7, 1976 between 1120 and 1150 UT..... 53

LIST OF FIGURES (Continued)

- Figure 29. Temporal and spatial comparisons of 2.94 μm
and 3914A enhancement measured March 8, 1976...54
- Figure 30. Temporal and spatial comparisons of 2.94 μm
and 3914A enhancements measured March 26,
1976 between 0905 and 0935 UT.....55
- Figure 31. Temporal and spatial comparisons of 2.94 μm
and 3914A enhancements measured March 26,
1976 between 1010 and 1040 UT.....56
- Figure 32. Temporal and spatial comparisons of 2.94 μm
and 3914A enhancements measured March 26,
1976 between 1120 and 1150 UT.....57
- Figure 33. All sky camera pictures showing auroral
conditions during periods when infrared
enhancements were measured on March 3, 1976...59
- Figure 34. All sky camera pictures showing auroral
conditions on March 26, 1976 for time periods
corresponding to the data presented in
Figure 30.....60
- Figure 35. All sky camera pictures showing auroral
conditions on March 26, 1976 for time periods
corresponding to the data presented in
Figure 31.....61
- Figure 36. All sky camera pictures showing auroral
conditions on March 26, 1976 for time periods
corresponding to the data presented in
Figure 32.....62

LIST OF FIGURES (Continued)

APPENDIX A

Figure A.1.	Pictorial of the AFGL Flying Laboratory NKC-135A, Serial Number 53120, showing the optical view locations which were used.....	73
Figure A.2.	Liquid nitrogen cooled chopper and radiometer system.....	75
Figure A.3.	Optical layout of 1.0 to 1.75 μm radiometer.....	77
Figure A.4.	Some typical upper atmospheric night airglow emission intensities compared with emissions from a 300 ⁰ K blackbody.....	79
Figure A.5.	Example of the All-Sky Camera Format....	80
Figure A.6.	Optical and Electrical Layout of 3914A Photometer.....	82

APPENDIX C

Figure C.1.	Measured data for March 1, 1976 showing significant NO enhancements which are correlated with aurora.....	89
Figure C.2.	Measured data for March 1, 1976 from 0930 to 1000 UT plotted on an expanded time scale to illustrate the temporal and spatial correlation between the emissions.....	90
Figure C.3.	Measured data for March 1, 1976 from 1015 to 1115 UT plotted on an expanded time scale to illustrate the temporal and spatial correlation between the emissions.....	91
Figure C.4.	Measured data for March 3, 1976 which includes significant auroral enhancements and a sunset transition.....	92
Figure C.5.	Measured data for March 3, 1976 from 0450 to 0530 plotted on an expanded time scale to illustrate the temporal and spatial correlation between the emissions.....	93
Figure C.6.	Measured data for March 3, 1976 from 0200 to 0500 showing intensities during daylight and sunset transition conditions.....	94

LIST OF FIGURES (Continued)

Figure C.7	Measured data for March 8, 1976 showing significant NO enhancements which are correlated with the aurora.....	95
Figure C.8	Measured data for March 2, 1975 showing correlation between the 2.83 μ m emissions and the 1.7 μ m (OH) emissions during a period when the auroral activity was minimal.....	96
Figure C.9	Measured data for March 11, 1975 showing small enhancements in the 3914A and 2.83 μ m emissions.....	97

APPENDIX D

Figure D.1	Flight description for measurements performed 2 Mar 75.....	99
Figure D.2	Flight description for measurements performed 10 Mar 75.....	100
Figure D.3	Flight description for measurements performed 11 Mar 75.....	101
Figure D.4	Flight description for measurements performed 15 Mar 75.....	102
Figure D.5	Flight description for measurements performed 1 Mar 76.....	103
Figure D.6	Flight description for measurements performed 3 Mar 76.....	104
Figure D.7	Flight description for measurements performed 7 Mar 76.....	105
Figure D.8	Flight description for measurements performed 8 Mar 76.....	106
Figure D.9	Flight description for measurements performed 26 Mar 76.....	107
Figure D.10	Cross section of Alaska showing footprint of 100 km Intercept with 2 ⁰ , 10 ⁰ , and 160 ⁰ airborne instrument fields of view.....	108

LIST OF TABLES

Table 1.	Summary of Instrumentation and Measurements for Infrared Experiment.....	25
Table 2.	Data Characteristics of Measurement Conditions.....	27
Table 3.	Comparisons of the 2.94 μm Enhancements and 3914A Emissions.....	64
Table 4.	Photo-Energy Efficiencies of Aurorally Excited 2.94 μm Emissions.....	68
Table 5.	Photo-Energy Efficiencies of Overtone NO Emissions.....	70

APPENDIX B

Table B.1.	Summary of Measurement Modes of the DNA 617 Backscatter Radar for the Nights of the 1976 Aircraft Measurements.....	84
------------	---	----

APPENDIX C

Table C.1.	Table of Figure Descriptions.....	85
------------	-----------------------------------	----

ACKNOWLEDGEMENTS

The principal AFGL ICECAP investigator was Dr. A.T. Stair, Jr. The Utah State University airborne investigation reported herein was under the technical direction of R.J. Huppi. The overall Flying Laboratory preparation and field effort was the responsibility of AFGL Project Officer, J.W. Reed, Major, USAF, including realtime telecommunications through the Geophysical Institute of University of Alaska. Airborne coordination and support was very ably accomplished by R.E. Pierce and John W. LaSpina of AFGL's Radiation Effects Branch, Optical Physics Division. Charles Eastman of Utah State University is to be commended for his concerted data reduction efforts. The authors would like to acknowledge the continued interest and collaborative effort on the part of Dr. I.L. Kofsky of Photometrics, Inc., who provided technical support and airborne camera and photometer support, and Dr. D. Baker of Utah State University for providing ground based photometer and low level T-V support. The support of E. Ray Huppi who significantly contributed to the development of the instrumentation is gratefully acknowledged. The gracious assistance by the University of Alaska's Geophysical Institute and Drs. T.N. Davis and J. Romick, and N. Brown and M. Holmgren, was directly responsible for the smooth operation during the critical measurement period. The excellent support provided in operating and maintaining the NKC-135A (Serial Number 53120) Infrared Flying Laboratory is acknowledged for the 1975 ICECAP missions to the 4900th Test Group, Air Force Special Weapons Center, Kirtland AFB, New Mexico; and for the 1976 ICECAP missions to the 4950th Test Wing, Wright-Patterson AFB, Ohio; and for both years, the professional support given by the entire Eielson AFB, Alaska team. Special acknowledgement is due to the AFSWC project officer, Capt. M. Hunter, and senior project pilot, Major W. Brown, and the 4950th T.W. Project Officer, Capt. J. Sillup, and senior project pilot, Capt. P. Larkin, and their operations and maintenance crews.

The support and encouragement of our colleagues and of our DNA Project Officer, Dr. C. Fitz, are gratefully acknowledged.

INTRODUCTION

Apparent enhancements of infrared emissions in the 2.75 to 3.04 μm region have been measured with a radiometer operated from the AFGL NKC-135 aircraft in the auroral region. The enhancements appear to co-vary spatially and temporally with the ionization-prompt fluorescence of N_2^+ as monitored by a 3914A photometer. However, better spatial resolution measurements are needed to more accurately study the correlation between the emissions.

The enhancements were measured during the 1975 and 1976 ICECAP programs supported by the Defense Nuclear Agency. The basic goals of the experiments were to confirm the existence of 2.75 to 3.04 μm enhancements in the auroral region, to measure the intensity of the enhancements, and to obtain spatial information about the enhancements. Also, concurrent measurements were made to aid in the determination of the source creating the enhancements. These concurrent measurements confirm that the enhancements cannot result from the airglow mechanisms producing OH emissions which fall within the spectral measurement bands. Thus, consideration is given to other probable sources, one of the most viable sources being the overtone of nitric oxide (NO).

In this report the instrumentation, the basic experiment, the measured results, and a fundamental analysis are discussed in detail. The absolute intensities of the emissions at the aircraft are provided, but to obtain absolute intensities of the emissions at the source one should correct the measured intensities for atmospheric transmittance losses using a high spectral resolution model.

EXPERIMENT DESCRIPTION

The experiment was planned to radiometrically measure enhancements in the 2.75 to 3.04 μm region during periods of auroral activity. When planning such an experiment it is

necessary to give consideration to possible emissions that may be present in the spectral region of interest. Specifically, in the 2.75 to 3.04 μm region, known sources of energy include the following: OH fundamental, H_2O , CO_2 and the NO overtone. Synthetic spectra of these sources are shown in Figure 1, Figure 2, Figure 3, and Figure 4, respectively, Gibson [1977]. The NO and OH vibrational distributions are the result of chemiluminescent reactions occurring above 80 km. The CO_2 and H_2O radiations observed by the aircraft are in thermal equilibrium and therefore most intense at low altitudes (near the aircraft) due to decreasing molecular density with altitude.

From Figures 1 through 4 it is apparent that the spectral wavelength regions of the various emissions overlap. All spectral wavelength bands, which are sufficiently broad to be compatible with the resolution limitations of a filtered radiometer, have a possibility of including NO and OH and to a lesser degree CO_2 and H_2O . Therefore it is necessary to discriminate against or prove the insignificance of the CO_2 , OH, and H_2O emissions if the auroral enhancements are to be assigned to NO.

Probably the best discrimination technique would be to perform a high spectral resolution measurement which would allow one to spectrally identify the emissions. This measurement could be accomplished through the use of a highly sensitive cryogenically cooled Michelson interferometer. However, such an instrument was not available, although it is being fabricated for future missions.

Therefore it was necessary to plan a simpler experiment using radiometric and spatial scanning techniques to perform the desired measurements. To accomplish this goal two IR radiometers, a photometer, and an all sky camera were installed in the AFGL flying laboratory, NKC 135A, serial number 53120. All instruments were coaligned and looked vertically out of the top of the aircraft. The aircraft not only provides a convenient platform to avoid low altitude atmospheric problems such as atmospheric thermal emissions, atmospheric transmittance

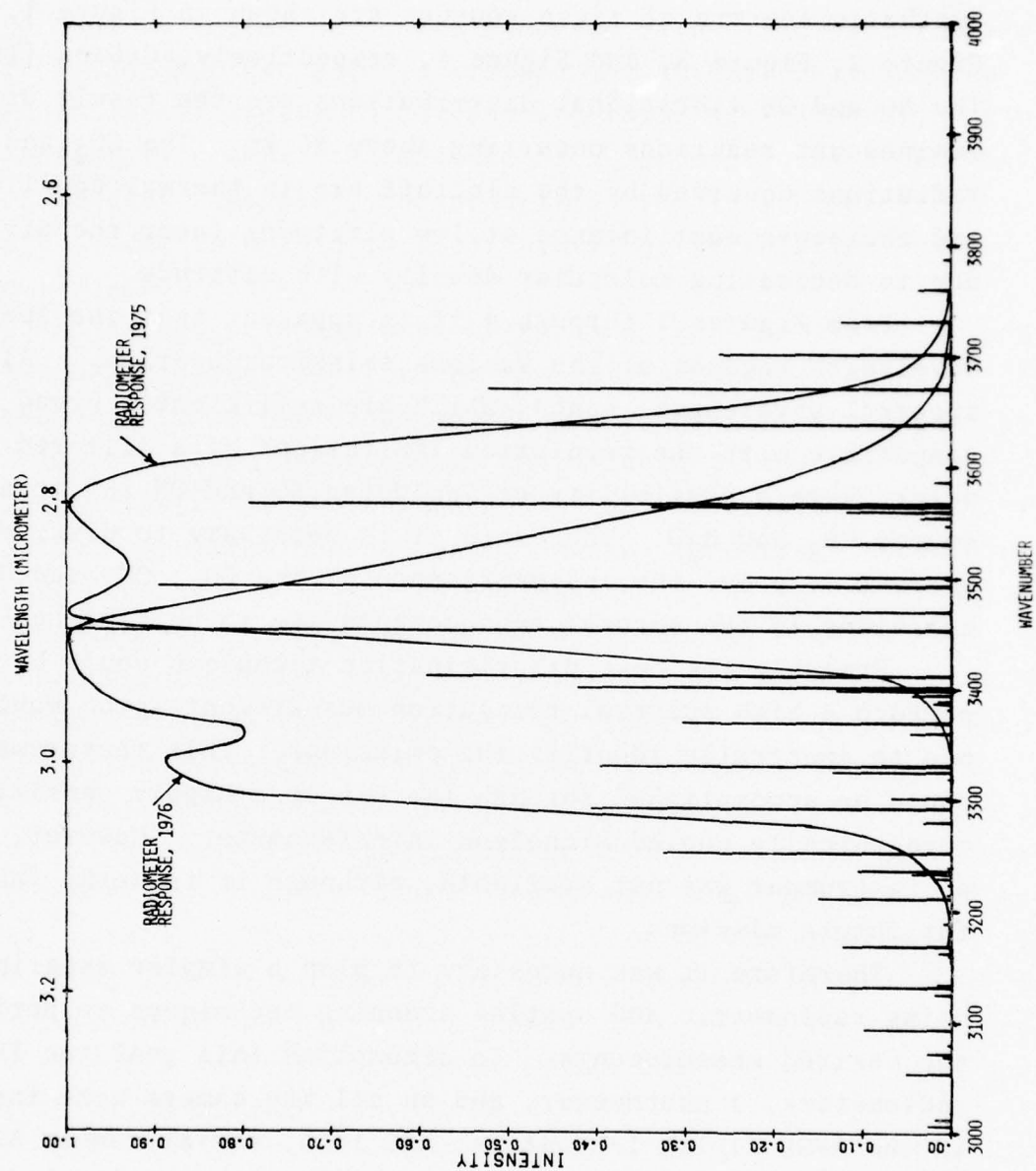


Figure 1. Radiometer response curves overlaid on a synthetic spectrum of OH $\Delta V = 1$ computed for $T_R = 220^\circ\text{K}$, $T_V = 5000^\circ\text{K}$, and resolution $= 1 \text{ cm}^{-1}$.

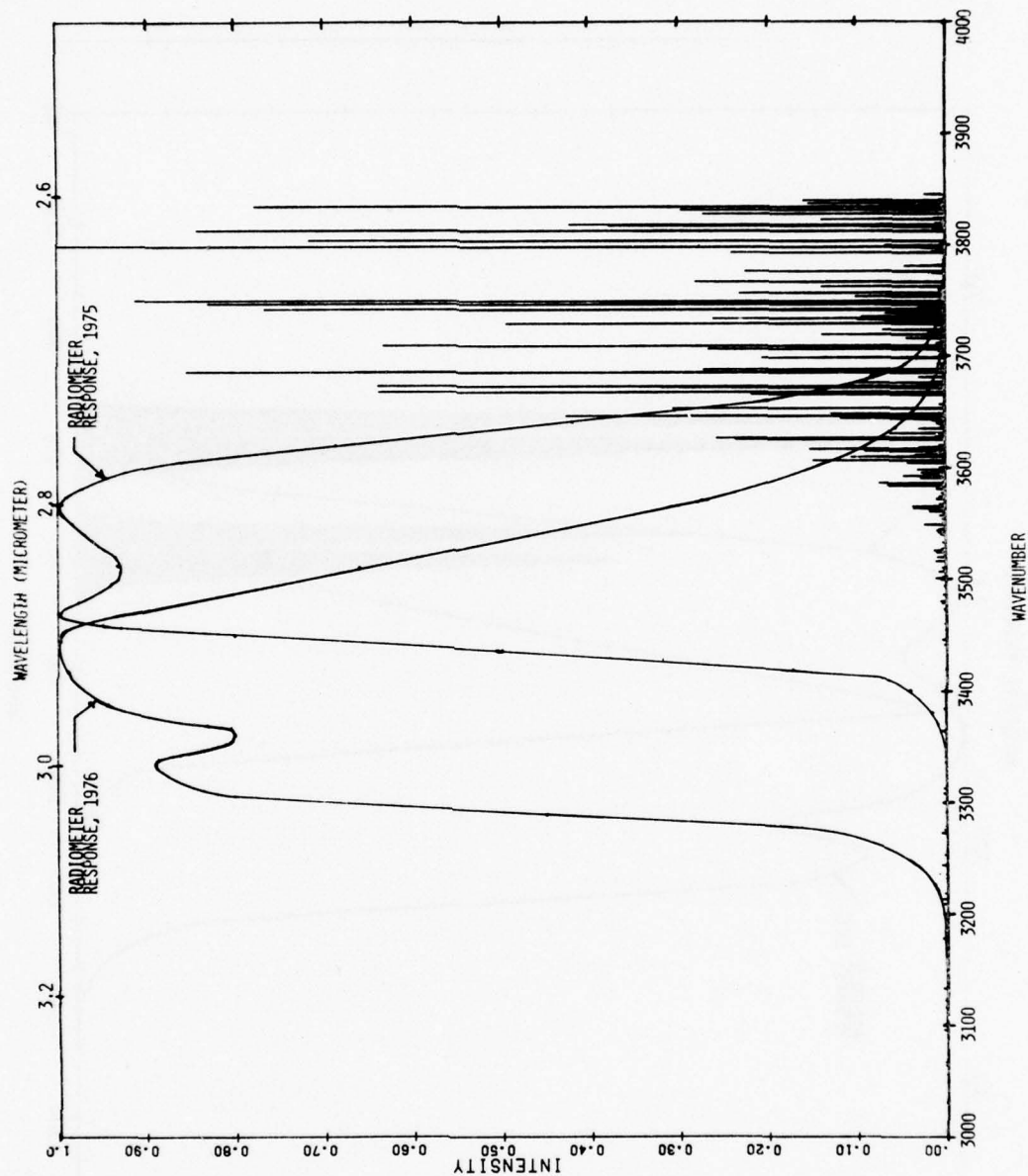


Figure 2. Radiometer response curves overlaid on a synthetic spectrum of H_2O computed for $T_R = 220^\circ K$, $T_V = 220^\circ K$ and resolution = 1 cm^{-1} .

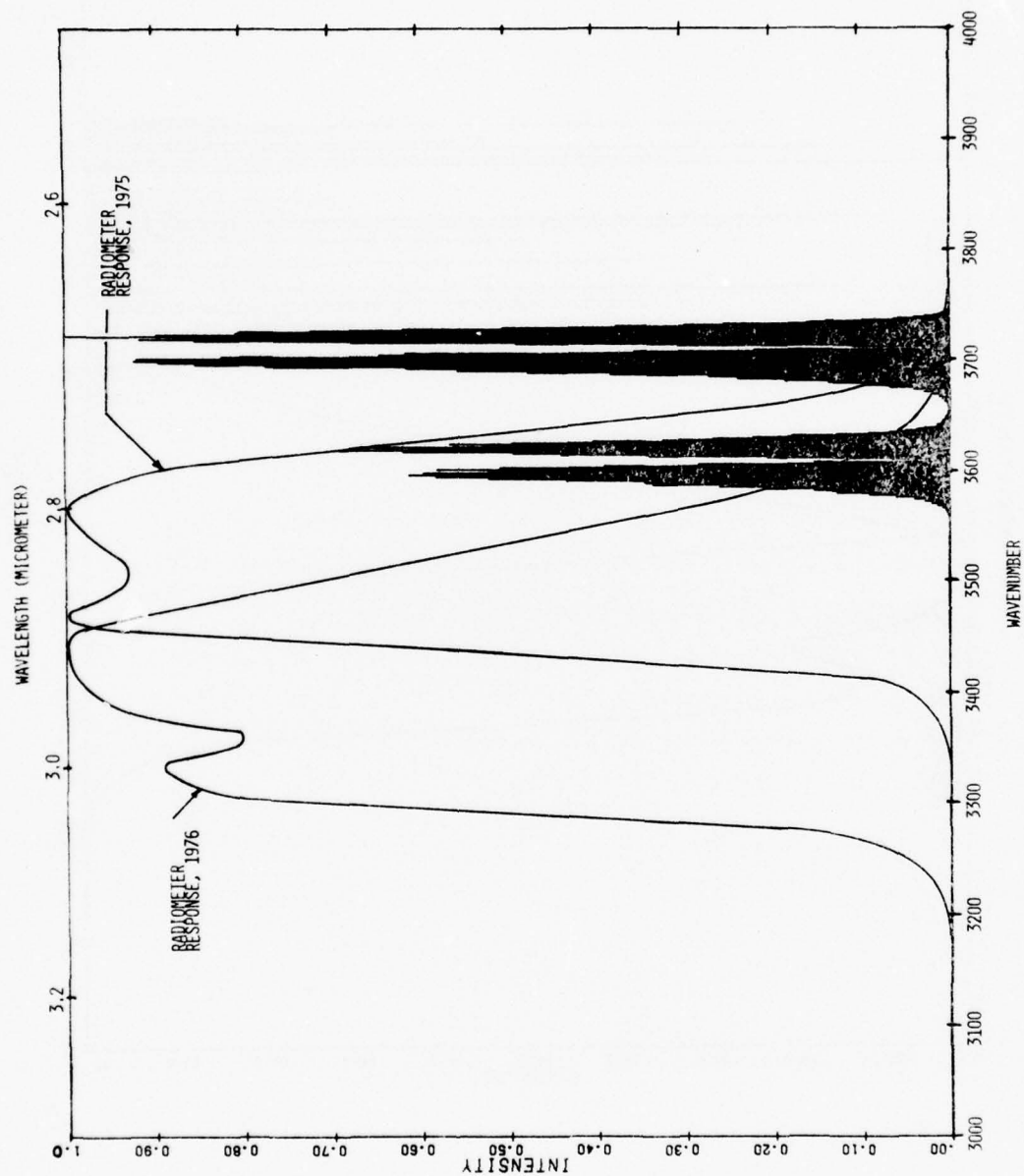


Figure 3. Radiometer response curves overlaid on a synthetic spectrum of $2.7 \mu\text{m CO}_2$ computed for $T_R = T_V = 220^\circ\text{K}$ and resolution $= 1 \text{ cm}^{-1}$.

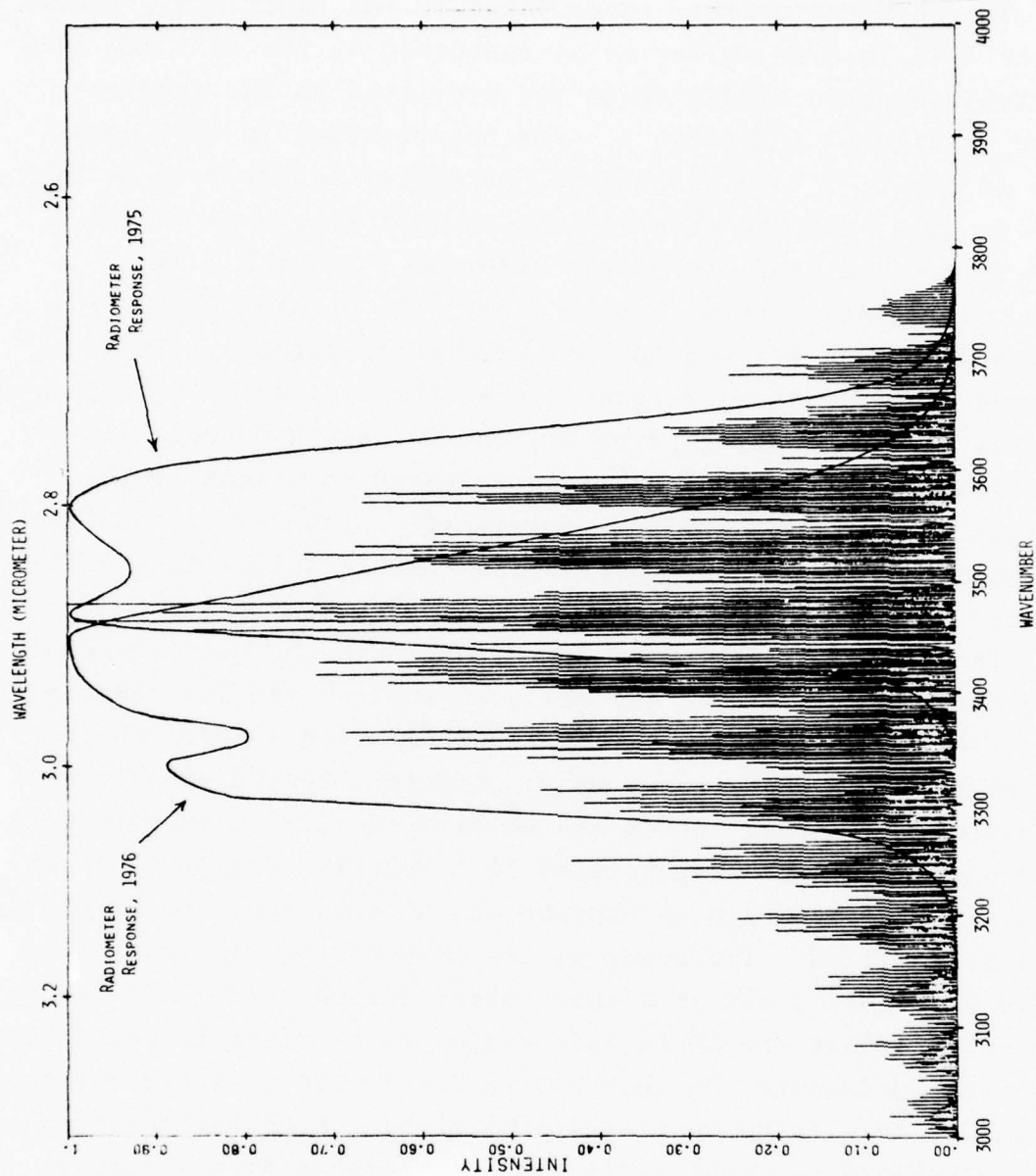


Figure 4. Radiometer response curves overlaid on a synthetic spectrum of NO $\Delta V = 2$ computed for $T_R = 220^\circ\text{K}$, $T_V = 5000^\circ\text{K}$, resolution = 1 cm^{-1} .

losses, and clouds; but it also provides the capability of limited scanning by virtue of its motion.

The main radiometer, fundamental to the experiment, looked in the 2.75 to 3.04 μm region as indicated by the 1975 and 1976 spectral response curves which are overlayed on the spectra shown in Figures 1 through 4. The observations in 1975 were made in the 2.75 to 2.90 μm band, hereafter referred to as the 2.83 μm data; and the observations in 1976 were made in the 2.84 to 3.04 μm band, hereafter referred to as the 2.94 μm data. The general term, 2.8 μm data, will be used whenever a common reference is made to both wavelength regions. It is obvious from Figures 1 through 4 that the radiometer's bandpasses were such that emissions from NO , OH , CO_2 and H_2O could all contribute to the measured 2.8 μm infrared emissions if the various sources have sufficient intensity. Therefore, additional instrumentation was needed to define the characteristics of the source.

The selected instrumentation supporting the main radiometer were useful for defining the emission sources and for removing the effects of non-aurorally enhanced emission sources which contaminate the measurement band. Consider the OH emissions. To allow the subtraction of the OH from the 2.8 μm measurement, a second radiometer was operated in a spectral region, 1.7 μm , which is free from H_2O absorption and NO emissions and primarily includes only OH . The spectral response of this instrument is shown in Figure 5 and it mainly covers the OH $\Delta V=2$ (5,3) transition. One would expect the OH in this region to be directly correlated with the fundamental OH near 2.8 μm Baker, [1976]. Therefore the amount of OH airglow contamination in the 2.8 μm radiometer channel should be predictable and subtractable at all times.

The H_2O and CO_2 thermal emissions are typically a factor of 5 to 10 less than the hydroxyl airglow emissions at 2.8 μm in a non-aurorally excited atmosphere. This is demonstrated by Stair [1976] (his Figure 2) where the hydroxyl spectral radiance is compared with blackbody emissions at various

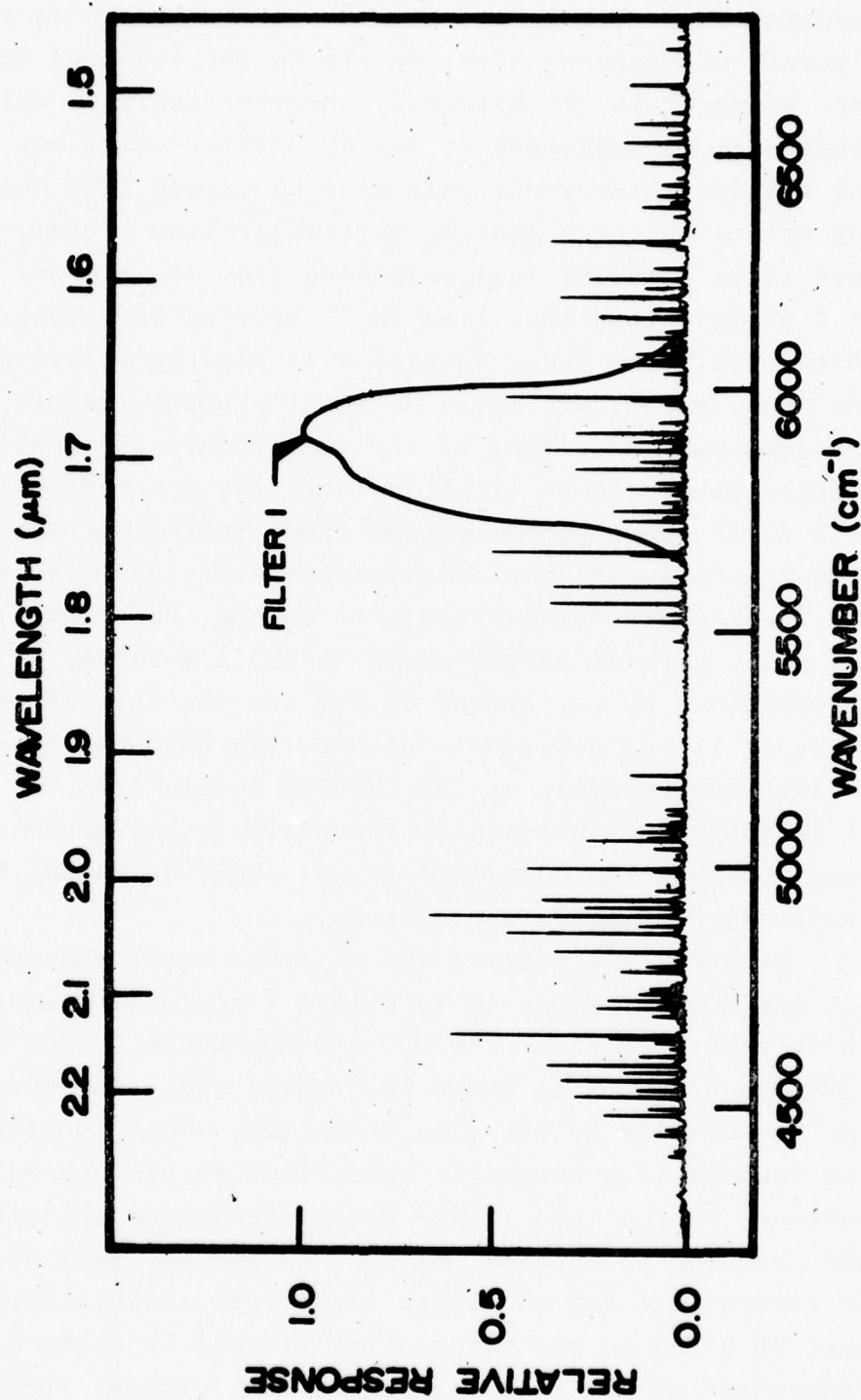


Figure 5. Relative spectral response of the OH radiometer overlaid on an OH $\Delta V = 2$ spectrum.

temperatures. Typically, outside air temperatures at the aircraft measurement altitude are on the order of 220°K . At this temperature the blackbody spectral radiance emission is comparable in magnitude to the OH airglow emissions. However, the atmosphere does not emit as a blackbody (H_2O and CO_2 are not optically thick looking vertically from 11 km), and therefore it is apparent that emissions from the H_2O and CO_2 species will be less than that from OH. Spatial and temporal variations which occur from these species will also be relatively small. Any small variations which do occur probably result from spatial and temporal variations of the temperature and density of the species at altitudes slightly above the aircraft. Therefore, as a first order approximation these variations should correlate with the measured outside air temperature near the aircraft, and it is therefore desirable to monitor this temperature. In any case, auroral enhancements in the $2.8\text{ }\mu\text{m}$ region could not be explained by variations of H_2O and CO_2 thermal emissions. However, if one desired to measure the absolute intensity of the NO $\Delta V=2$ enhancements or the OH $\Delta V=1$ levels from the aircraft, it is important to consider the absorption effects of these species since the OH originates at about 85 km and NO (aurorally produced) originates above 80 km.

Probably the easiest way to avoid being contaminated by H_2O and CO_2 emissions is to select a spectral measurement band which rejects most of the H_2O and CO_2 bands. This was done in the 1976 measurements as shown in Figures 2,3. The absorption problem can be avoided by the same technique. This is illustrated in the Lowtran II atmospheric transmittance plot shown in Figure 6. However, in the 1975 ICECAP measurements the spectral band was not selected to be clear of the H_2O and CO_2 regions as shown in Figures 2,3 and 6. Under these conditions, consideration must be given to the attenuation effects by using a line by line comparison of the absorptions and the spectral features of the emissions being measured. Based on an analysis of the measured data, the emission effects of H_2O and CO_2 in the 1975 and 1976

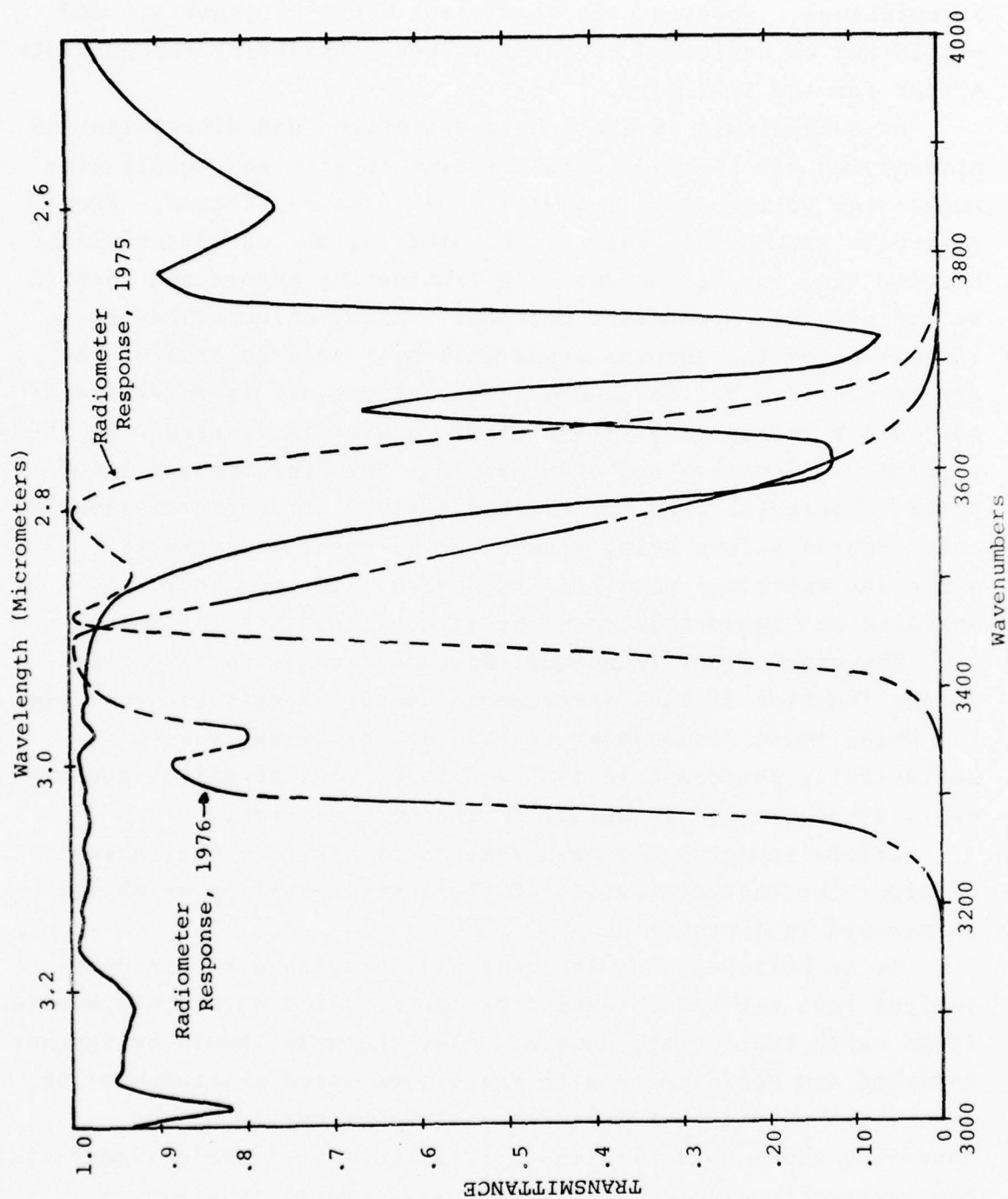


Figure 6. Radiometer instrument responses overlaid on atmospheric transmittance calculated from Lowtran program for 10.5 km.

aircraft data are insignificant in comparison to the OH and NO emissions. However, the absorption might be important and should not be neglected especially when considering the absolute number for the 1975 data.

As a final aid in the source definition and discrimination process, an all sky camera can be used to give an overall wide angle view of the visible aurora as a function of time. From this data and the aircraft flight profile, one can discriminate between time variations due to a fluctuating aurora and spatial variations due to aircraft movement. Also, an uncalibrated indication of the auroral conditions over a large area of the sky is provided by the camera. This allows one to determine if any aurora exists in a region prior to when it is viewed by the aircraft radiometers and photometers. This information is of specific interest when the visible auroral intensity dissipates only seconds before being viewed by the other instruments, since any emissions with long radiative lifetimes would still be enhanced and measurable once the aircraft reaches the scene.

The measurement techniques discussed above as they relate to the function of each instrument used are summarized in Table 1. Using these measurement techniques, experiments were successfully performed in 1975 and 1976. The resulting measurements are discussed in detail in the next section.

Before studying the measurements it might be desirable to consider the characteristics of the instrumentation which are summarized in Appendix A.

It is believed that the data will provide a significant insight into our understanding of the infrared emission processes. It is worth mentioning, however, that the data should be further analyzed and coordinated with the ground-based instrumentation to perform an altitude dependency study by combining the Chatinika radar data with the aircraft data. A table summarizing the expected overlap of the radar measurements is given in Appendix B.

TABLE 1. SUMMARY OF INSTRUMENTATION AND MEASUREMENTS FOR INFRARED EXPERIMENT

INSTRUMENT	EXPECTED EMISSIONS	INSTRUMENTS PRIME FUNCTION	CONSIDERATIONS & COMMENTS
RADIOMETER (2.8 μ m REGION)	NO ($\Delta V=2$), OH ($\Delta V=1$), & POSSIBLE H ₂ O & CO ₂ .	MEASURE AURORALLY ENHANCED NO ($\Delta V=2$).	NEED TO DISCRIMINATE AGAINST OH, H ₂ O, & CO ₂ EMISSIONS.
RADIOMETER (1.7 μ m REGION)	OH ($\Delta V=2$) 5, 3	REMOVE OH EMISSIONS FROM 2.8 μ m DATA.	NEED TO CONSIDER H ₂ O ABSORPTION.
PHOTOMETER (3914 Å)	N ₂ ⁺ (FIRST NEGATIVE BAND)	PROVIDE AN ABSOLUTE REFERENCE OF IONIZATION-PROMPT FLORESCENCE FOR SPATIAL AND TIME CORRELATIONS WITH THE 2.8 μ m DATA.	ASSUMES OH ($\Delta V=2$ AND OH ($\Delta V=1$) EMISSIONS HAVE SAME BEHAVIOR.
ALL SKY CAMERA	VISIBLE AURORA	TIME HISTORY MONITOR OF LARGE PORTION OF THE SKY. PROVIDES TIME AND SPATIAL MONITOR OF AURORA.	PROVIDES ABSOLUTE ENERGY INPUT MEASUREMENTS OF THE AURORA BEING VIEWED.
NAVIGATION AIDS		PROVIDE ALTITUDE, POSITION AND OUTSIDE AIR TEMPERATURE OF MEASUREMENT PLATFORM.	PROVIDES INFORMATION ON AURORA PRIOR TO AIRCRAFT ARRIVAL INTO A REGION, WHICH IS USEFUL IF AN EMISSION WITH A LONG RADIATIVE LIFETIME EXISTS. ALTITUDE IS IMPORTANT WHEN MODELING THE ATMOSPHERIC ABSORPTION. POSITION IS IMPORTANT FOR COORDINATION WITH GROUND DATA. OUTSIDE AIR TEMPERATURE SHOULD BE SOMEWHAT CORRELATED WITH H ₂ O & CO ₂ THERMAL EMISSIONS

MEASURED INFRARED ENHANCEMENTS

Significant enhancements of the atmospheric emissions in the 2.8 μm region were observed from the AFGL NKC-135A aircraft during the 1975 and 1976 ICECAP measurement series. These enhancements are believed to be increases in the nitric oxide emissions created by a relatively prompt process in an aurorally excited atmosphere, *Stair et al.* [1975], *Hurd et al.* [1977].

A sample or overview of the measured data will be presented and discussed in detail in this section. Noise levels, response times, and fields of view are tabulated in Table 2 for the various measurement days. A significant amount of additional data which is similar to the data being discussed is cataloged in Appendix C.

The first extensive 2.8 μm enhancements that were observed by the aircraft during an aurorally excited atmosphere occurred on March 10, 1975. Figure 7 shows this data for the entire period of the flight. In contrast to this aurorally excited data is the data presented in Figure 8, measured March 15, 1975 during relatively quiet auroral conditions which shows the 2.83 μm emissions co-varying with the uncontaminated 1.7 μm OH emissions. From top to bottom the figures present the aircraft latitude, the aircraft longitude, the air temperature at the aircraft altitude, the aircraft altitude, the 3914A ionization-prompt N_2^+ emissions, the 2.83 μm emissions and the 1.7 μm OH emissions.

The correlation between the 2.83 μm emissions and the 1.7 μm OH emissions under non-auroral conditions shown in Figure 8 is further illustrated in Figure 9. The ratio of the two emissions remain almost constant for large variations in time, location and emission intensity. This indicates that the 2.8 μm emissions primarily result from OH processes during non-auroral conditions, and apparently H_2O emissions at 2.83 μm are insignificant in the selected measurement band. If H_2O emissions were significant, the ratio of the 2.83 μm emissions and the water free 1.7 μm OH emissions would not remain constant for different OH intensity

TABLE 2. DATA CHARACTERISTICS AND MEASUREMENT CONDITIONS

MEASUREMENT DATE	FIGURE NUMBERS	NOISE EQUIVALENT RADIANCE (KILO RAYLEIGHS) RMS				DATA FILTERING [†]	INSTRUMENTATION F O V [*]
		3914A	2.83 μm	2.94 μm	1.7 μm		
10 MAR. 1975	7, 10, 11, 12, 13	.007 ^{**}	3.9	NA	1	3 SEC. - 3 POLE LOW PASS	10° CIRCULAR
15 MAR. 1975	8 & 9	.007 ^{**}	2.75	NA	.71	6 SEC. - 3 POLE LOW PASS	10° CIRCULAR
26 MAR. 1976	17, 18, 19, 20	.007 ^{**}	NA	6.0	1	3 SEC. - 3 POLE LOW PASS	10° CIRCULAR
7 MAR. 1976	22, 23, 24, 25	.007 ^{**}	NA	6.0	3	3 SEC. - 3 POLE LOW PASS	10° CIRCULAR

* ALL THREE INSTRUMENTS ARE CO-ALIGNED WITH IDENTICAL FIELDS OF VIEW.

** NOISE LEVEL IS LIMITED BY THE DARK CURRENT OF THE PHOTOMULTIPLIER TUBE.

† NOISE EQUIVALENT BANDWIDTH IS EQUAL TO $1/(4 \times \text{No. poles} \times \text{No. sec.})$

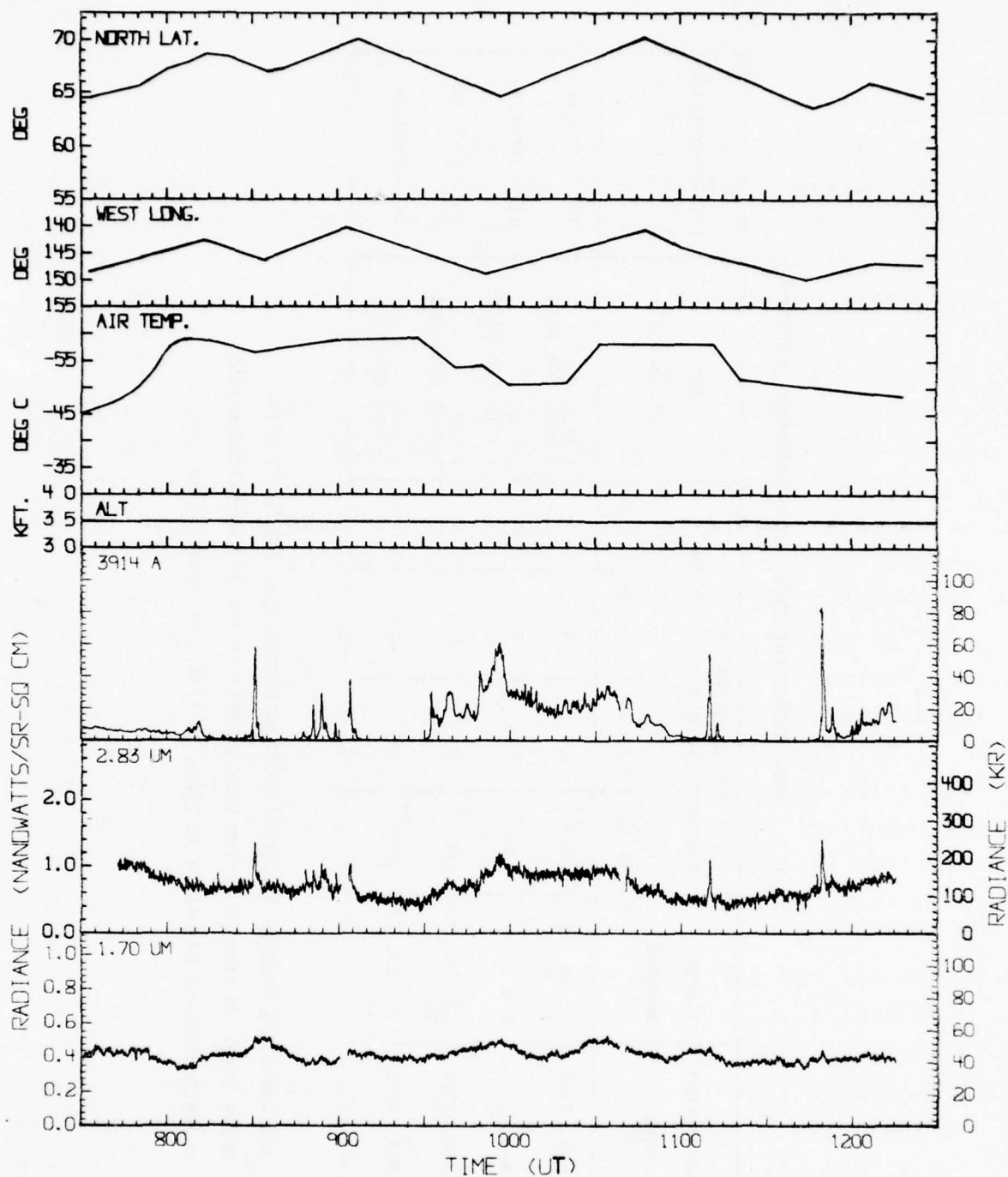


Figure 7. Measurements from aircraft-borne instrumentation for March 10, 1975, showing significant 2.83 μm enhancements correlated with various auroral formations.

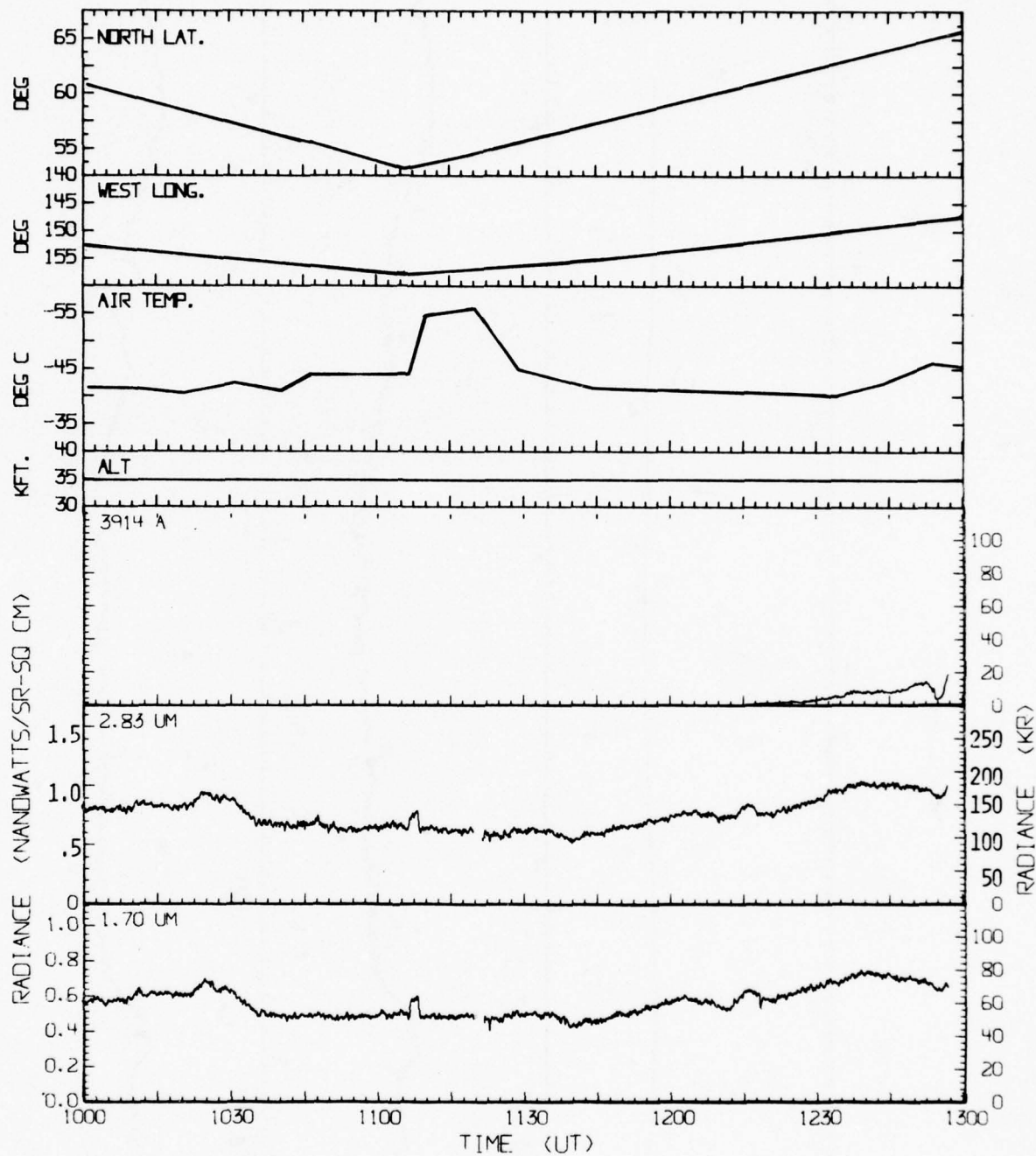


Figure 8. Measurements made from aircraft borne instrumentation on March 15, 1975 showing correlation of OH $\lambda_v = 2$ during a period of minimal auroral activity.

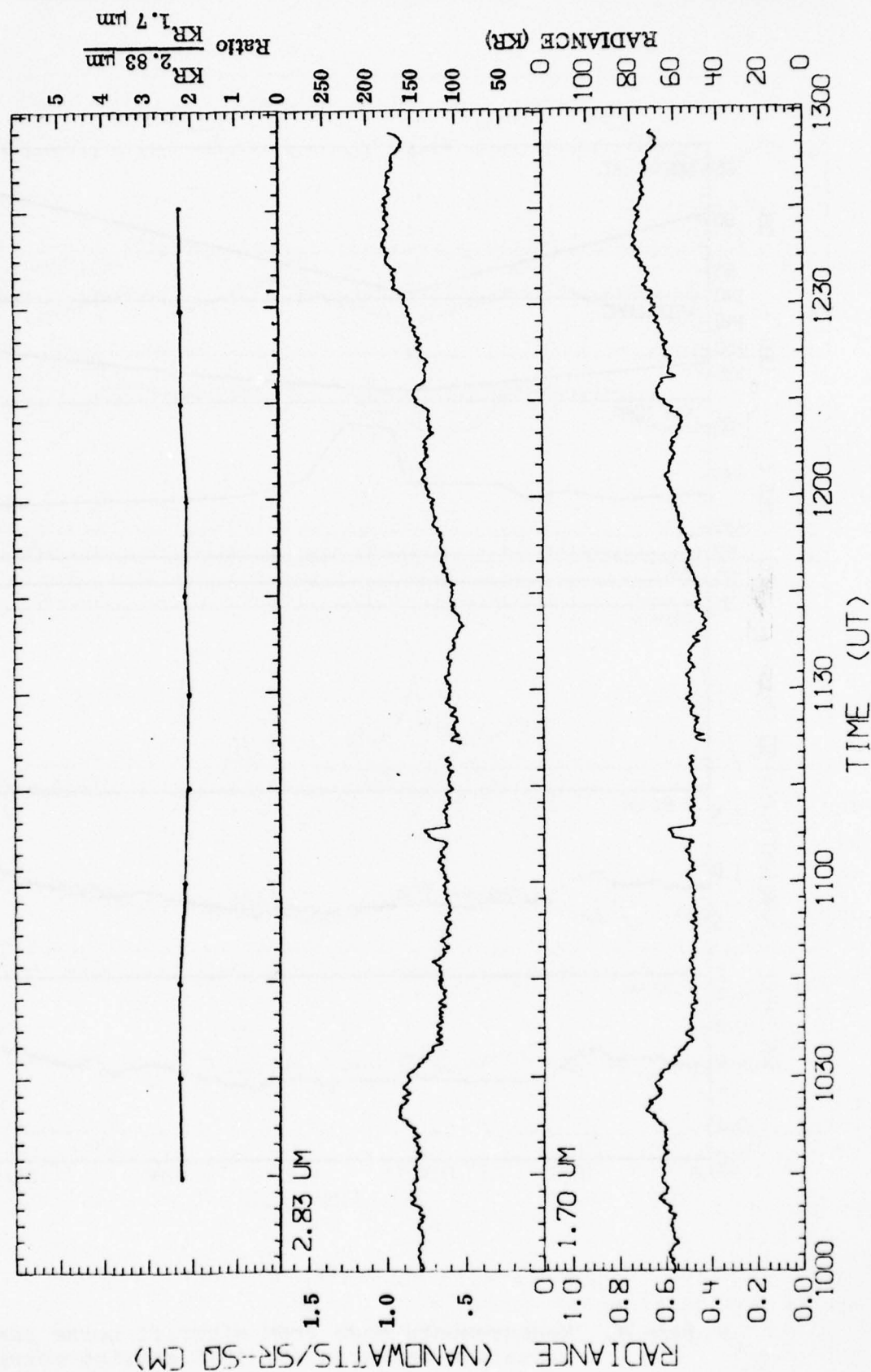


Figure 9. Measured correlation between the 2.83 μm data and the 1.7 μm (OH) data measured March 15, 1975 during a period of minimal auroral activity.

levels. This would also indicate that the H_2O emissions were not significant in the 1976 measurements at $2.94\ \mu\text{m}$, since the selected spectral measurement band was even less contaminated by H_2O emission lines.

Under auroral conditions the ratio of the $2.83\ \mu\text{m}$ and $1.7\ \mu\text{m}$ emissions do not remain constant, and it is apparent from Figure 7 that $2.83\ \mu\text{m}$ enhancements occur, and they are directly related to the aurora as monitored by the 3914A photometer emissions. This is even more evident in Figures 10 through 14 which are time expanded plots of the various enhancement periods displayed in Figure 7. Also, it is important to note that variations of the $1.7\ \mu\text{m}$ emissions, which are primarily generated by the 5,3 band of the OH overtone, are minimal during the time periods when the $2.83\ \mu\text{m}$ enhancements occur, and there does not appear to be any direct correlation of these OH emissions with the aurora. Since one would expect the $2.8\ \mu\text{m}$ OH fundamental emissions to behave similar to $1.7\ \mu\text{m}$ OH overtone emissions as shown in Figures 8 and 9, the measured $2.83\ \mu\text{m}$ enhancements cannot be explained by variations in the OH fundamental emissions.

The expanded plots presented in Figures 10 through 14 tend to indicate that the $2.83\ \mu\text{m}$ enhancements are created by a relatively prompt process, since the data correlate so well with the ionization-prompt 3914A emissions. This direct correlation exists for all types of auroral forms and during periods of time when the aurora is dynamic and varying rapidly in intensity. The all-sky camera pictures shown in Figure 15 and Figure 16 document these various auroral forms during the enhancements. They also tend to show the dynamic variations which occurred during the measurements. These direct correlations between the $2.83\ \mu\text{m}$ enhancements with the enhancements of the prompt 3914A emissions tend to rule out the possibility that the measured increases result from long radiative life-time emissions. This presents a strong argument that the measured enhancements are generated from a NO photochemical emission process, since the characteristics of all other feasible sources do not fit the measured data.

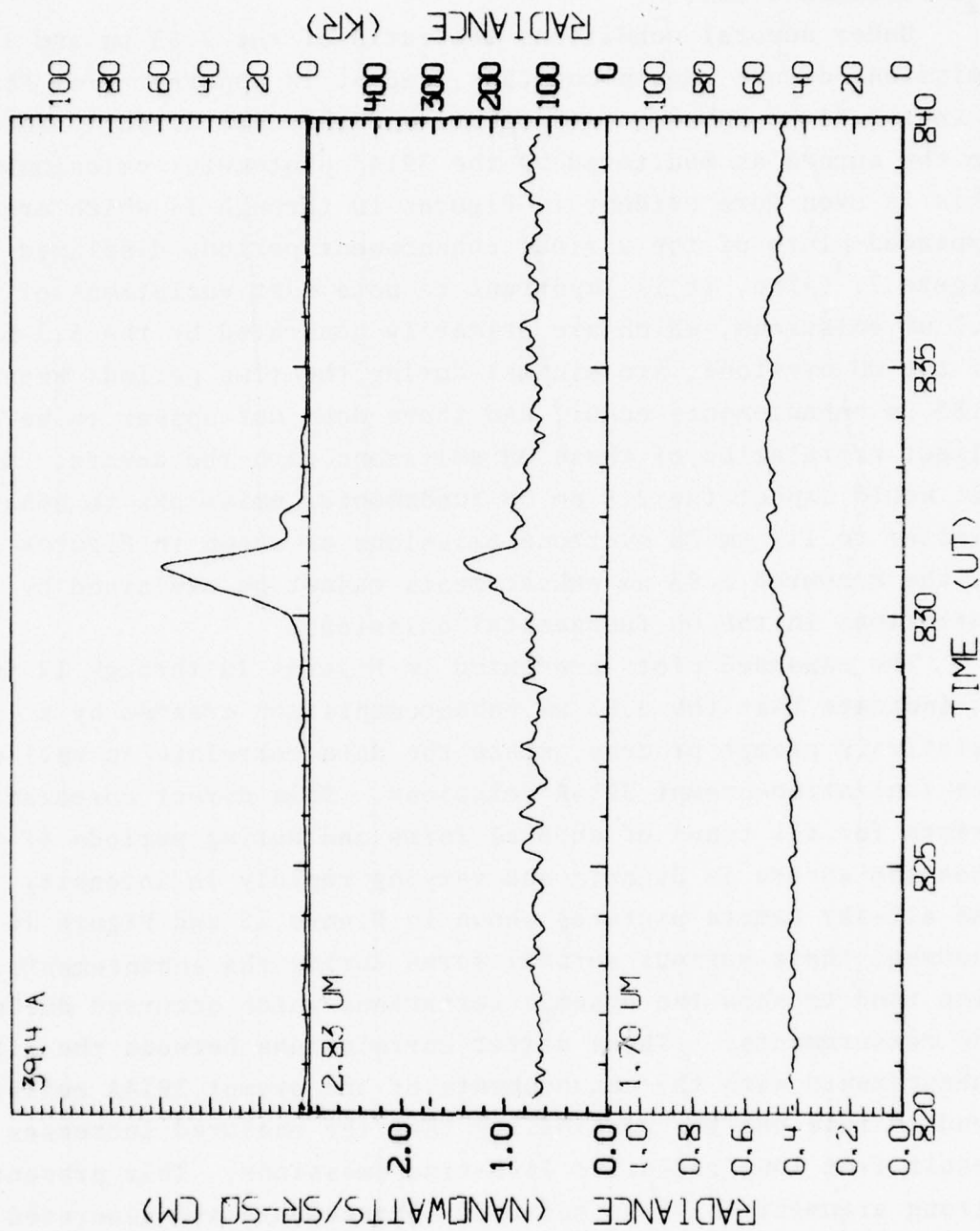


Figure 10. Measured data for March 10, 1975 plotted with an expanded time scale to illustrate the time and spatial correlation between the 2.83 μm emissions and the 3914Å emissions while viewing an auroral arc.

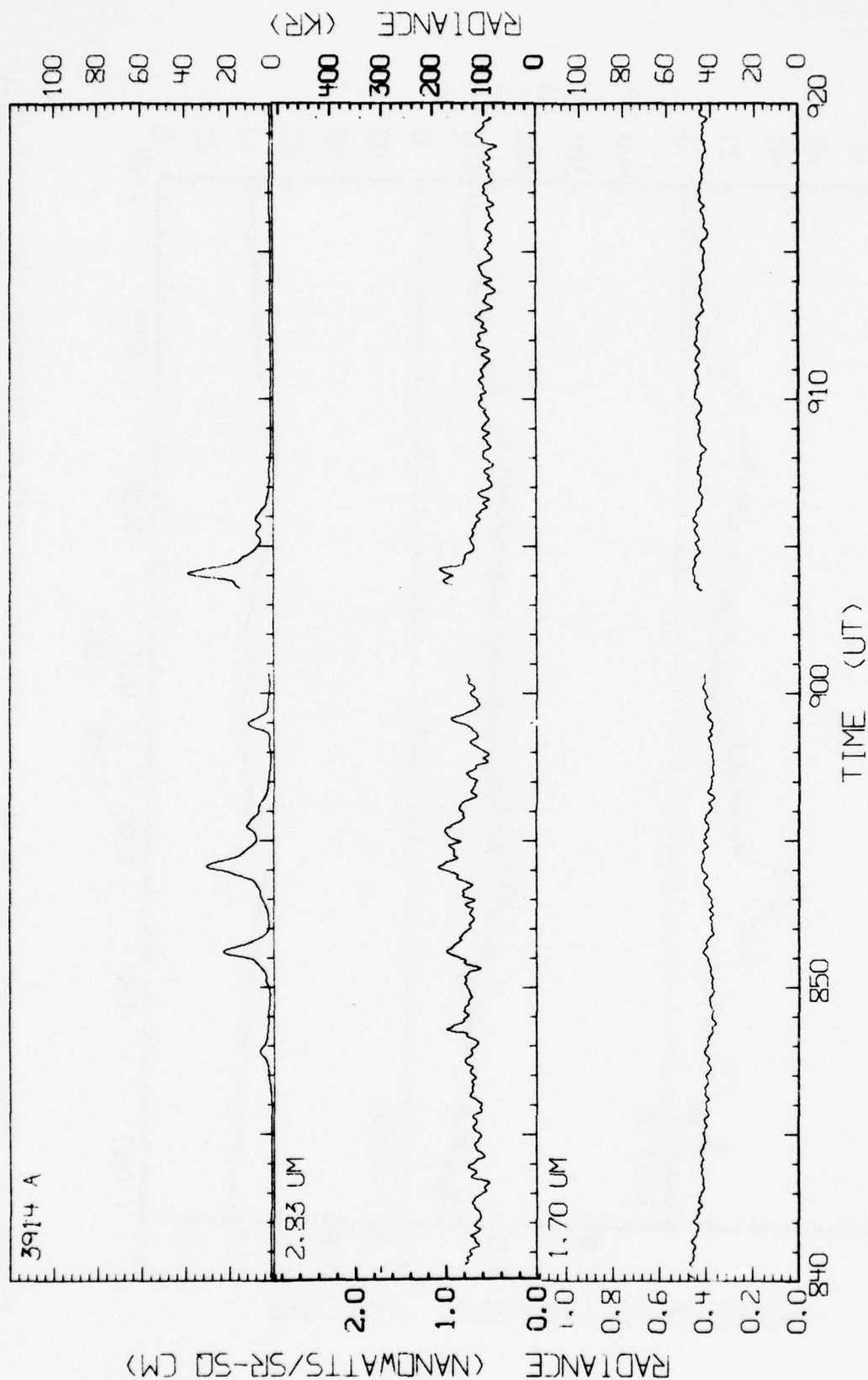


Figure 11. Measured data for March 10, 1975 plotted with an expanded time scale to show small enhancements of the 2.83 μm emissions which are correlated with small enhancements of the 3914A fluorescence.

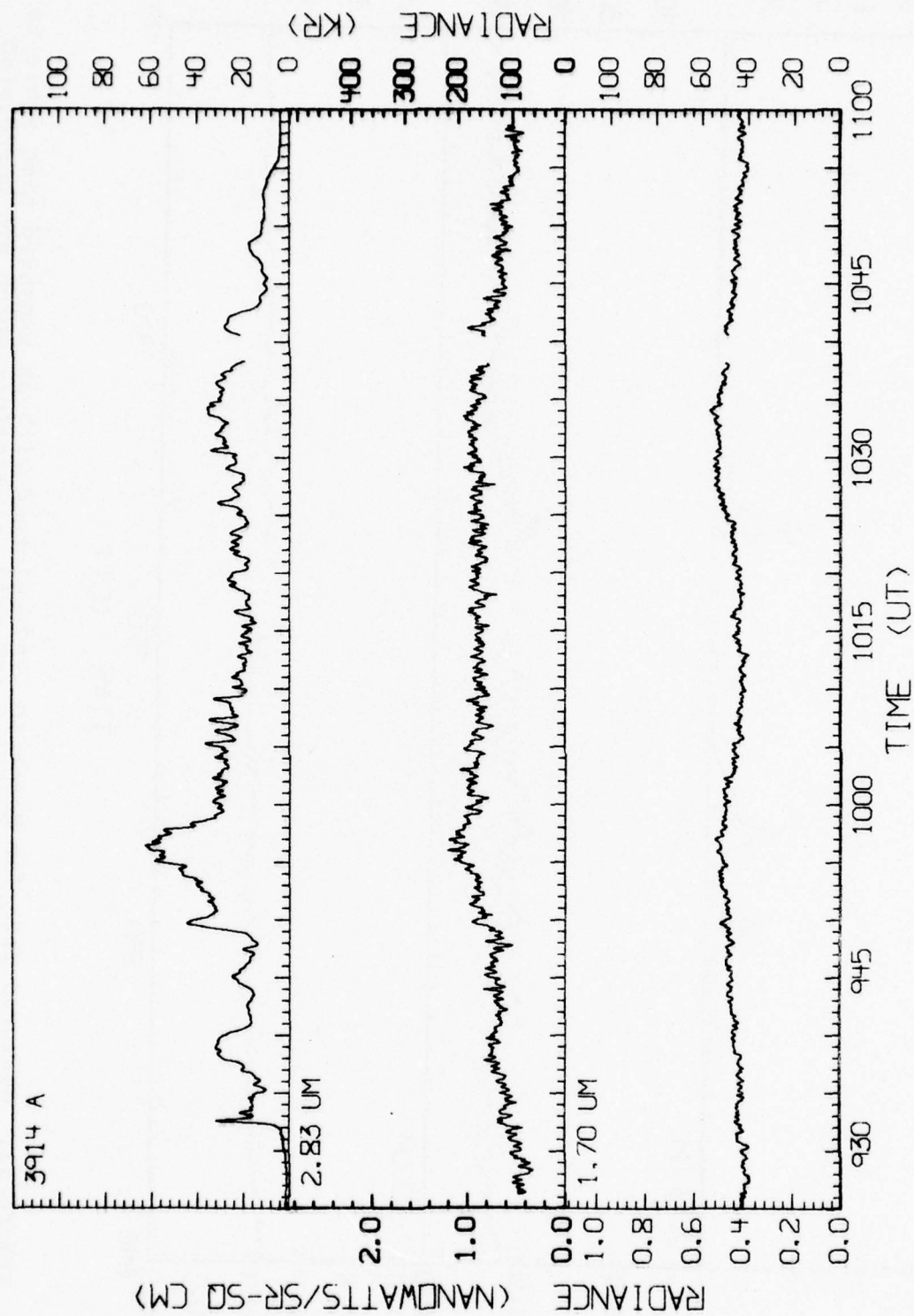


Figure 12. Measured data for March 10, 1975 plotted with an expanded time scale to show detailed structure of 2.83 μm enhancement which are correlated with a 3914A enhancement caused by a broad, diffused aurora.

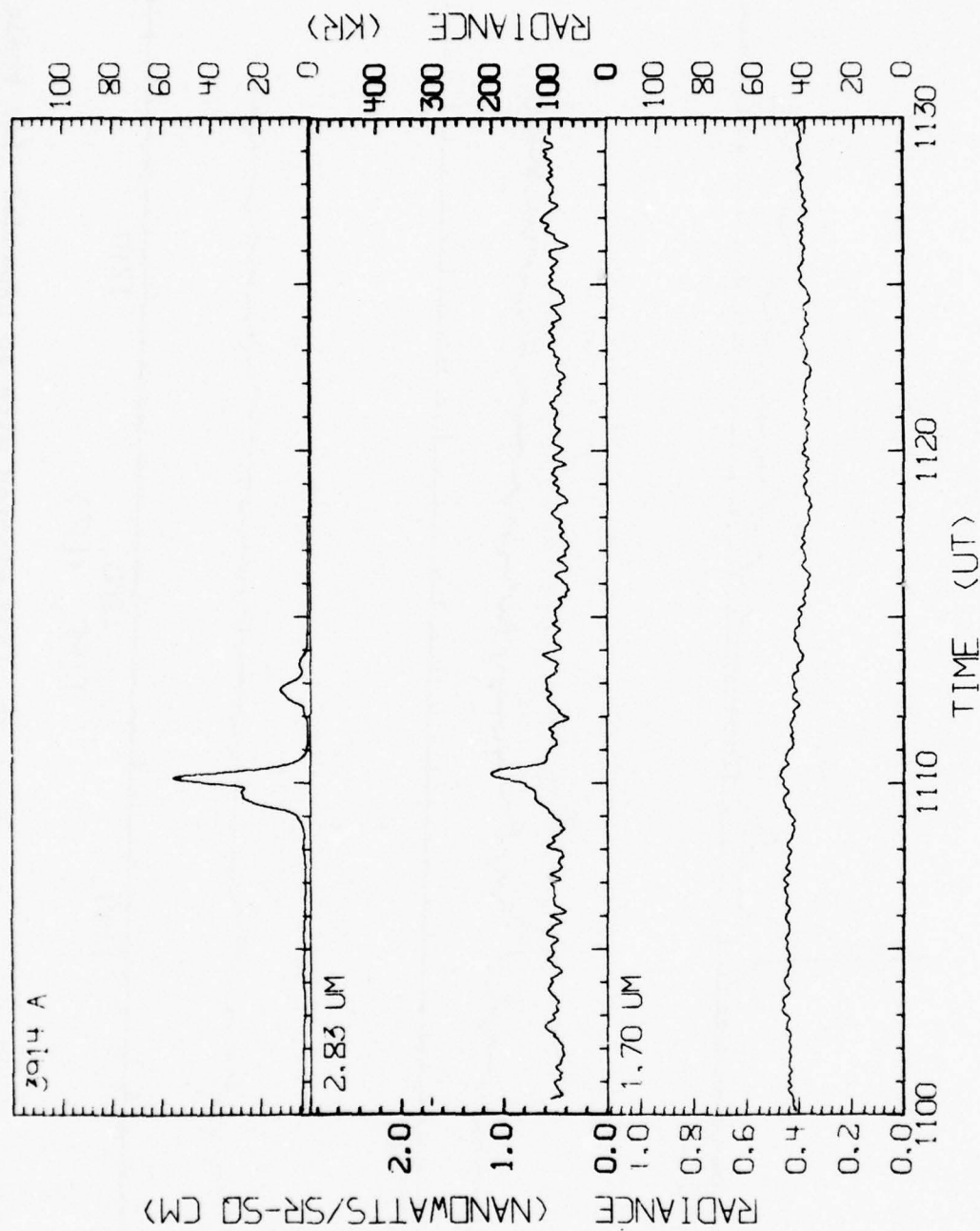


Figure 13. Measured data for March 10, 1975 plotted with an expanded time scale to show time and spatial correlation between 2.83 μ m emissions and 3914A emissions while viewing a narrow auroral arc.

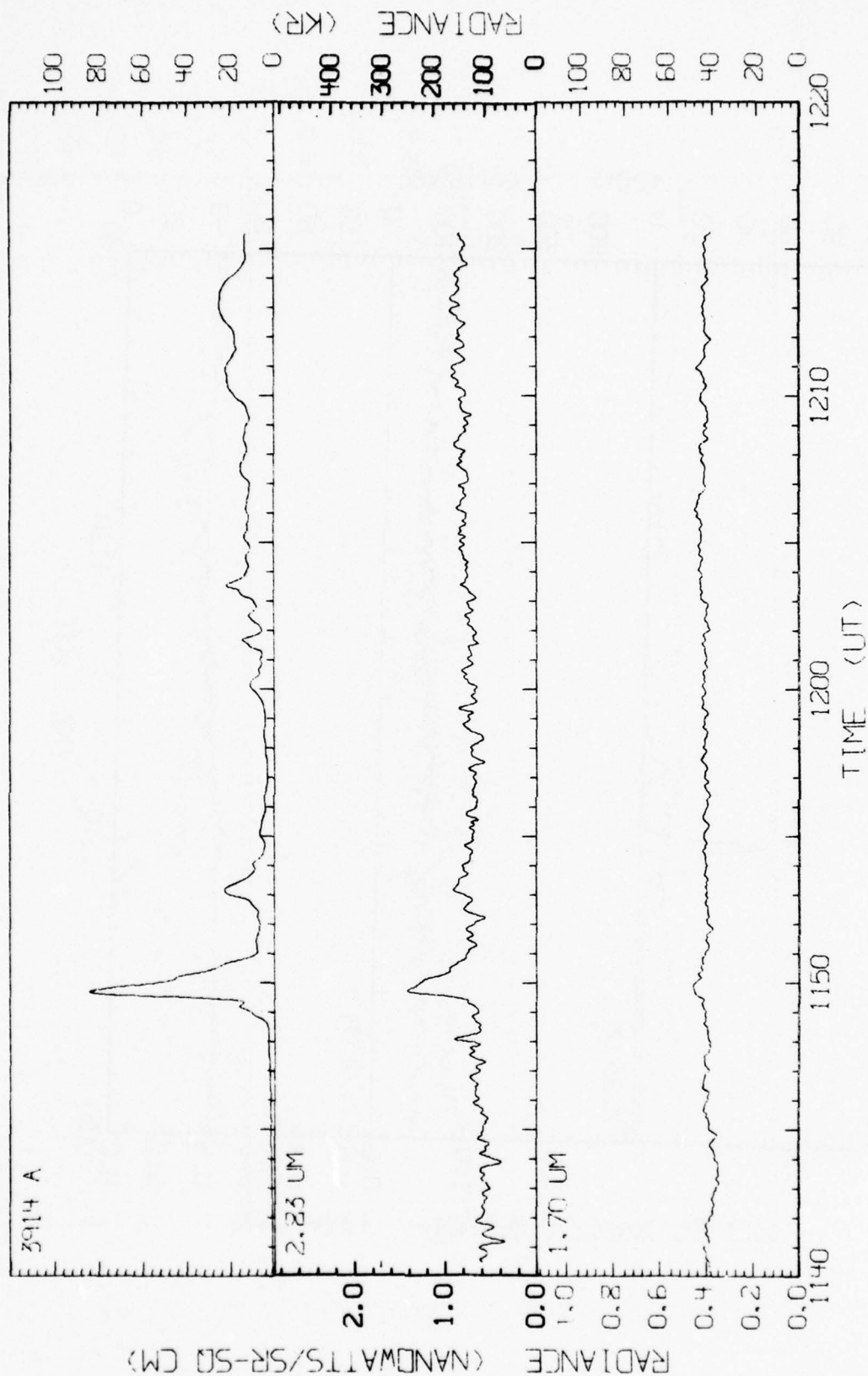


Figure 14. Measured data for March 10, 1975 plotted with an expanded time scale to show time and spatial correlation between 2.83 μm emissions and 3914A emissions while viewing an auroral patch.

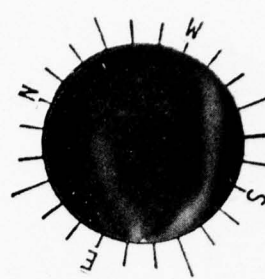
→ Forward Movement of Aircraft →



0827:00 UT



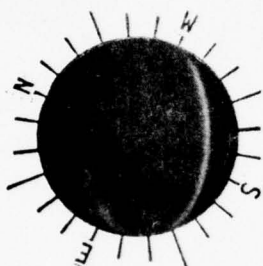
0831:00 UT



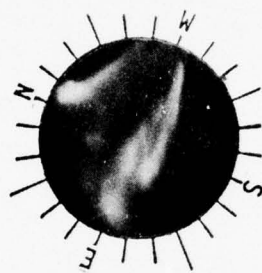
0837:00 UT

A. All sky camera pictures illustrating the auroral conditions during the measurement period shown in Figure 10. The measured enhancement was caused by the auroral arc at 0831 UT.

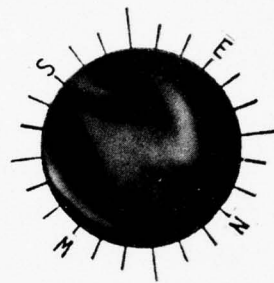
→ Forward Movement of Aircraft →



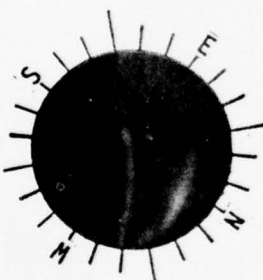
0842:14 UT



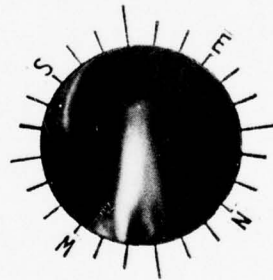
0851:06 UT



0854:09 UT



0858:44 UT



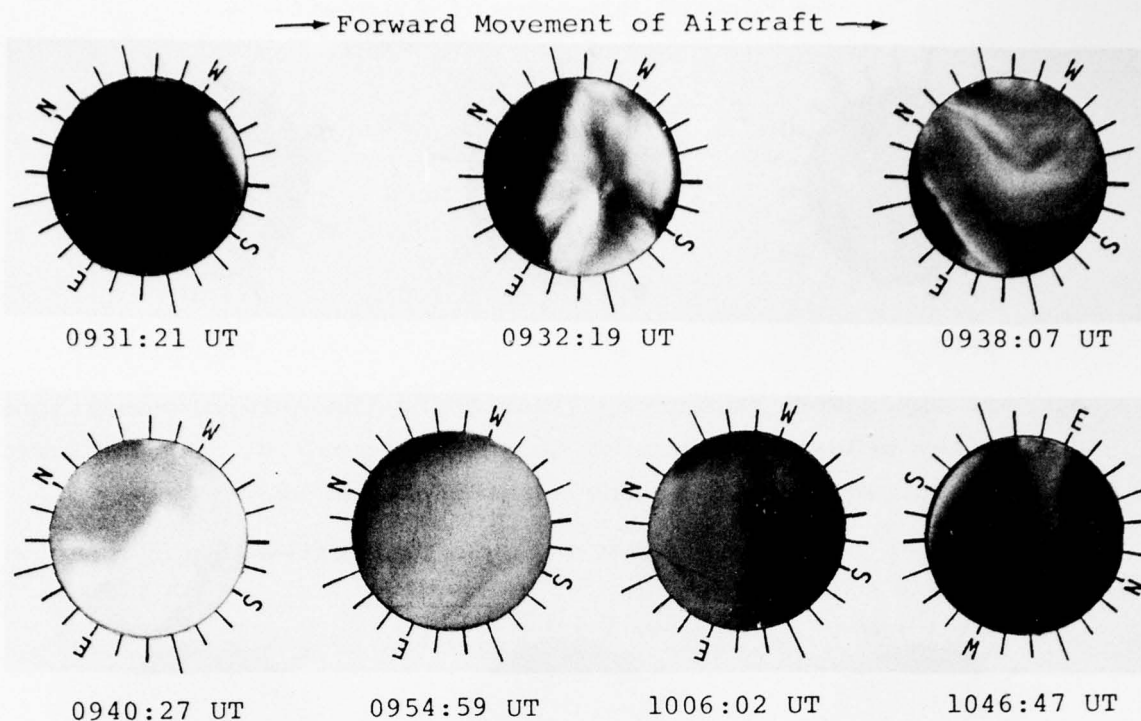
0903:59 UT



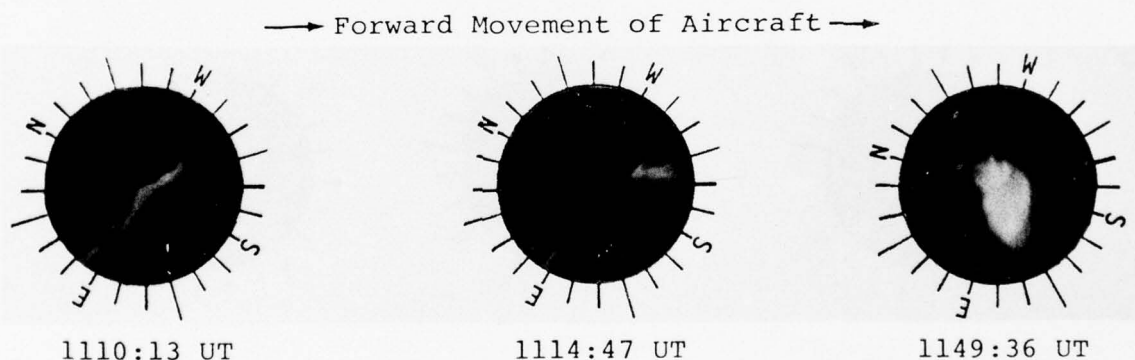
0906:10 UT

B. All sky camera pictures illustrating the auroral conditions during the measurement period shown in Figure 11. The enhancements were caused by broad diffuse aurorae.

Figure 15. All sky camera pictures taken March 10, 1975 by Photometrics Incorporated from the AFGL NKC-135 aircraft with a 160° FOV camera.



A. All sky camera pictures illustrating the various auroral forms and varying conditions for the measurement period shown in Figure 12.



B. All sky camera pictures illustrating the auroral enhancements and conditions for the measurement periods shown in Figure 13 and 14.

Figure 16. Continuation of all sky camera pictures taken March 10, 1975 with a 160°FOV camera viewing vertically from the AFGL NKC-135 aircraft.

Many additional flights verified that $2.8\text{ }\mu\text{m}$ enhancements are measurable above the OH background anytime the 3914A emissions are in excess of 20 KR. Some of the best examples of these measurements are given in Figures 17 through 25, which present the data measured in the $2.94\text{ }\mu\text{m}$ spectral band for March 26 and March 7 of 1976. As in the data of March 10, 1975, the enhancements appear to be directly correlated with the 3914A fluorescence, but not with the $1.7\text{ }\mu\text{m}$ OH emissions.

These extensive absolutely calibrated measurements should provide an excellent data base for analyses of infrared enhancements in the 2.75 to $3.04\text{ }\mu\text{m}$ region under auroral conditions. A brief analysis of some of the data is presented in the next section. The analysis specifically addresses the problem of determining the photo-energy efficiencies for several of the measured enhancements.

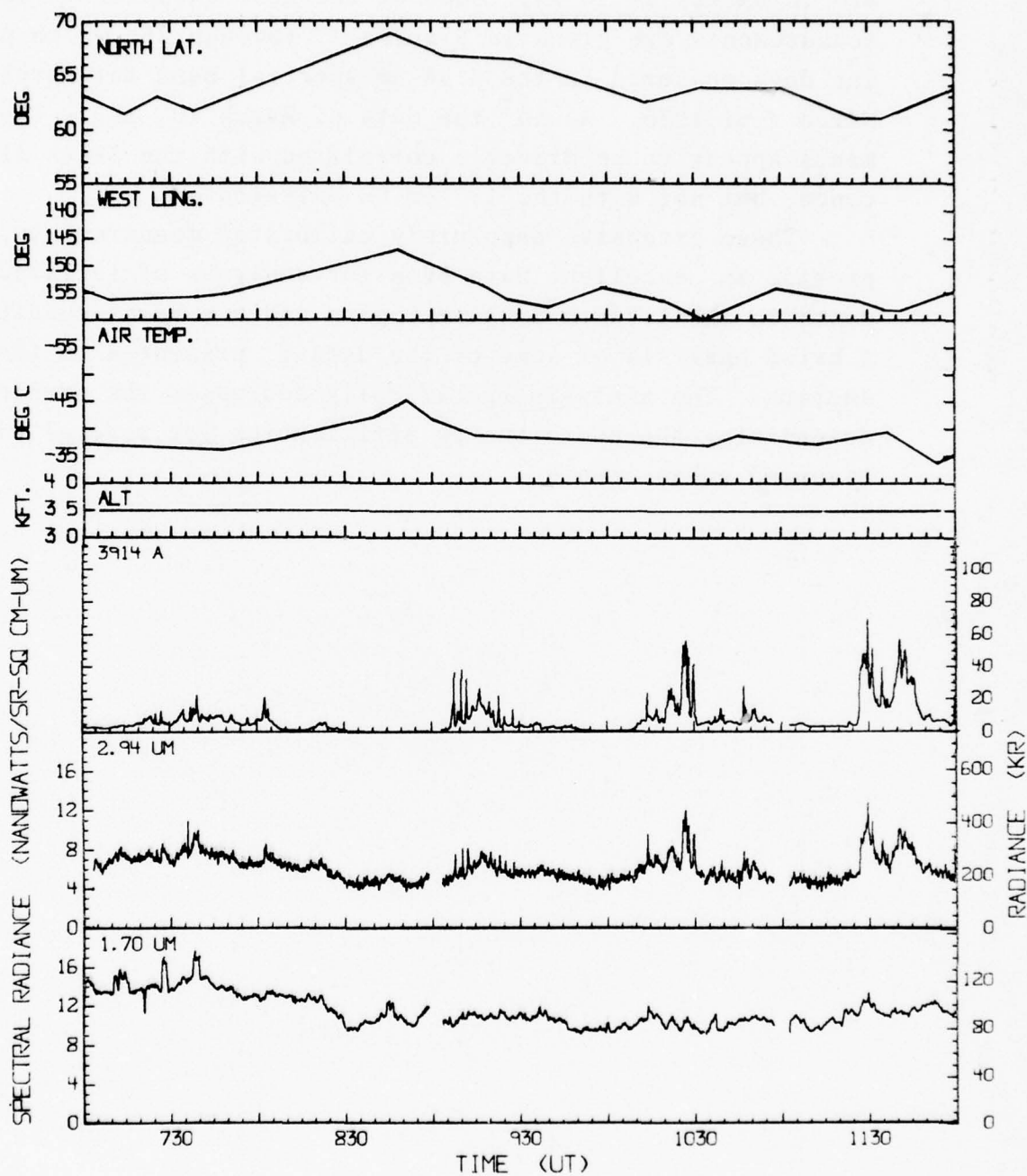


Figure 17. Measurements from aircraft-borne instrumentation for March 26, 1976, showing significant 2.94 μm enhancements correlated with the aurora.

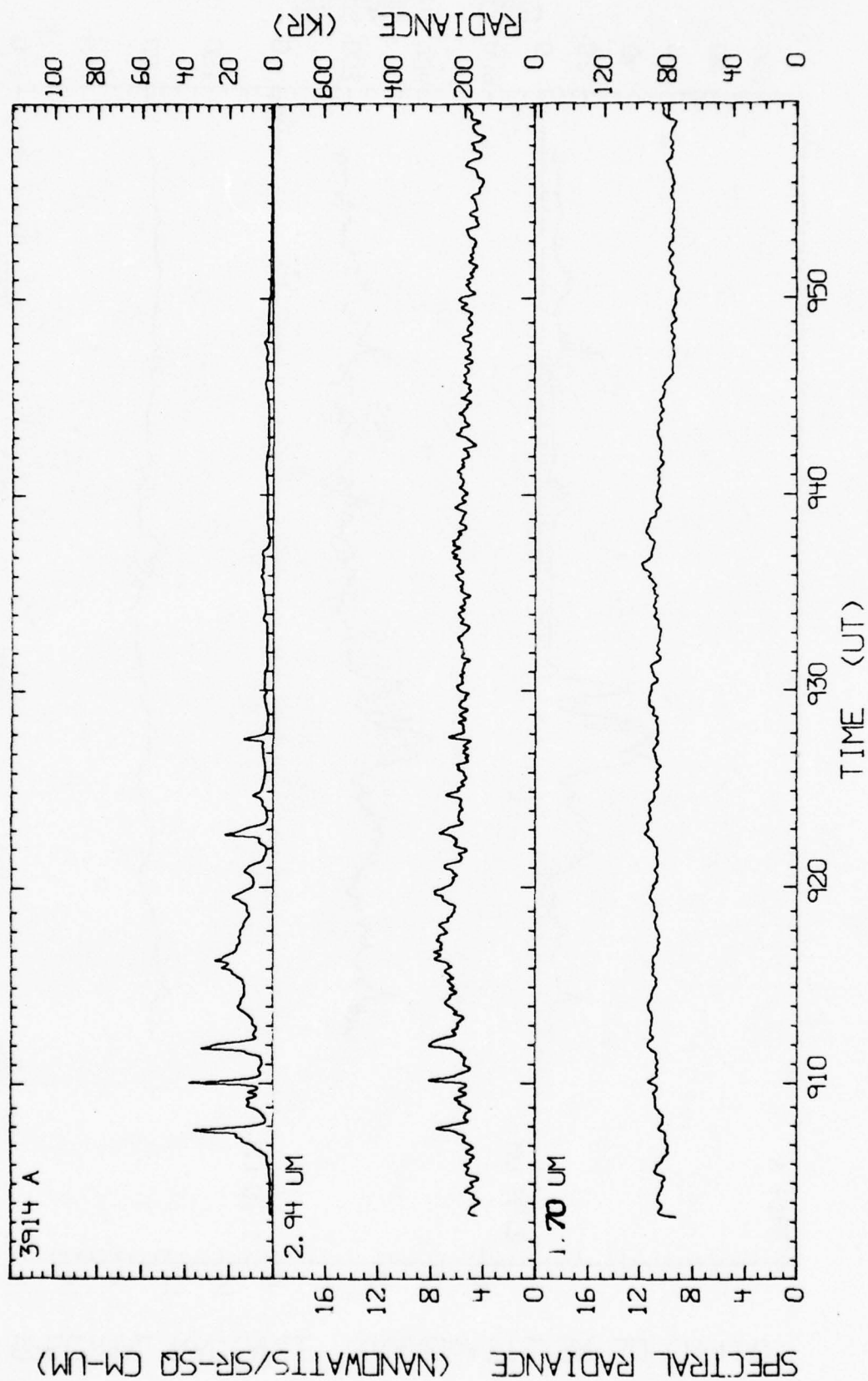


Figure 18. Measured data for March 26, 1976 plotted with an expanded time scale to show the detailed correlation between the 2.94 μm emissions and the 3914 Å emissions during rapidly varying auroral conditions.

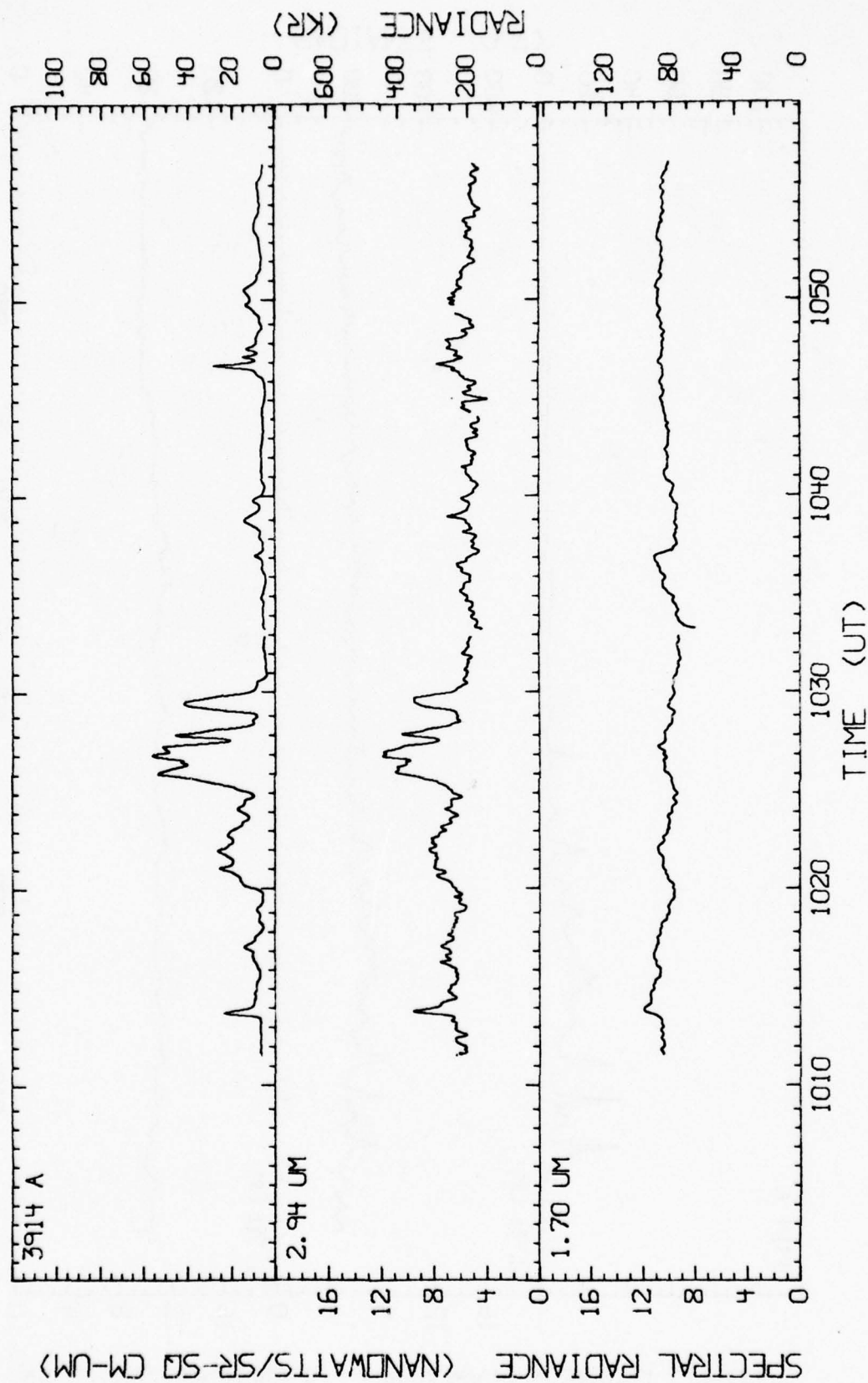


Figure 19. Measured data for March 26, 1976 showing the detailed structure and correlation of the 2.94 μ m and 3914 Å emissions while viewing an auroral arc.

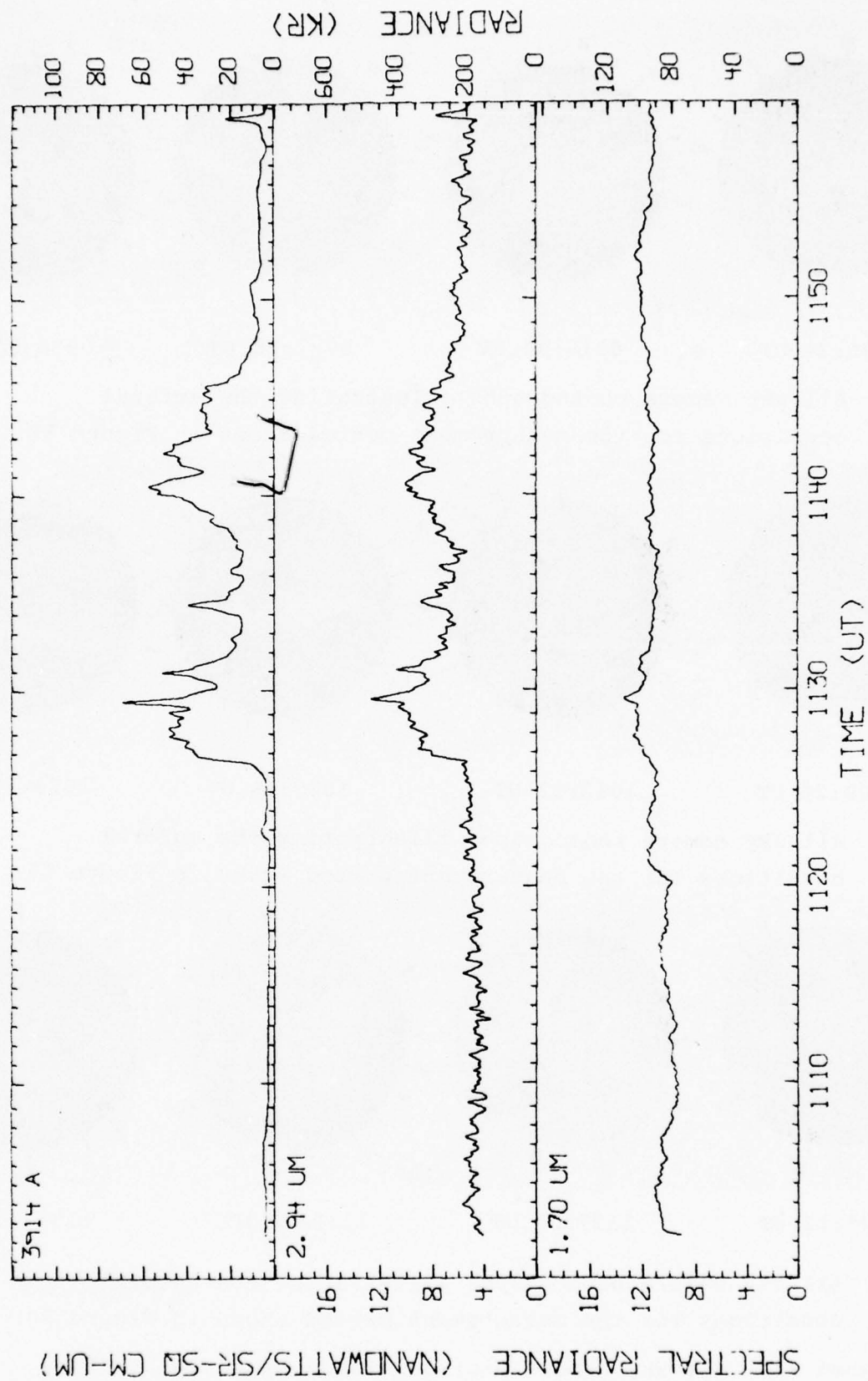


Figure 20. Measured data for March 26, 1976 showing the detailed correlation between the 2.94 μm emissions and the 3914 A emissions during an auroral breakup.

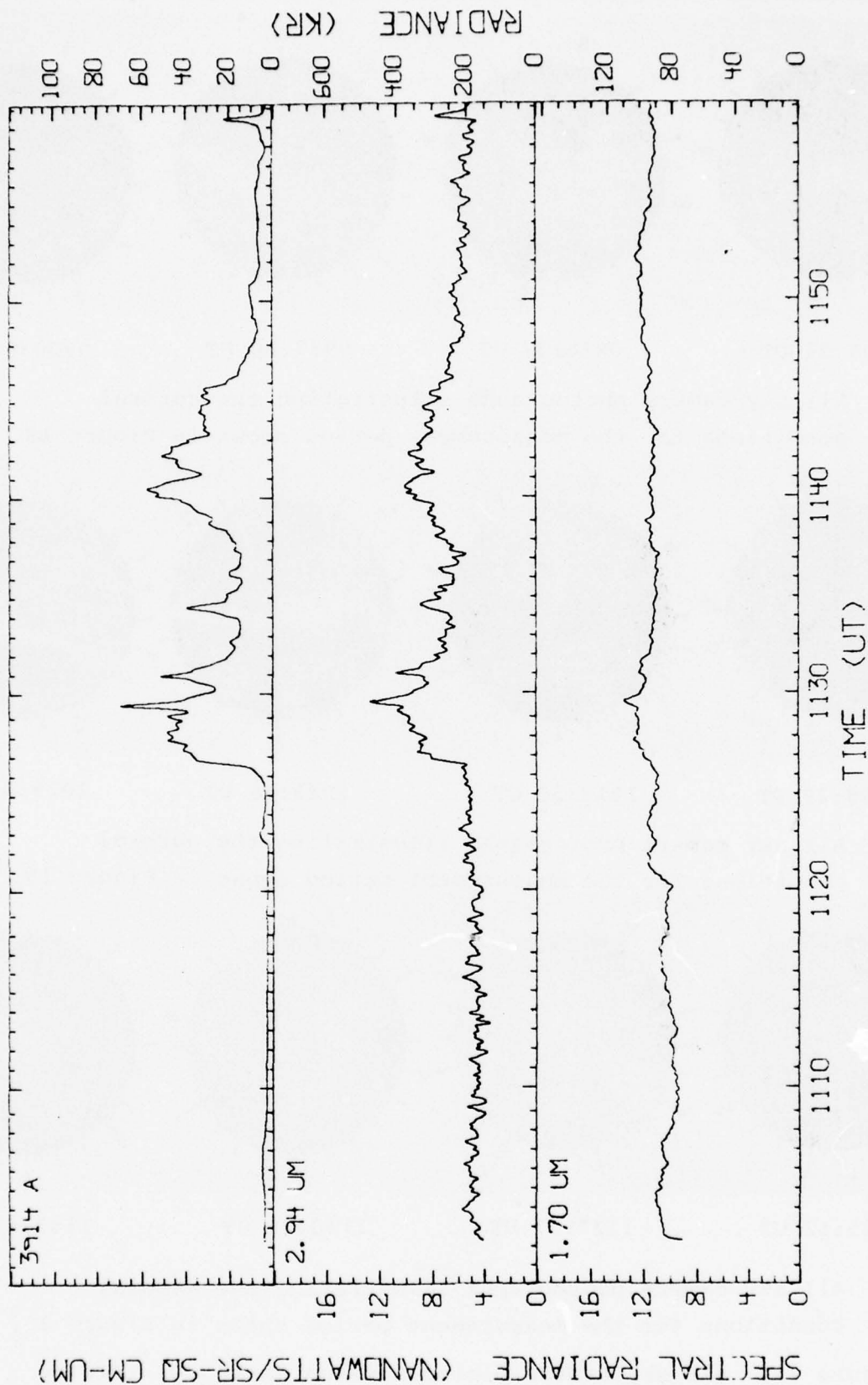
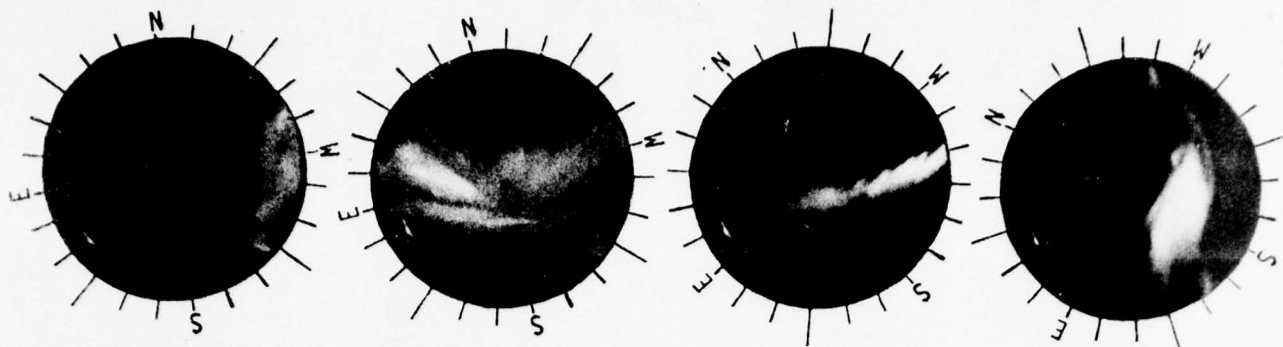


Figure 20. Measured data for March 26, 1976 showing the detailed correlation between the 2.94 μm emissions and the 3914 Å emissions during an auroral breakup.



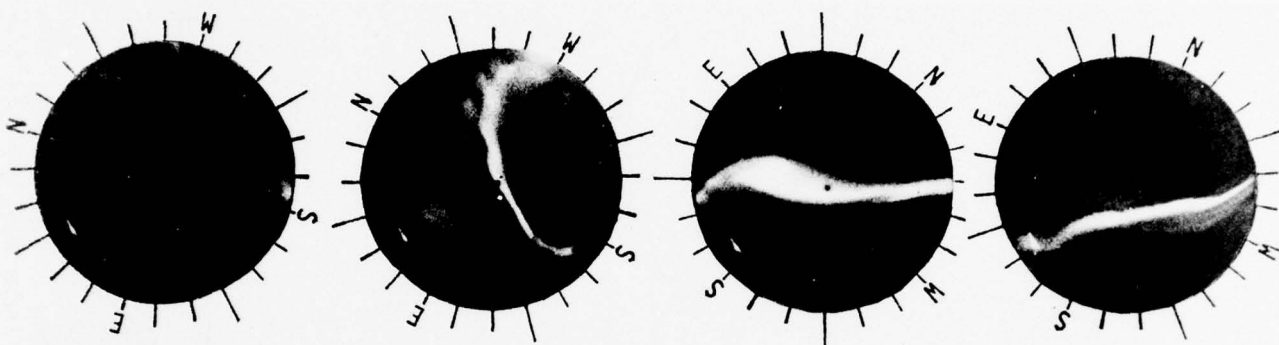
0905:24 UT

0916:37 UT

0927:28 UT

0930:00 UT

A. All sky camera photographs illustrating the auroral conditions for the measurement period shown in Figure 18.



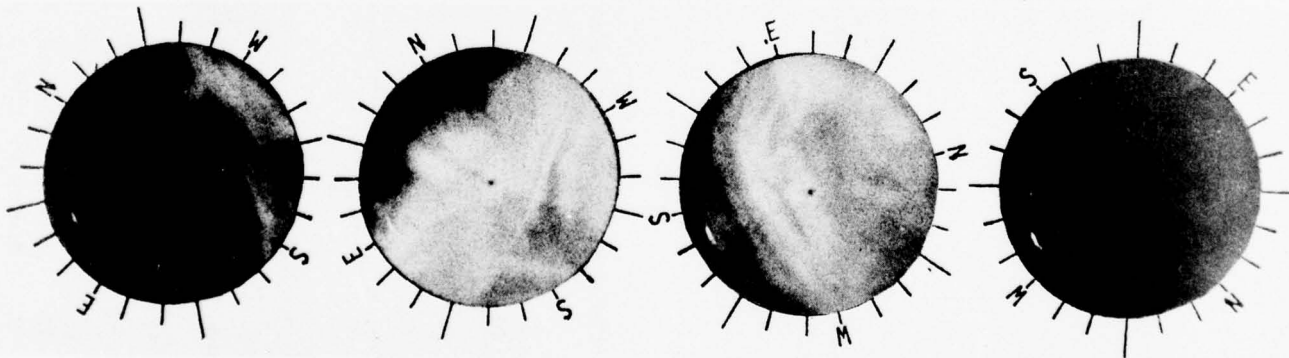
1008:29 UT

1013:32 UT

1025:56 UT

1029:53 UT

B. All sky camera photographs illustrating the auroral conditions for the measurement period shown in Figure 19.



1125:12 UT

1127:57 UT

1140:24 UT

1153:37 UT

C. All sky camera photographs illustrating the auroral conditions for the measurement period shown in Figure 20.

Figure 21. All sky camera pictures taken March 26, 1976 by Photometrics Incorporated from the KC-135 aircraft with a 160° FOV camera viewing vertically.

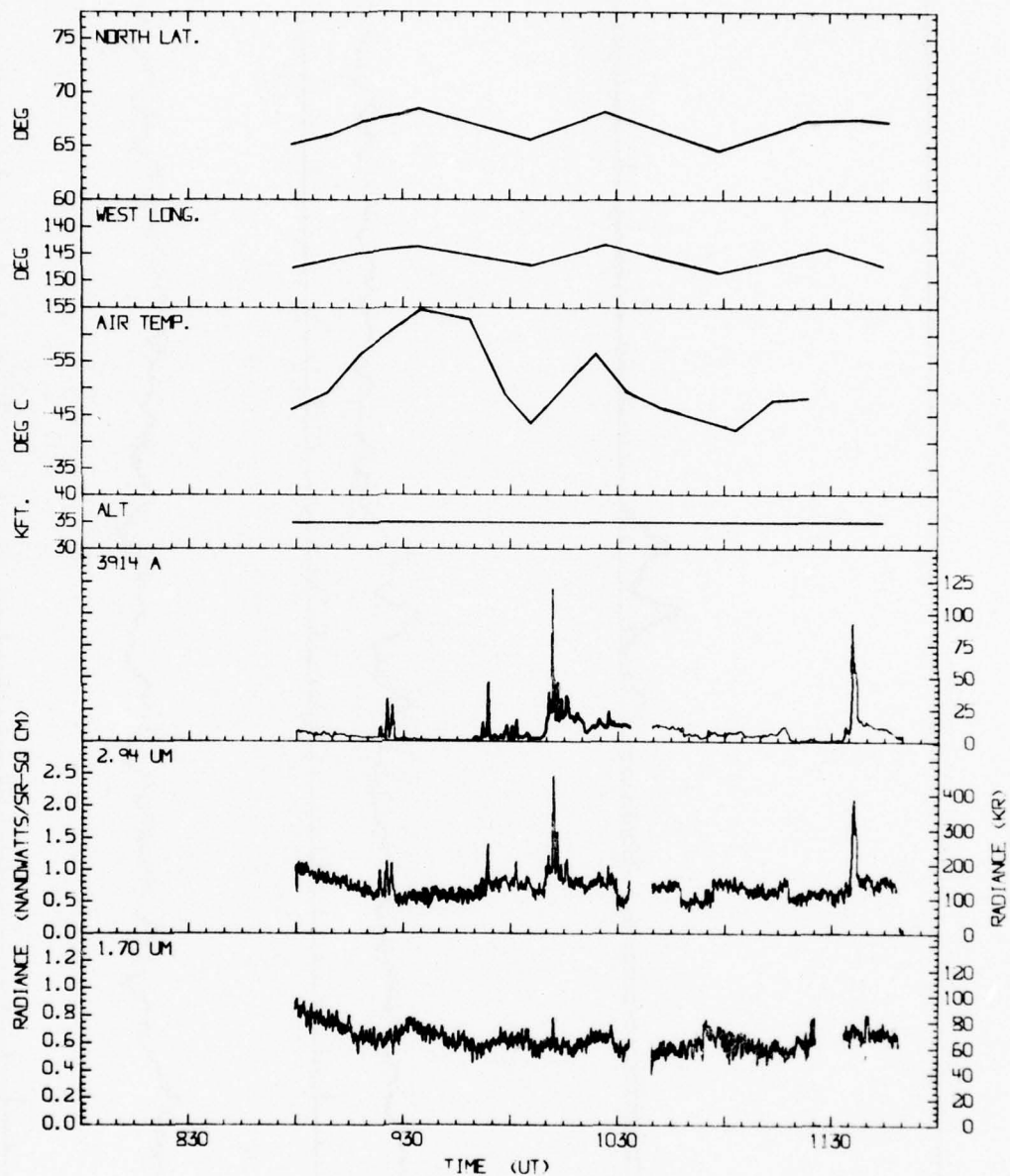


Figure 22. Measurements made with aircraft-borne instrumentation on March 7, 1976 showing significant infrared enhancements which are correlated with aurora.

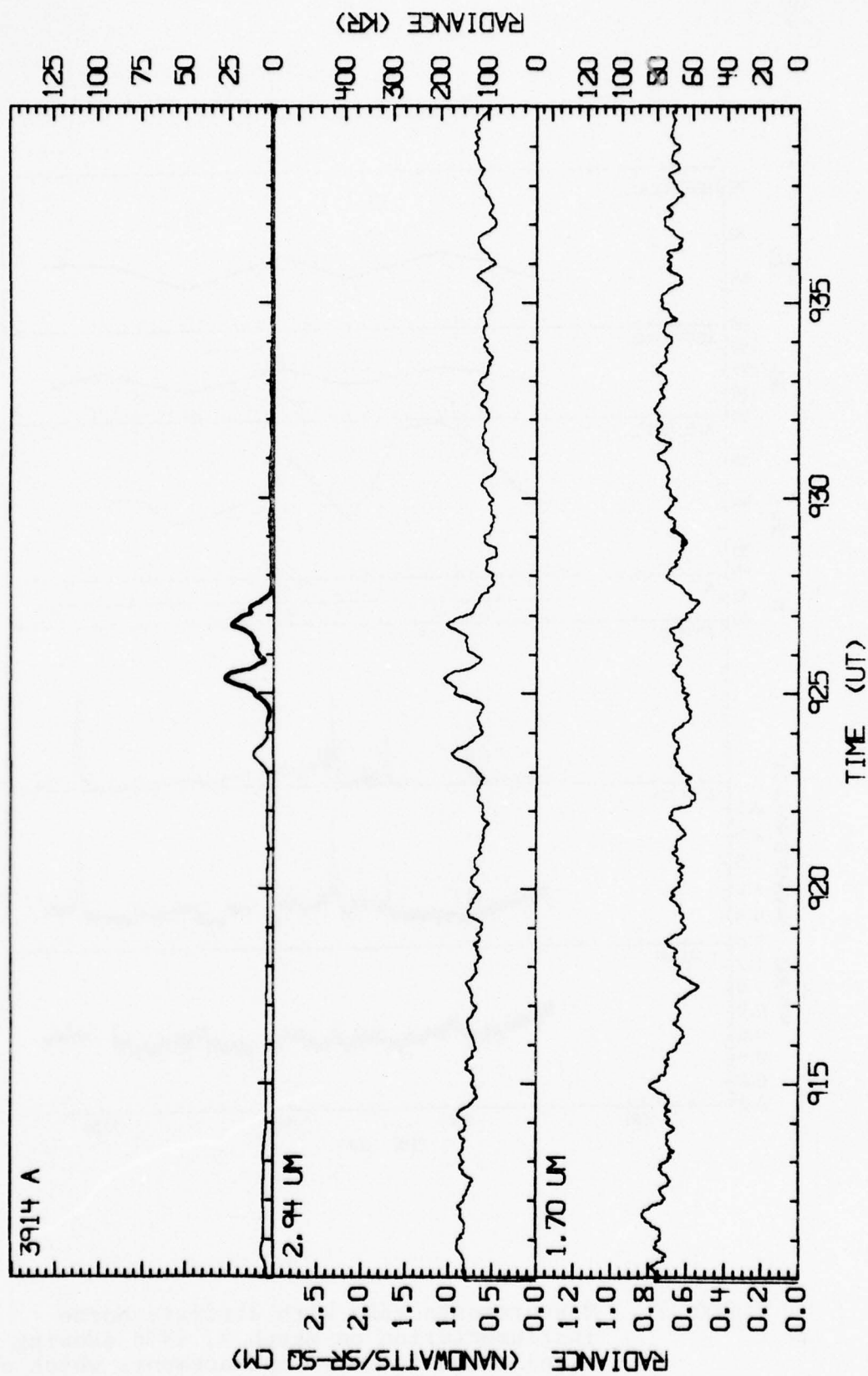


Figure 23. Measured data for March 7, 1976 plotted on an expanded time scale to show the correlation between the 2.94 μm emissions and the 3914 Å emissions during a period when small enhancements occurred.

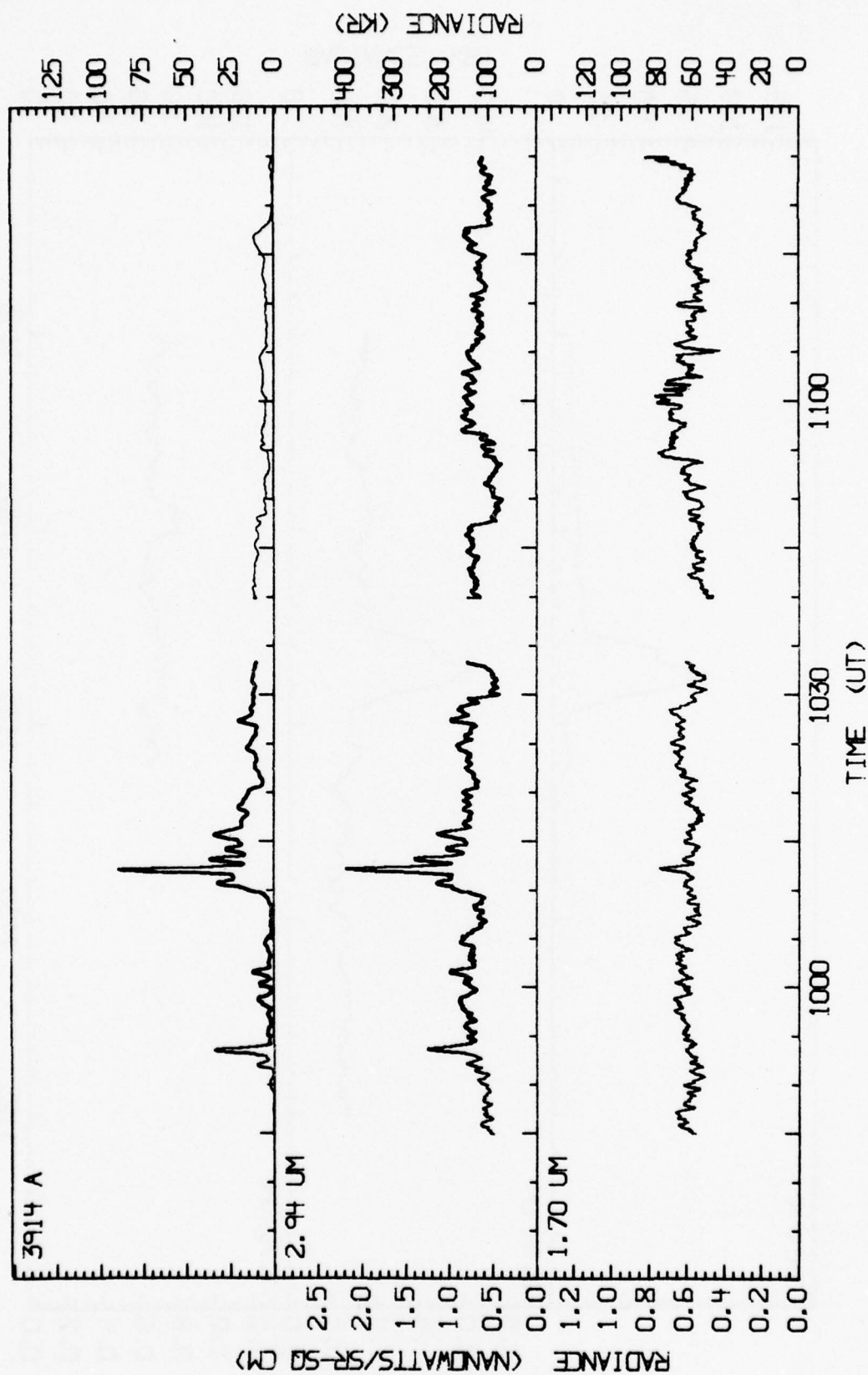


Figure 24. Measured data for March 7, 1976 plotted on an expanded time scale to show the excellent spatial and time correlation between the 3914A emissions and the 2.94 μm emissions during rapidly fluctuating auroral conditions.

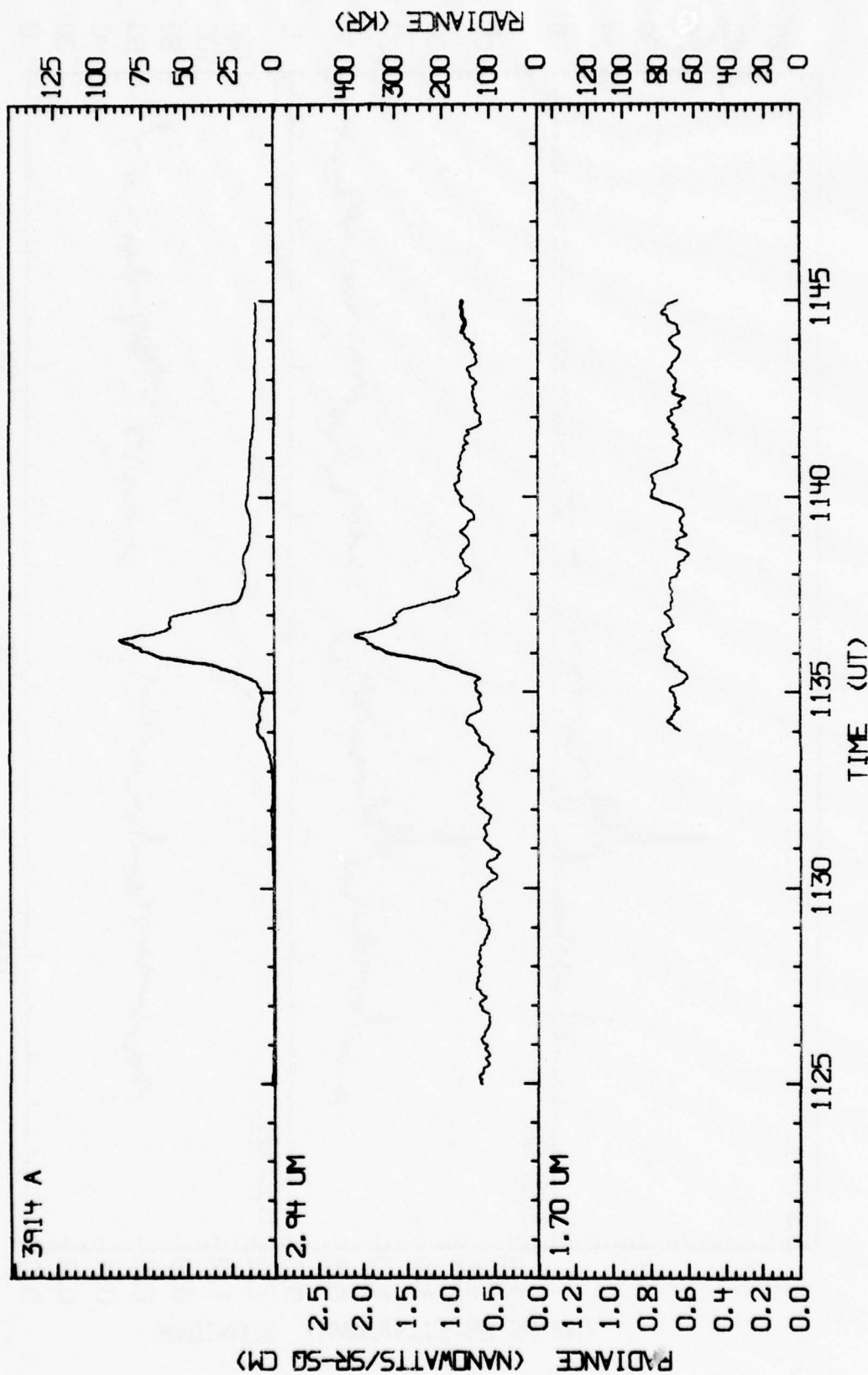


Figure 25. Measured data for March 7, 1976 plotted on an expanded time scale to illustrate the correlation between the 3914 Å emissions and the 2.94 μm emissions during a period when a large enhancement occurred.

DATA ANALYSIS

Atmospheric emission enhancements in the $2.8 \mu\text{m}$ region appear to occur whenever auroral activity exists. These enhancements are readily apparent in the data measured from the aircraft anytime the N_2^+ (3914A) emissions exceed 20 kiloRayleighs. Enhancements during less intense aurorae still exist, but they are not as apparent because they are relatively small in comparison to the OH background emissions and the instrument noise.

To provide a better understanding of the measured $2.8 \mu\text{m}$ enhancements, several analysis procedures and calculations were performed. The analyses include the following: (1) A detailed spatial and temporal correlation analysis which compares the $2.8 \mu\text{m}$ enhancements with the 3914A enhancements during various auroral intensities and conditions; (2) A linearity analysis comparing the measured intensities of the $2.8 \mu\text{m}$ enhancements with the intensities of the 3914A auroral monitor for various auroral conditions; and (3) Photo-energy efficiency calculations to determine what percentage of the total incoming auroral electron energy is emitted as photons in the 1976 $2.94 \mu\text{m}$ measurement band and what percentage is emitted as NO overtone photons assuming the enhancement is produced by a NO process.

The above named analyses are separately described below.

Spatial and Temporal Correlation

Between 3914A(N_2^+) Emissions and $2.8 \mu\text{m}$ Enhancements

Spatial and temporal correlation studies between the measured 3914A(N_2^+) emissions and the $2.8 \mu\text{m}$ emissions during an aurorally enhanced period can be made by comparing the radiance versus time plots of the two emissions. However, before the comparison is made it is desirable to subtract or remove any background emissions from the data which are not correlated with the auroral enhancements. The 3914A backgrounds are typically less than 100 Rayleighs

which are insignificant in comparison to the levels measured during enhancement periods. Thus, no background subtraction is required for the 3914A emissions. On the other hand, the 2.8 μm data includes emissions from OH fundamental sequences, which are not directly correlated with the aurora. These OH emissions should be directly related to the OH overtone emissions measured at 1.7 μm , and therefore they can be removed from the 2.8 μm data by subtracting a radiance level proportional to the radiance values measured at 1.7 μm . The proportionality constant required for the subtraction can be calculated from a report by Baker [1976], which relates the amplitudes of the OH $\Delta V = 1$ bands to the amplitudes of the OH $\Delta V = 2$ bands. Using Baker's results, Schummers [1977] calculated the expected ratio between the radiance levels of two OH measurement bands for the 1976 aircraft data. The results are

$$\frac{\text{Rayleigh Radiance of OH } \Delta V = 1, 2.94 \mu\text{m Band}}{\text{Rayleigh Radiance of OH } \Delta V = 2, 1.7 \mu\text{m Band}} = 2.2$$

If one ratios the measured radiances of the 2.94 μm band and the 1.7 μm band for the 1976 ICECAP data during quiet auroral conditions, values ranging from 1.7 to 2.1 are obtained. This is in good agreement with the calculated value which indicates that OH emissions can account for the entire background level. Any differences and variations between the calculated and measured ratios can be accounted for by accuracy limitations of the instrumentation calibrations and the measurement techniques. Therefore, a feasible method of subtracting the OH background from the 2.8 μm data is to subtract an amount proportional to the 1.7 μm data which will reduce the 2.8 μm radiance to zero during quiet auroral conditions. This method was used for our analyses.

Once the OH subtraction is completed, comparisons can more readily be made between the aurorally enhanced emissions in the 2.8 μm region and the 3914A, N_2^+ emissions. Figures 26 through 32 present data measured March 3, March 7, March 8, and March 26, 1976 which have the OH emissions subtracted from the total

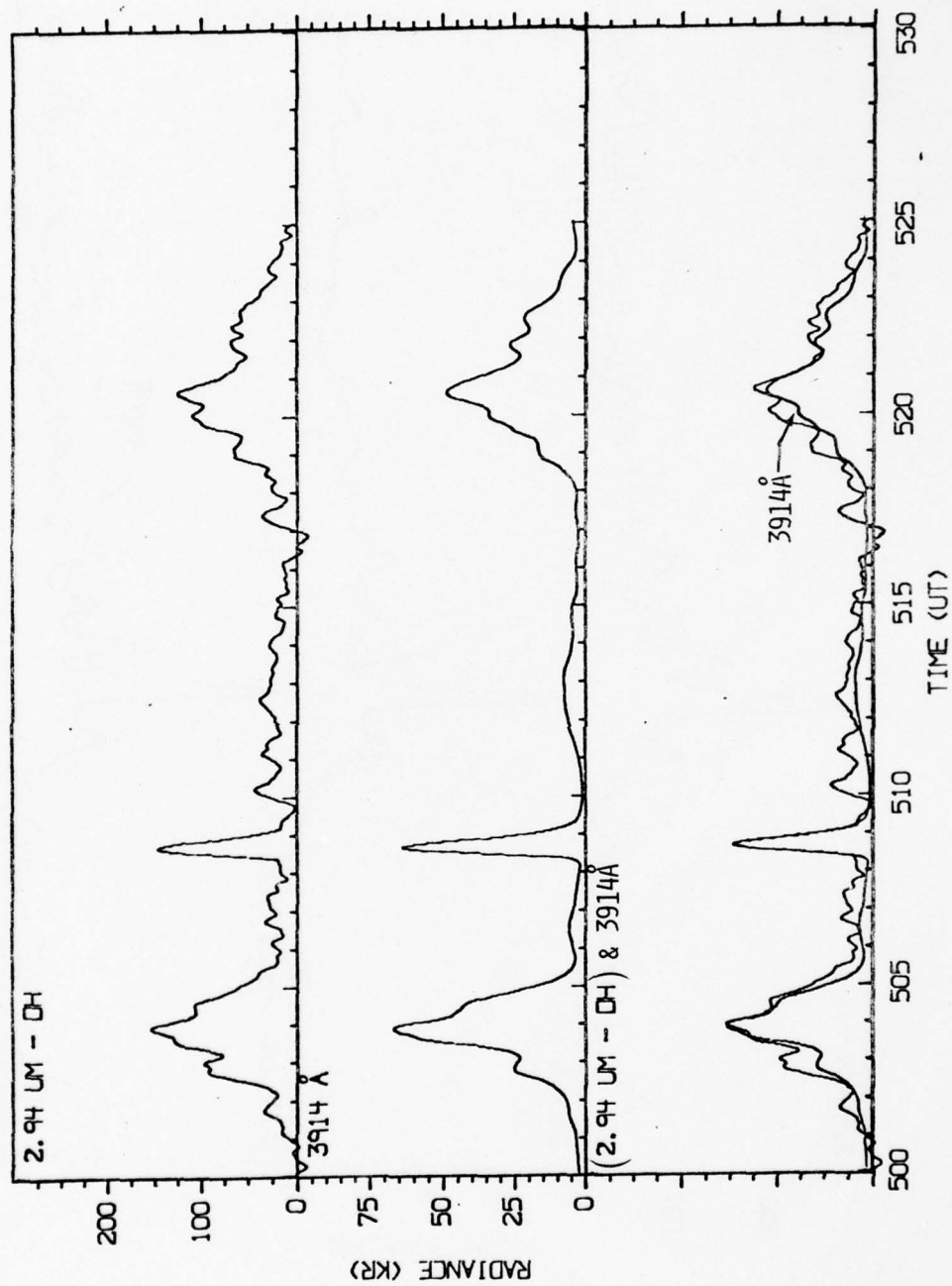


Figure 26. Temporal and spatial comparisons of 2.94 μm and 3914 Å enhancements measured March 3, 1976.

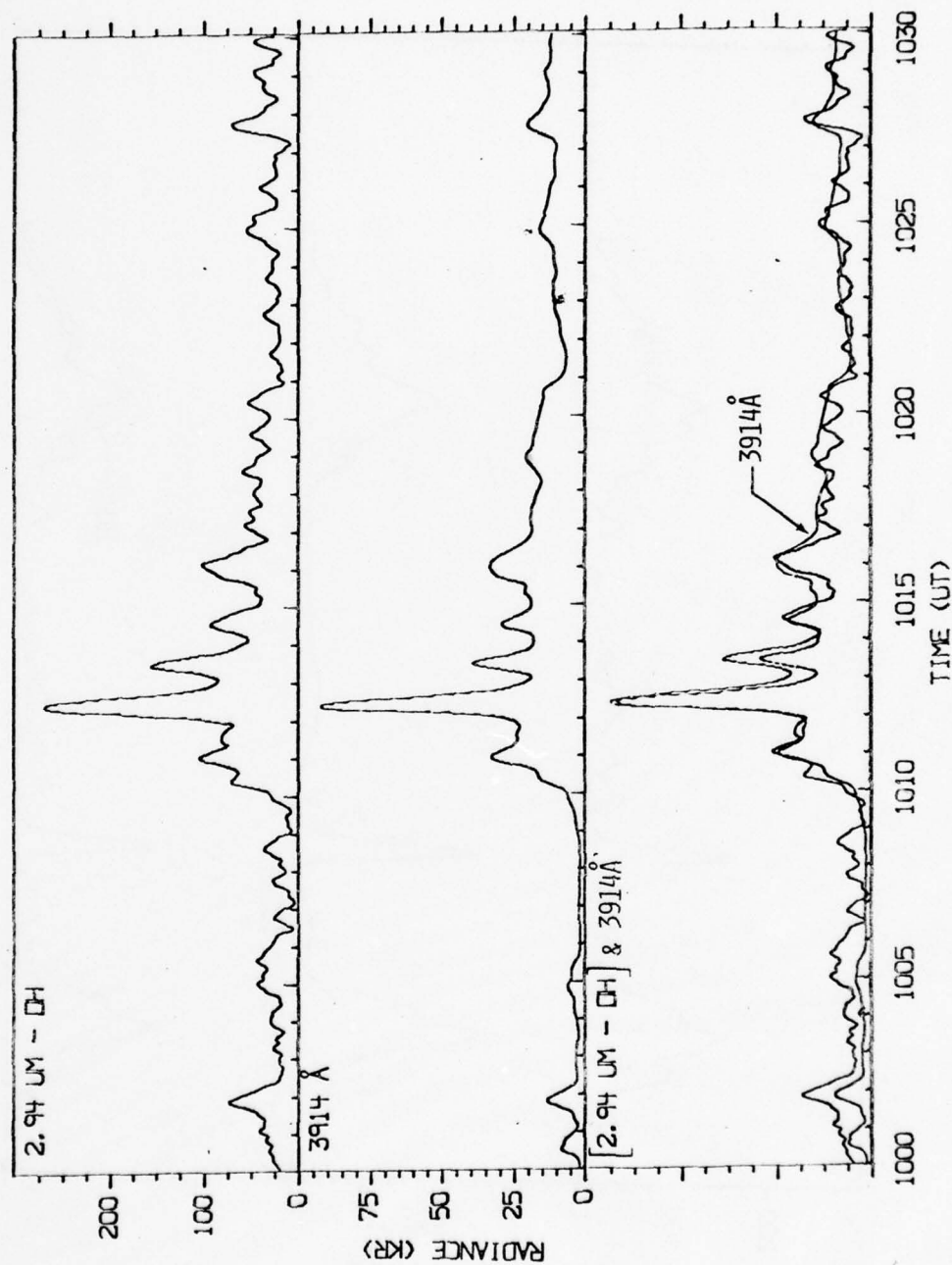


Figure 27. Temporal and spatial comparisons of 2.94 μm and 3914 Å enhancements measured March 7, 1976 between 1000 and 1030 UT.

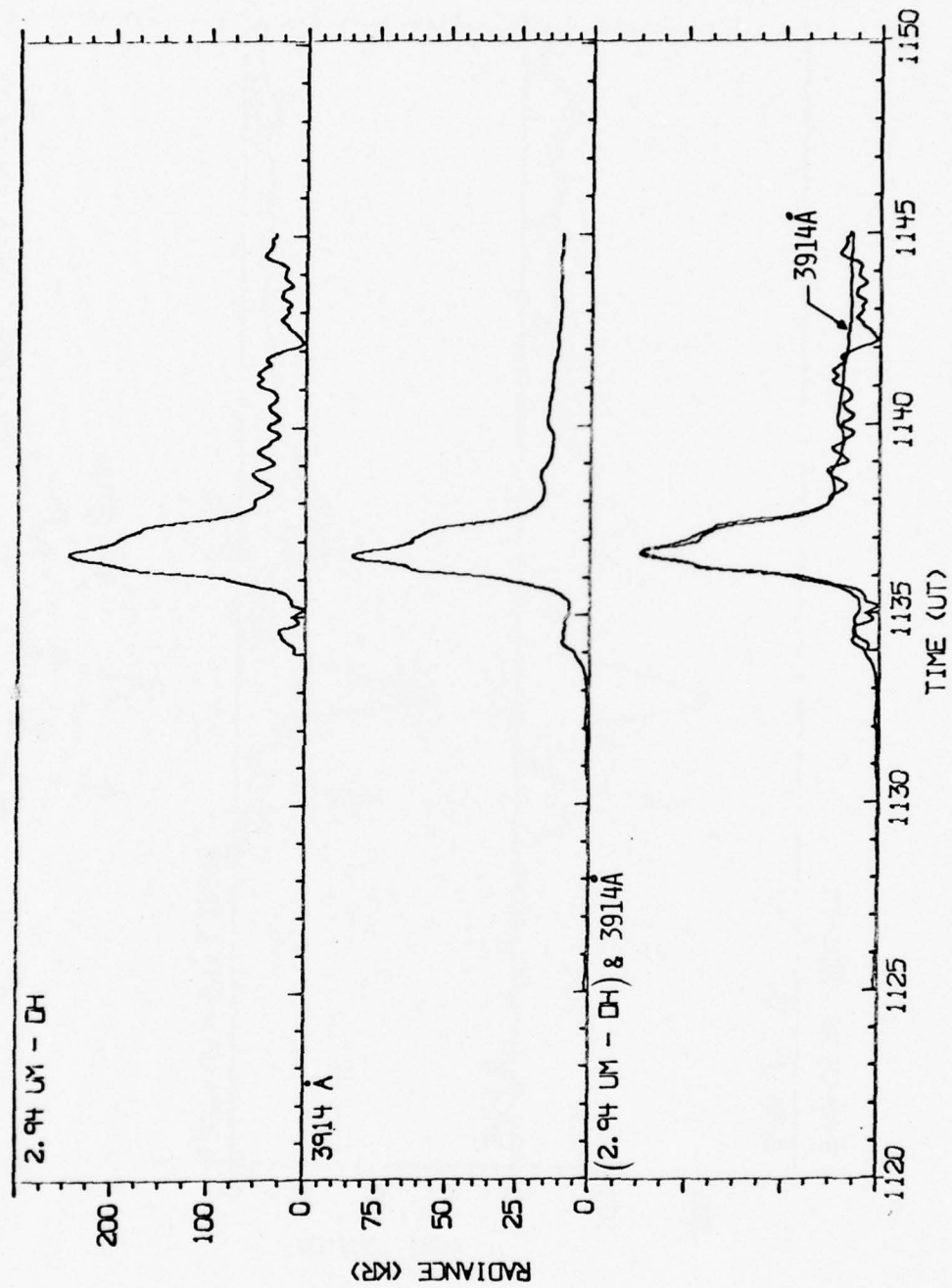


Figure 28. Temporal and spatial comparisons of 2.94 μm and 3914 Å enhancements measured March 7, 1976 between 1120 and 1150 UT.

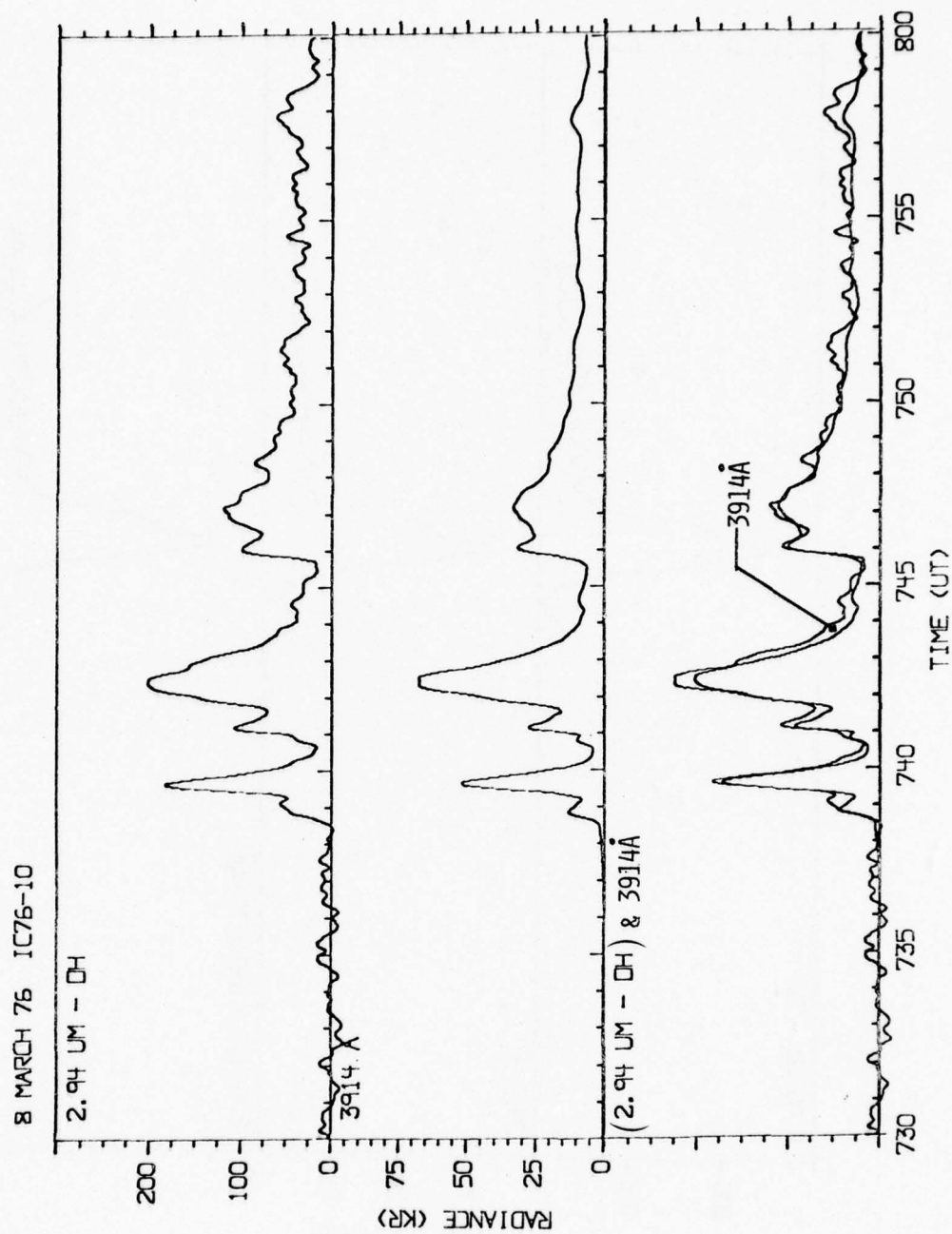


Figure 29. Temporal and spatial comparisons of 2.94 μm and 3914 Å enhancement measured March 8, 1976.

26 MARCH 76 IC76-16

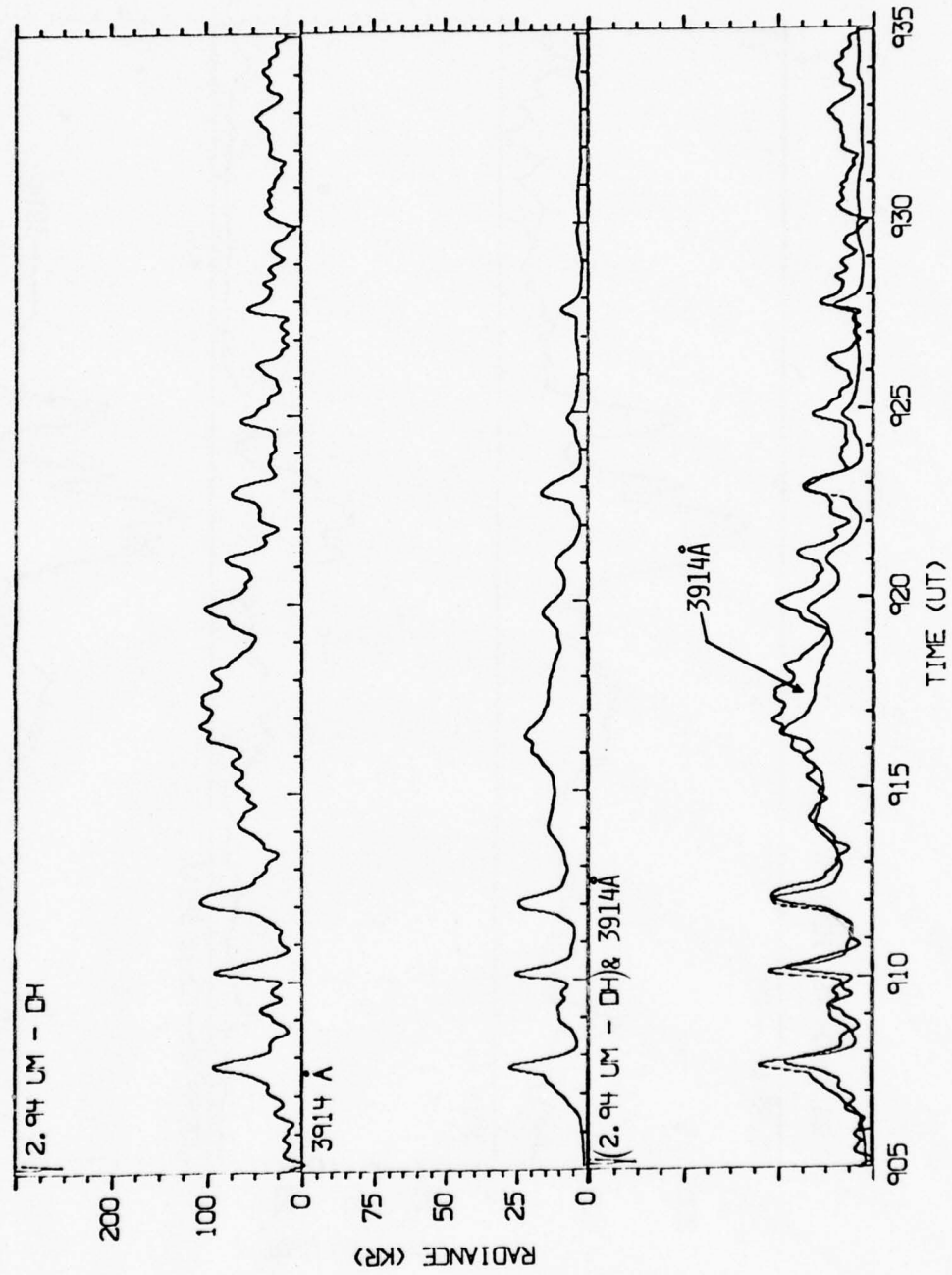


Figure 30. Temporal and spatial comparisons of 2.94 μm and 3914 Å enhancements measured March 26, 1976 between 0905 and 0935 UT.

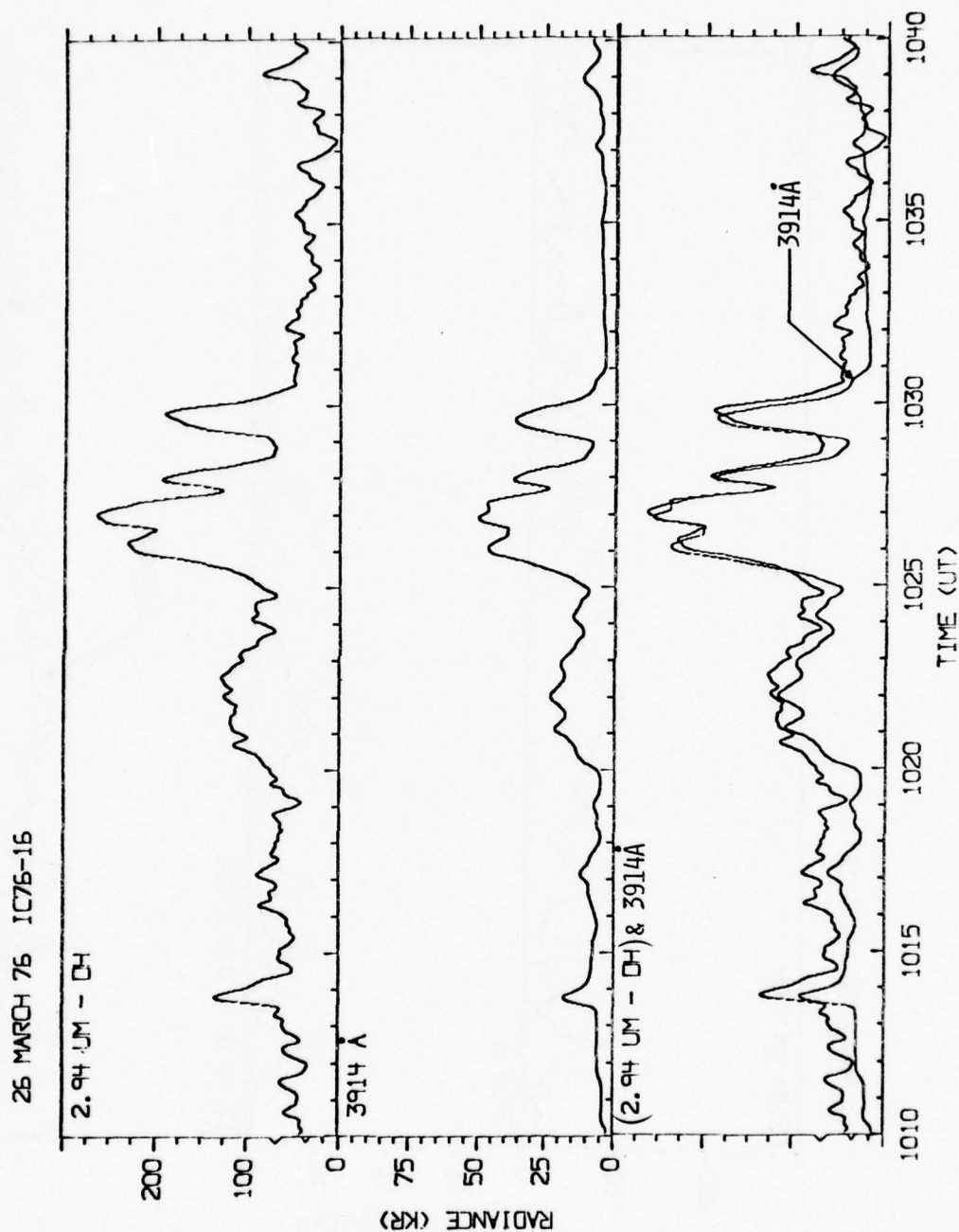


Figure 31. Temporal and spatial comparisons of 2.94 μm and 3914 Å enhancements measured March 26, 1976 between 1010 and 1040 UT.

26 MARCH 76 IC76-16

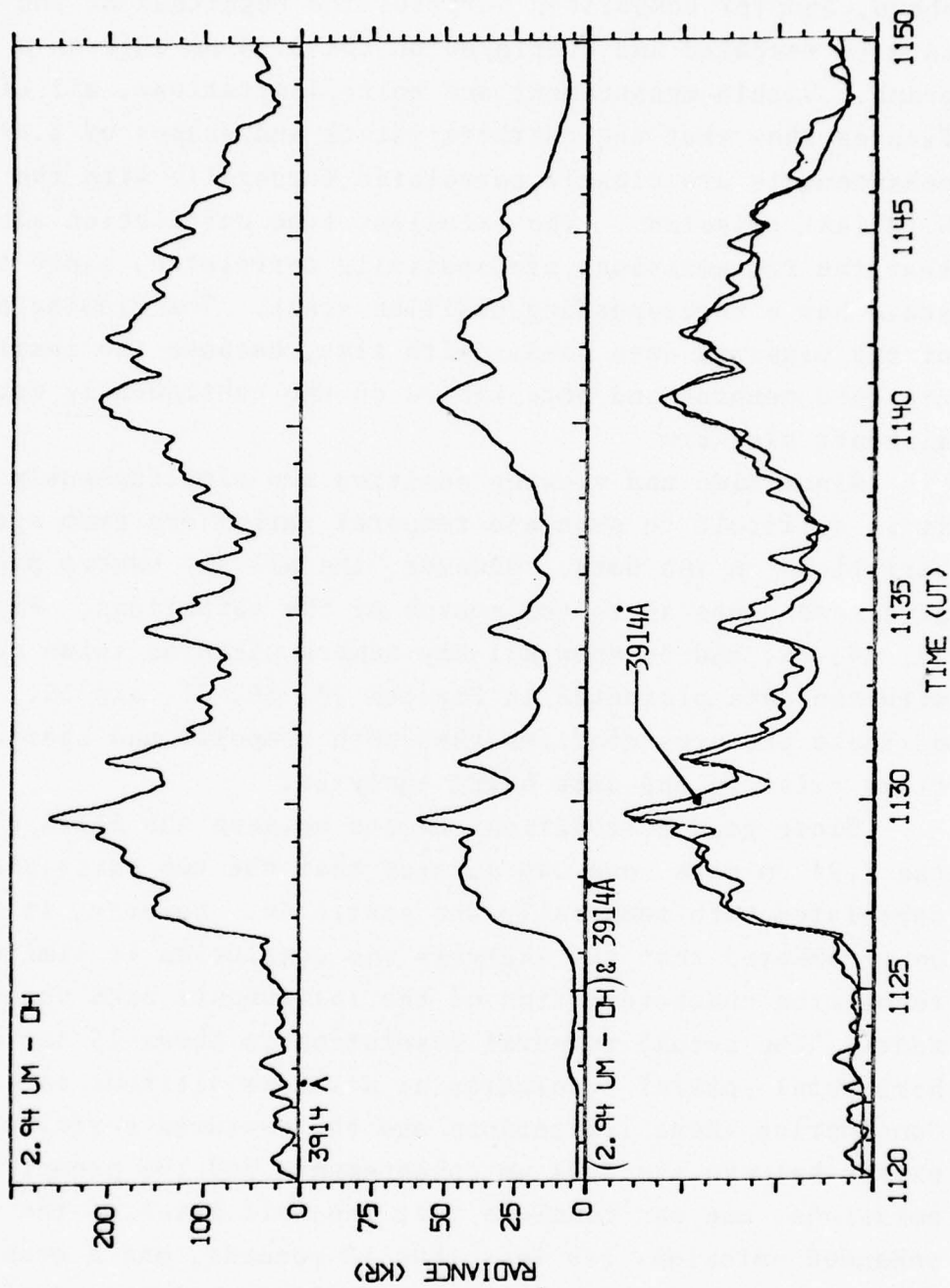


Figure 32. Temporal and spatial comparisons of 2.94 μm and 3914 Å enhancements measured March 26, 1976 between 1120 and 1150 UT.

2.94 μm emissions. The corresponding 3914A emissions are also shown, and for comparison purposes the magnitude of the 3914A data is rescaled and overlayed on the 2.94 μm data on a separate graph. Within measurement and noise limitations, all of the figures show that the characteristics and shapes of 2.94 μm enhancements are closely correlated temporally with the prompt N_2^+ (3914A) emissions. The excellent time correlation also implies that the two emissions are spatially correlated, since the time scale has a corresponding position scale. The viewing position of the measured data varies with time, because the instruments are hard mounted and boresighted on the continuously moving aircraft platform.

Since time and viewing position are simultaneously varying, it is difficult to separate temporal variations from spatial variations in the data. However, the all-sky camera pictures do give some clues as to the source of the variations. Figures 33, 34, 35, and 36 show all-sky camera pictures taken concurrent with the data presented in Figures 27, 30, 31, and 32. A study of these pictures confirms that both temporal and spatial variations exist in the data being analyzed.

Since good correlation exists between the 3914A data and the 2.94 μm data, one can surmise that the two emissions are correlated both temporally and spatially. However, it should be remembered that the analysis and conclusion is limited by the resolution characteristics of the instruments used for the measurements. The actual temporal resolution is about 15 sec and the horizontal spatial resolution at a 100 km altitude is 14 km. Considering these limitations and the measured correlation which exists between the 2.94 μm enhancements and the prompt 3914A emissions, one can conclude that the half lives of the 2.94 μm enhanced emissions are less than 15 seconds, and a considerably faster instrument response is needed to accurately determine the exact half life.

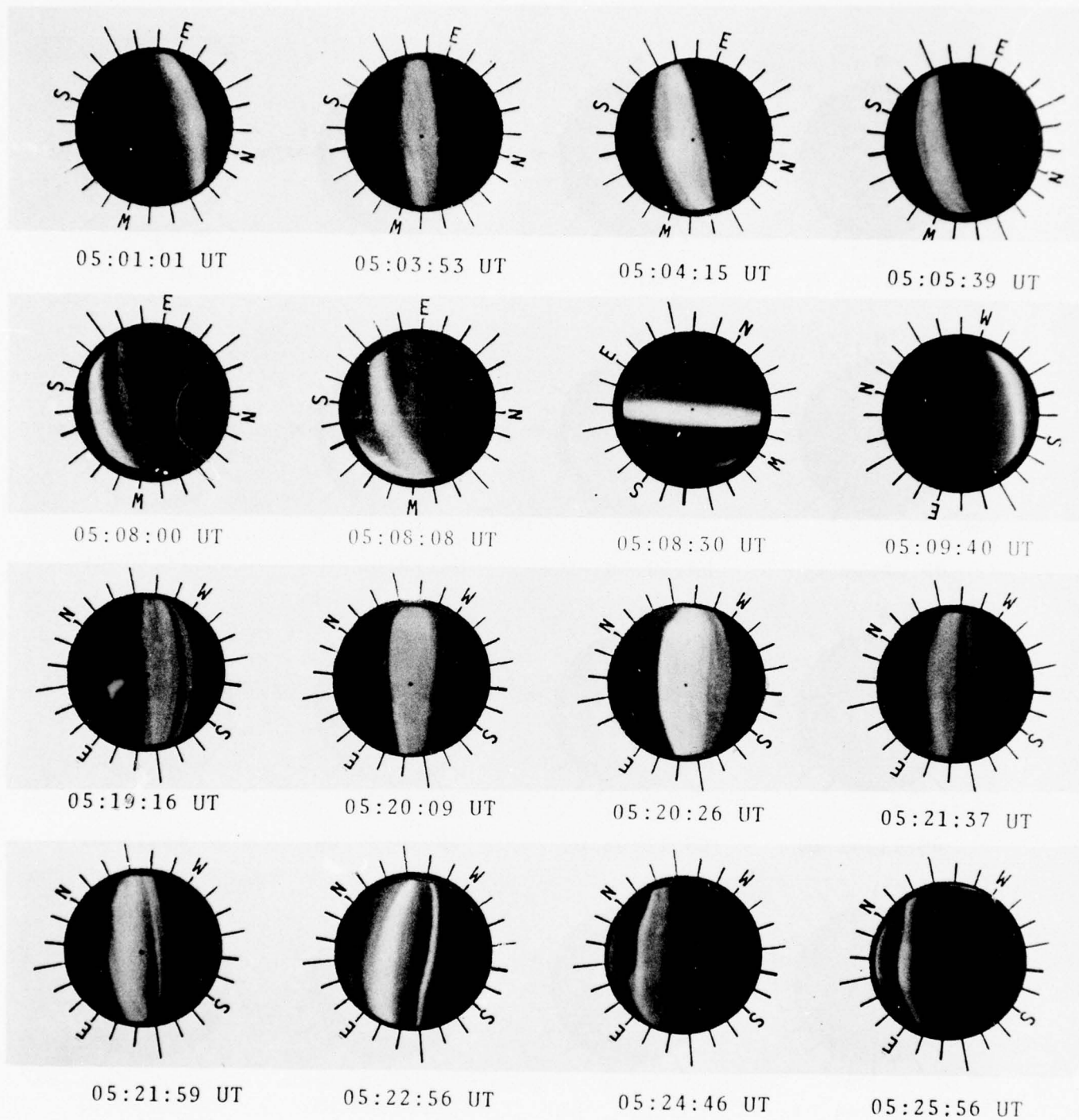


Figure 33. All Sky Camera pictures showing auroral conditions during periods when infrared enhancements were measured on 3 March 1976.

→ Forward Movement of the Aircraft →

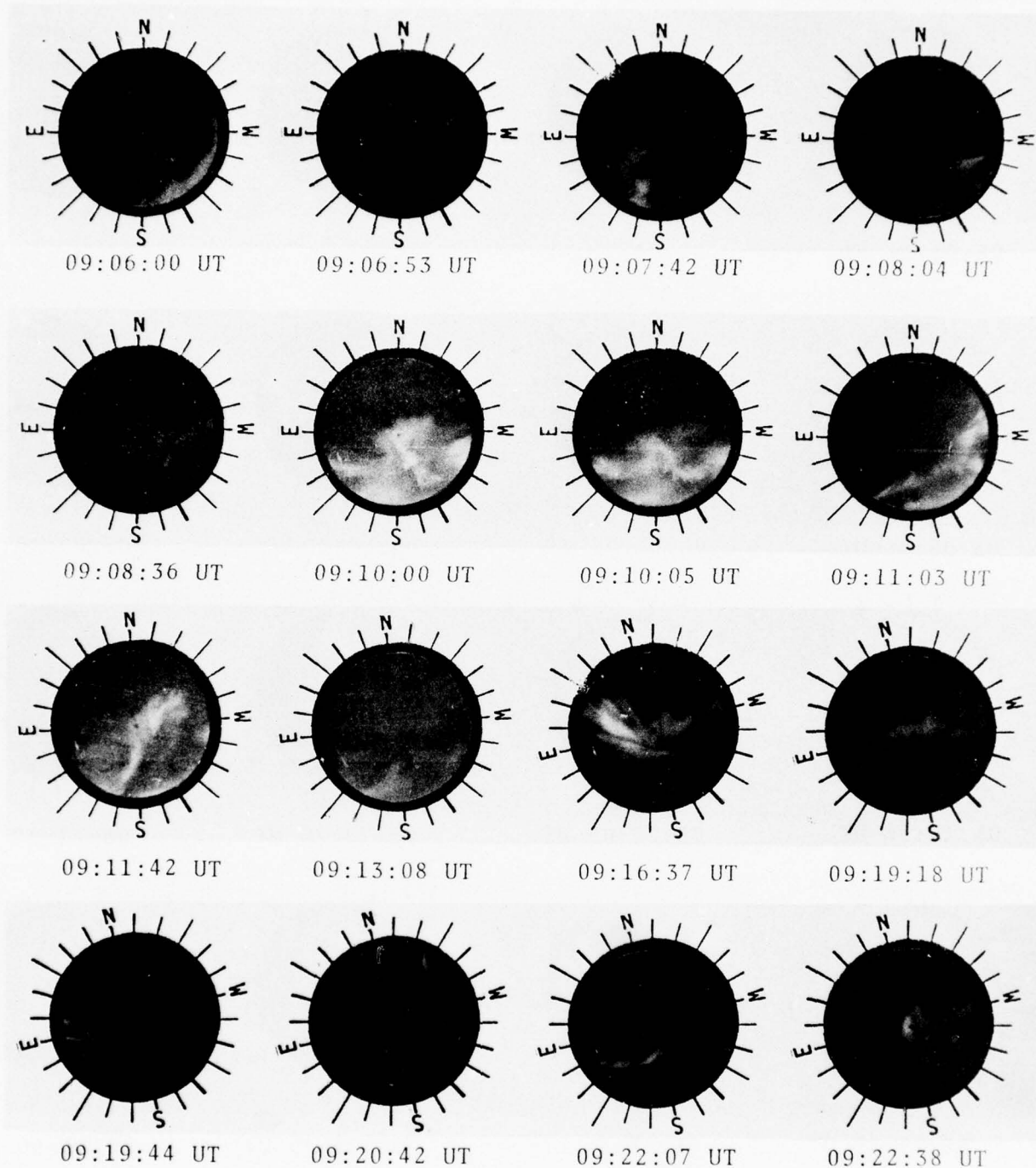
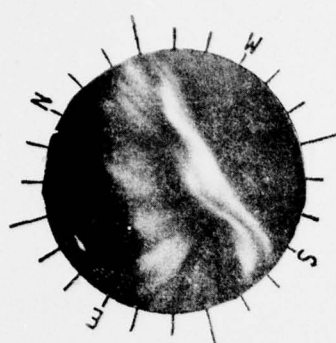
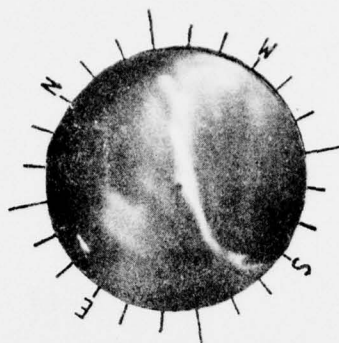


Figure 34. All sky camera pictures showing auroral conditions on March 26, 1976 for time periods corresponding to the data presented in Figure 30.

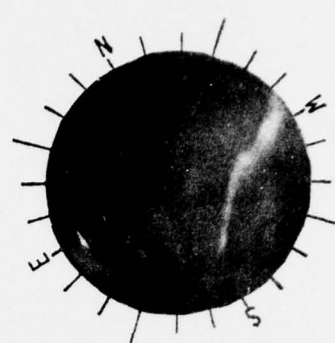
→ Forward Movement of Aircraft →



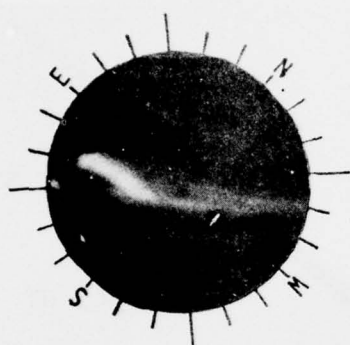
10:11:58 UT



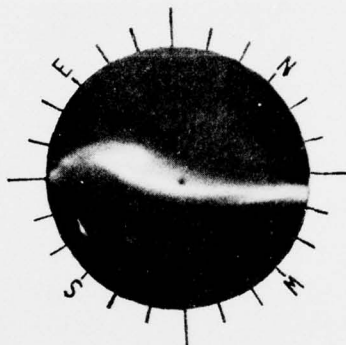
10:13:36 UT



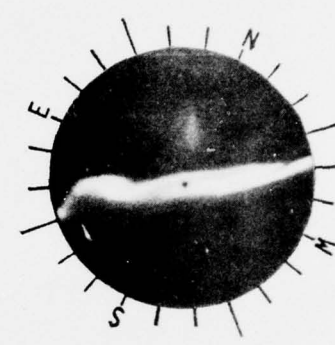
10:14:12 UT



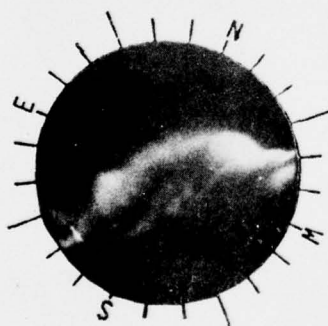
10:25:03 UT



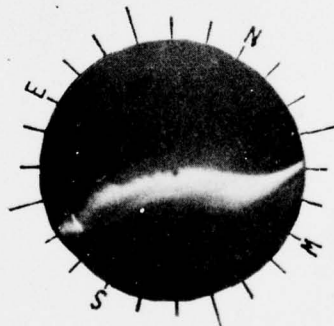
10:26:01 UT



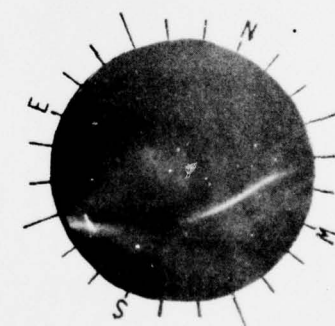
10:26:54 UT



10:28:46 UT



10:29:30 UT



10:30:28 UT

Figure 35. All sky camera pictures showing auroral conditions on March 26, 1976 for time periods corresponding to the data presented in Figure 31.

→ Forward Movement of the Aircraft →

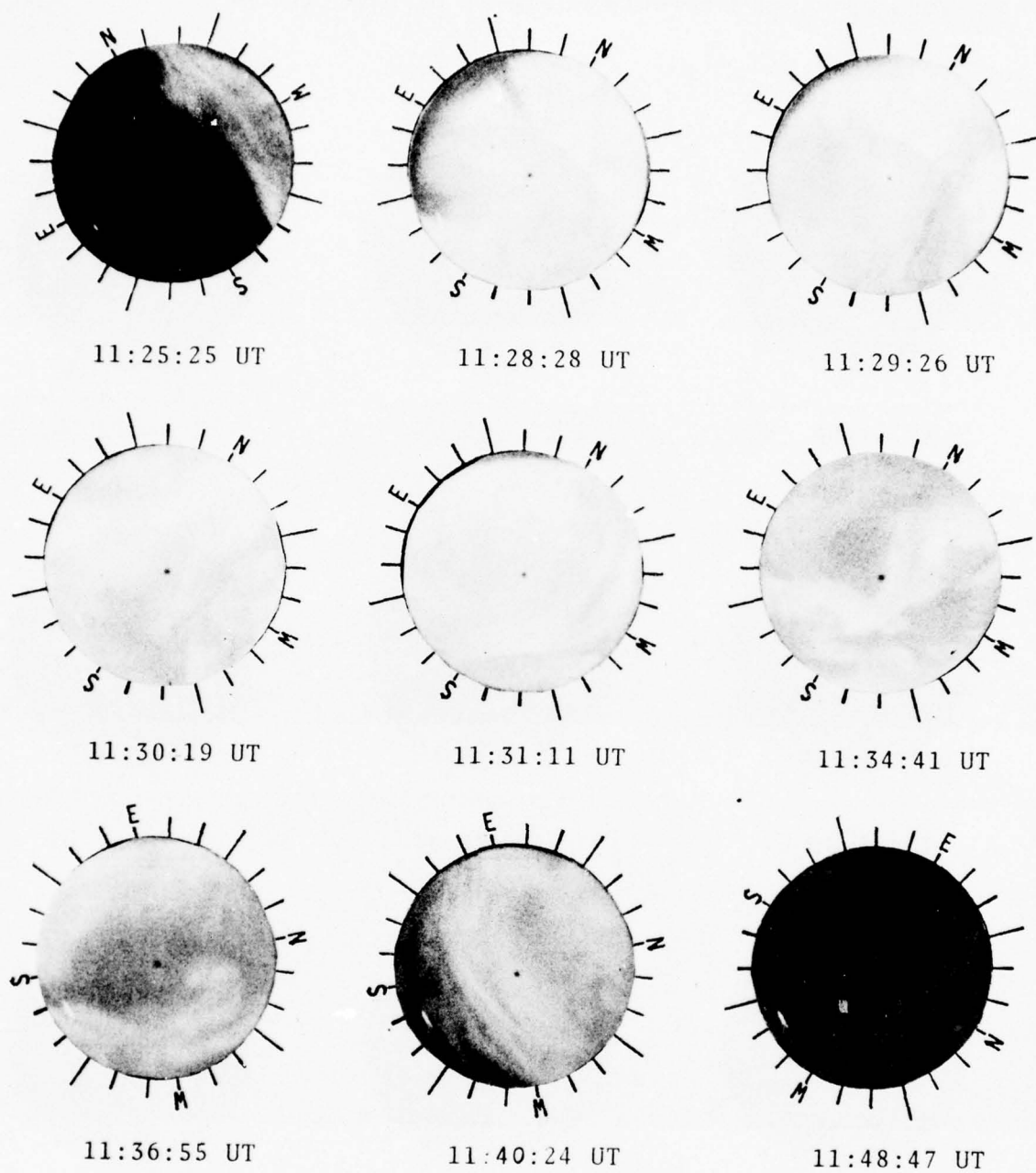


Figure 36. All sky camera pictures showing auroral conditions on March 26, 1976 for time periods corresponding to the data presented in Figure 32.

Linearity Studies

Since the enhanced emissions at $2.8\ \mu\text{m}$ are directly correlated with the visible aurora as monitored by a 3914A photometer, further analyses were performed to investigate the relationship between the magnitude of the $2.8\ \mu\text{m}$ enhancements and the incoming auroral energy. A study was performed to determine whether the amplitude of the enhancement portion of the $2.8\ \mu\text{m}$ emissions are linearly proportional to the 3914A emissions for various auroral conditions. Since the 3914A emissions provide an approximate monitor of the total incoming auroral electron energy, the study also indicates whether the $2.8\ \mu\text{m}$ enhancements vary linearly with the incoming auroral energy for various auroral intensities and conditions. The linearity study was made using the data presented in Figures 26 through 32 which were measured on March 3, 7, 8 and 26, 1976 during various levels of auroral excitation. The study was performed by directly comparing the amplitudes of the 3914A emissions with the amplitudes of the $2.94\ \mu\text{m}$ enhancements at times corresponding to a variety of auroral excitation levels. The results are given in Table 3, where the comparison is accomplished by taking the ratio of the kiloRayleigh amplitudes of the two emissions.

It should be noted from Table 3 that the ratios between the 3914A emissions and the $2.94\ \mu\text{m}$ emissions are not constant for the various auroral conditions. This indicates that the $2.94\ \mu\text{m}$ emissions are not linearly proportional to the 3914A emissions. Based on the premise that the 3914A emissions are proportional, within limits, to the total incoming auroral energy, one can also surmise that the $2.94\ \mu\text{m}$ enhancements are not linearly proportional to the total auroral energy. Explanations as to the cause of these non-linearities are not readily apparent from the presented data. However, one possible explanation is that the intensities of the enhanced $2.8\ \mu\text{m}$ emissions are affected by variations in the penetration depth into the atmosphere of the auroral electrons. The Chatanika

Table 3. Comparisons of the 2.94 μm Enhancements and 3914A Emissions.			
Date/Mission	Time (UT)	3914A Radiance (kR)	Ratio [*] $\frac{\text{kR}_{(2.94 \mu\text{m})}}{\text{kR}_{(3914\text{A})}}$
3 Mar 76 IC 76-6	0503:45	67	2.313
	0508:40	65	2.23
	0520:30	49	2.55
7 Mar 76 IC 76-9	1012:20	92	2.95
	1013:30	40	3.875
	1016:00	34	2.94
	1136.35	84	3.04
8 Mar 76 IC 76-10	0739:40	52	3.42
	0742.25	68	3.01
	0746.05	33	3.18
26 Mar 76 IC 76-16	0907.40	27.5	3.45
	0912:00	25	4.2
	1027:00	50	5.2
	1028:00	37	5.2
	1129:40	59	4.4
	1140:25	52	4.03

* The kiloRayleigh value for the 2.94 μm emission has the OH background removed leaving only the enhancement portion.

radar measurements outlined in Appendix B may provide some electron density and altitude data which can be used to partially check this explanation. As of yet these measurements have not been reduced, and therefore an analysis will not be made at this time. However, such an analysis is warranted and additional more refined experiments should be performed to study altitude effects.

Photo-Energy Efficiency of Aurorally Enhanced 2.94 μm Emissions

Since the measured enhancements in the 2.8 μm region are directly correlated with an aurorally excited atmosphere, it is of interest to use the measured data to calculate the percentage of the incoming auroral electron energy that is emitted as photon energy in the 2.8 μm measurement band. Also, since it is plausible that the enhancements could result from overtone nitric oxide emissions, it is of value to determine the percentage of auroral energy that would be radiated as overtone nitric oxide photons. The measured 3914A emission and background subtracted 2.94 μm emission presented in Figures 26 through 32 provide a good data base for these calculations.

To calculate the photo-energy efficiency of the 2.94 μm enhancements, we start with the following expression:

$$\text{Photo Energy Efficiency}_{(2.94 \mu\text{m})} = \frac{\text{eV}_{(2.94 \mu\text{m})}}{\text{eV}_{(\text{incident})}} \times 100\% \quad (1)$$

In this expression, the incoming energy in electron volts, $\text{eV}_{(\text{incident})}$, can be determined from the 3914A data. The conversion is accomplished by multiplying the measured 3914A photons by the number of ion pairs generated per photon and then multiplying the result by the number of electron volts absorbed per ion pair. *Baker and Pendleton [1976]* indicate that 18 ion pairs are formed per 3914A photon at 100 km, and *Tarr et al. [1974]*

indicates that 34 eV are absorbed per ion pair produced. Using these values we obtain the following expression for the total incident auroral energy:

$$\begin{aligned} \text{eV}_{(\text{incident})} &= \text{Photons}_{(3914\text{\AA})} \times \frac{18 \text{ ion pairs}}{3914\text{\AA} \text{ photon}} \times \frac{34\text{eV}}{\text{ion pair}} \\ &= 612 \times \text{Photons}_{(3914\text{\AA})} \end{aligned} \quad (2)$$

where $\text{Photons}_{(3914\text{\AA})}$ equals the number of photons produced by the $N_2^+(0,0)$ first negative band which is measured with a 3914Å photometer.

Substituting Equation (2) into Equation (1) we get

$$\text{Photo-Energy Efficiency}_{(2.94 \text{ }\mu\text{m})} = .163 \frac{\text{eV}_{(2.94 \text{ }\mu\text{m})}}{\text{Photons}_{(3914\text{\AA})}} \quad (3)$$

The 2.94 μm emission energy, $\text{eV}_{(2.94 \text{ }\mu\text{m})}$, can be determined from the 2.94 μm data by multiplying the enhanced portion of the measured photons by the energy per photon, and then dividing the result by the atmospheric transmittance. Thus,

$$\begin{aligned} \text{eV}_{(2.94\mu\text{m})} &= \frac{hc}{\lambda} \times \text{Photons}_{(2.94 \text{ }\mu\text{m})} \div \tau_{(2.94 \text{ }\mu\text{m})} \\ &= \frac{1.234}{\lambda \tau} \times \text{Photons}_{(2.94 \text{ }\mu\text{m})} \end{aligned} \quad (4)$$

where $\text{Photons}_{(2.94 \text{ }\mu\text{m})}$ is equal to the measured photons of the 2.94 μm enhancements, λ is the wavelength of the emission, and τ is the atmospheric transmittance from the emission altitude to the aircraft platform, at 2.94 μm .

Substituting Equation (4) into Equation (3) gives the following:

$$\text{Photo-Energy Efficiency}_{(2.94 \text{ } \mu\text{m})} = \frac{.201}{\lambda\tau} \times \frac{\text{Photons}_{(2.94 \text{ } \mu\text{m})}}{\text{Photons}_{(3914\text{A})}} \quad (5)$$

This expression can be equally stated as follows:

$$\text{Photo-Energy Efficiency}_{(2.94 \text{ } \mu\text{m})} = \frac{.201}{\lambda\tau} \times \frac{R_{(2.94 \text{ } \mu\text{m})}}{R_{(3914\text{A})}} \quad (6)$$

where $R_{(2.94 \text{ } \mu\text{m})}$ is the measured enhancement radiance in Rayleighs, and $R_{(3914\text{A})}$ is the measured radiance of the 3914A, $N_2^+(0,0)$ first negative band in Rayleighs.

Using Equation (6) and the measured data in Figures 26 through 33, the percentage of the incoming auroral energy that is radiated as 2.94 μm photons was calculated for various measurement periods. The calculated efficiencies are listed in Table 4. An atmospheric transmittance of .965 was calculated from the Lowtran II atmospheric model for an Arctic winter for a vertical path between 10.5 and 100 km, and this value was incorporated in the calculations.

Assuming that the 2.94 μm enhancements are generated by first overtone nitric oxide, Schummers [1977] calculates the percentage of auroral electron energy that is radiated as nitric oxide overtone photons. Basically, his calculations use the same process described above except he uses a synthetic nitric oxide spectrum, which was generated using a rotational temperature of 220⁰K and a vibrational temperature of 5400⁰K, to predict that 40% of the overtone nitric oxide radiation is included in the 2.94 μm spectral measurement band. Therefore, the measured 2.94 μm radiance must be multiplied by 2.5 to determine the radiance of the entire nitric oxide first overtone band. Knowing this, one can write the following expression for calculating the

TABLE 4. Photo-Energy Efficiencies of Aurorally Excited 2.94 μm Emissions.			
Date/Mission	Time UT	Ratio $\frac{R_{(2.94 \mu\text{m})}}{R_{(3914\text{\AA})}}$	% of Auroral Energy Radiated as Photons in the 2.94 μm Measurement Band
26 Mar 1976 IC 76-16	0905 - 0935	4.3	.305
	1010 - 1040	5.2	.368
	1120 - 1150	4.3	.305
8 Mar 1976 IC 76-10	0730 - 0800	3.3	.234
7 Mar 1976 IC 76-9	1000 - 1030	3.0	.213
	1120 - 1150	3.0	.213
3 Mar 1976 IC 76-6	0500 - 0530	2.3	.163

photo-energy efficiency of the nitric oxide overtone:

$$\text{Photo-Energy Efficiency}_{(\text{NO})} = \frac{.201}{\lambda \tau} \times \frac{2.5 \times R_{(2.94 \text{ } \mu\text{m})}}{R_{(3914\text{\AA})}}$$

Based on this expression and a λ equal to 2.9 μm , which is the center of the nitric oxide band (See Figure 4), photo-efficiencies ranging from .41 to .93% for the 1976 ICECAP measurements were calculated. These calculated values for seven measurement periods are given in Table 5. The values are in good agreement with those calculated by Schummers [1977].

The average of the calculated nitric oxide percentages presented in Table 5 is .65%. This is less than the lower limit of 1% which was presented by Hurd *et al.* [1977] for the data measured from the ICECAP A10.205-2 Paiute rocket launched March 24, 1973. However, this difference is not large considering our measurements show that variations as large as a factor of 2.3 occur for different auroral conditions.

TABLE 5. Photo-Energy Efficiencies of Overtone NO Emissions.

Date / Mission	Time UT	Ratio $\frac{R(2.94 \mu m)}{R(3914A)}$	% of Auroral Electron Energy Radiated as NO Overtone Photons
26 Mar 1976	0905 - 0935	4.3	.77
IC 76-16	1010 - 1040	5.2	.93
	1120 - 1150	4.3	.77
8 Mar 1976	0730 - 0800	3.3	.59
IC 76-10			
7 Mar 1976	1000 - 1030	3.0	.54
IC 76-9	1120 - 1150	3.0	.54
3 Mar 1976	0500 - 0530	2.3	.41
IC 76-6			

REFERENCES

1. Baker, D.J. [1976] "The Upper-Atmospheric Hydroxyl Airglow," Manuscript, Air Force Geophysics Laboratory, Hanscom AFB, Mass., and Utah State University, Logan, Utah, May 1976, p. 23.
2. Baker, D.J. and Pendleton, W.R., Jr. [1976] "Optical Radiation from the Atmosphere", Proc. Atmos. Radiometry, Vol. 91, August 1976, p. 50.
3. Gibson, J.J. [1977] Air Force Geophysics Laboratory, Hanscom Air Force Base, Mass., (private communication).
4. Hurd, A.G., Carpenter, J.W., Degges, T.C., et al., [1977] "Comparison of ICECAP and EXCEDE Rocket Measurements with Computer Code Predictions, HAES Report No. 61," AFGL TR-77-0060, VI-381, Final Report Contract F19628-74-C-0177, 15 Feb 77.
5. Schummers, J.H. [1977] Electro-Dynamics Laboratories, Utah State University, Scientific Report: EDL-SRL 77-01, "Analysis of ICECAP 1976 Aircraft Borne Measurements in 1.7 and 2.94 Micron Hydroxyl and Nitric Oxide Bands", June 13, 1977.
6. Tarr, P.W., Archer, D.H., and Utterbeck, N.G., [1974] Studies of Auroral Simulation, DNA 3937F, April, 1974 p. 32.
7. Stair, A.T., Jr., Ulwick, J.C., Baker, K.D., Baker, D.J., [1975] "Rocketborne Observations of Atmospheric Infrared Emissions in the Auroral Region", Atmospheres of Earth and the Planets, D.Reidel Pub. Co., Holland, 1975, p. 335.
8. Stair, A.T., Jr., [1976] "Cryogenic Spectrometry for the Measurement of Airglow and Aurora", Proc. Atmos. Radiometry, Vol. 91, August 1976, p. 71.

APPENDIX A

INSTRUMENTATION AND MEASUREMENT PLATFORM

The electro-optical instruments, which were used for the measurements reported herein, include two near infrared radiometers, two 3914A photometers, and an all sky camera. A discussion of the measurement platform and each instrument is presented in this appendix.

Measurement Platform

The instruments were operated from the AFGL Infrared Flying Laboratory. The flying laboratory is a modified Air Force NKC-135A aircraft which is similar in design and size to a Boeing 707 commercial aircraft.

All of the instruments viewed vertically out of the aircraft, and the center position of their fields of view were coaligned. Figure A.1 shows a pictorial view of the aircraft and the locations of the viewing windows.

The movement of the aircraft provides a means of spatially scanning the sky with the instruments. The scanning motion is predictable from the motion and maneuvers of the aircraft, since the instrumentation is mounted in a stationary manner to the flying platform. For the ICECAP measurement program, straight and level flights were maintained during the major portion of the measurement periods. Thus, the rate and direction of the scanning can be determined from the aircraft speed and heading, which is given in Appendix D for each of the reported measurements.

The aircraft provides a very convenient platform to accomplish auroral and airglow measurements. It has some definite advantages over ground sites, since it provides a means of selecting the viewing position of the instrumentation and a means of avoiding low altitude clouds and water vapor absorption. Also data measurements can be continuously performed for periods up

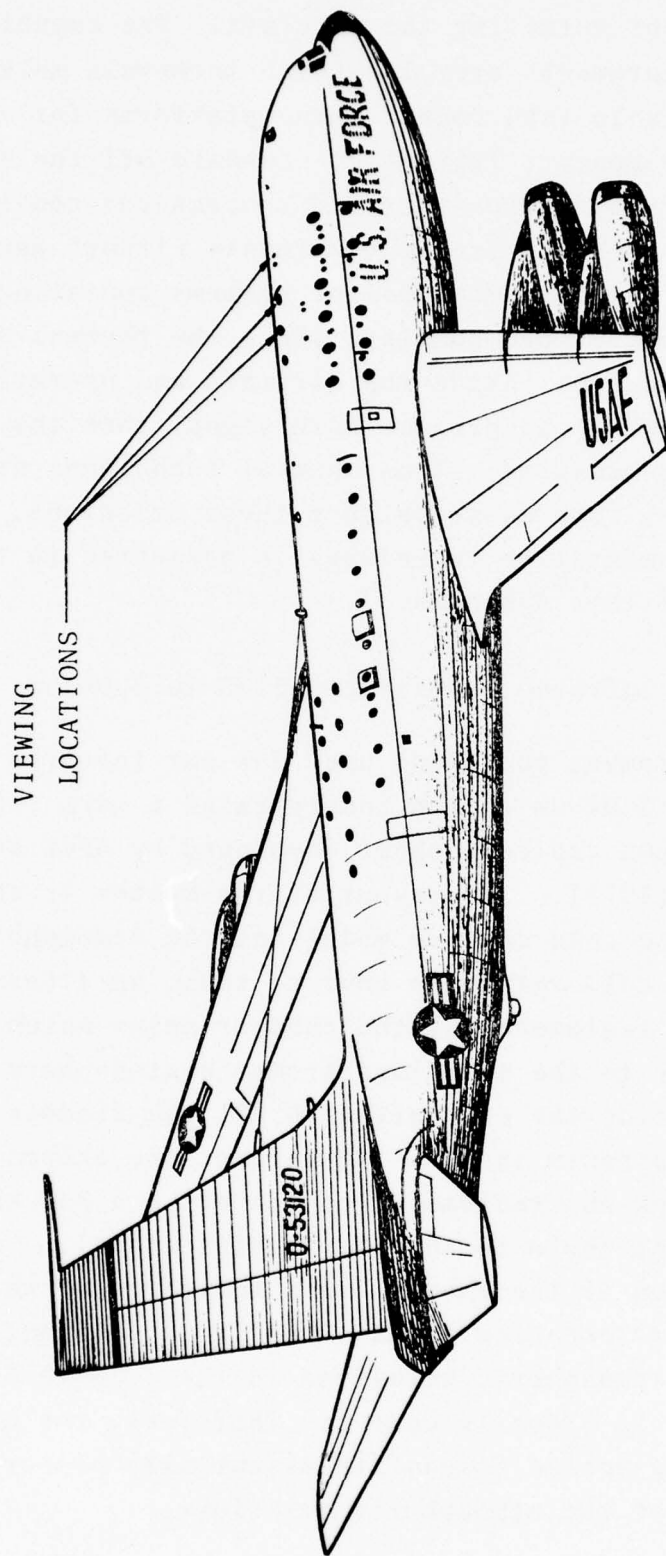


Figure A.1. Pictorial of the AFGL Flying Laboratory, NKC-135A, Serial Number 53120, showing the optical viewing locations which were used.

to 10 hrs without refueling the aircraft. The capability of performing measurements over long time intervals makes the platform more desirable than rocket-borne platforms for certain types of measurements. Typically, standard off the shelf visible instruments such as photometers and cameras can conveniently be mounted and operated from the aircraft without any major difficulties. However, measurement systems operating in the infrared region are more complex, since the thermal emissions of an instrument mounted inside the aircraft and operating at ambient temperature (300°K) can produce more signal than the atmospheric emissions being measured. Thus special techniques are necessary to discriminate, remove, or balance these emissions. A discussion of these instrumentation techniques is presented in the following two sections of this Appendix.

Near Infrared Radiometer, 2.75 to 3.04 μm

The measurement technique used for our infrared measurements in the 2.75 to 3.04 μm region incorporated a warm radiometer and a liquid nitrogen cooled chopper developed by AFGL and USU, *Huppi et al.*, [1974]. The layout of the system is shown in Figure A.2. The cold chopper modulates the atmospheric emission and provides a cold reference source; thus, an alternating signal is seen by the radiometer as the chopper spins which is due almost entirely to the emissions from the atmosphere. The chopper is mounted outside the aircraft with all the windows and the radiometer components inside. Therefore, the thermal emissions from the windows and radiometer components are not chopped, and they do not contribute to the alternating signal. However, the thermal emission of the chopper does introduce a small contribution to the alternating signal, but it is insignificant in comparison to atmospheric emissions in the 2.75 to 3.0 μm region if the chopper is properly cooled. Therefore, the magnitude of the alternating optical signal is essentially proportional to the intensity of the atmospheric emissions.

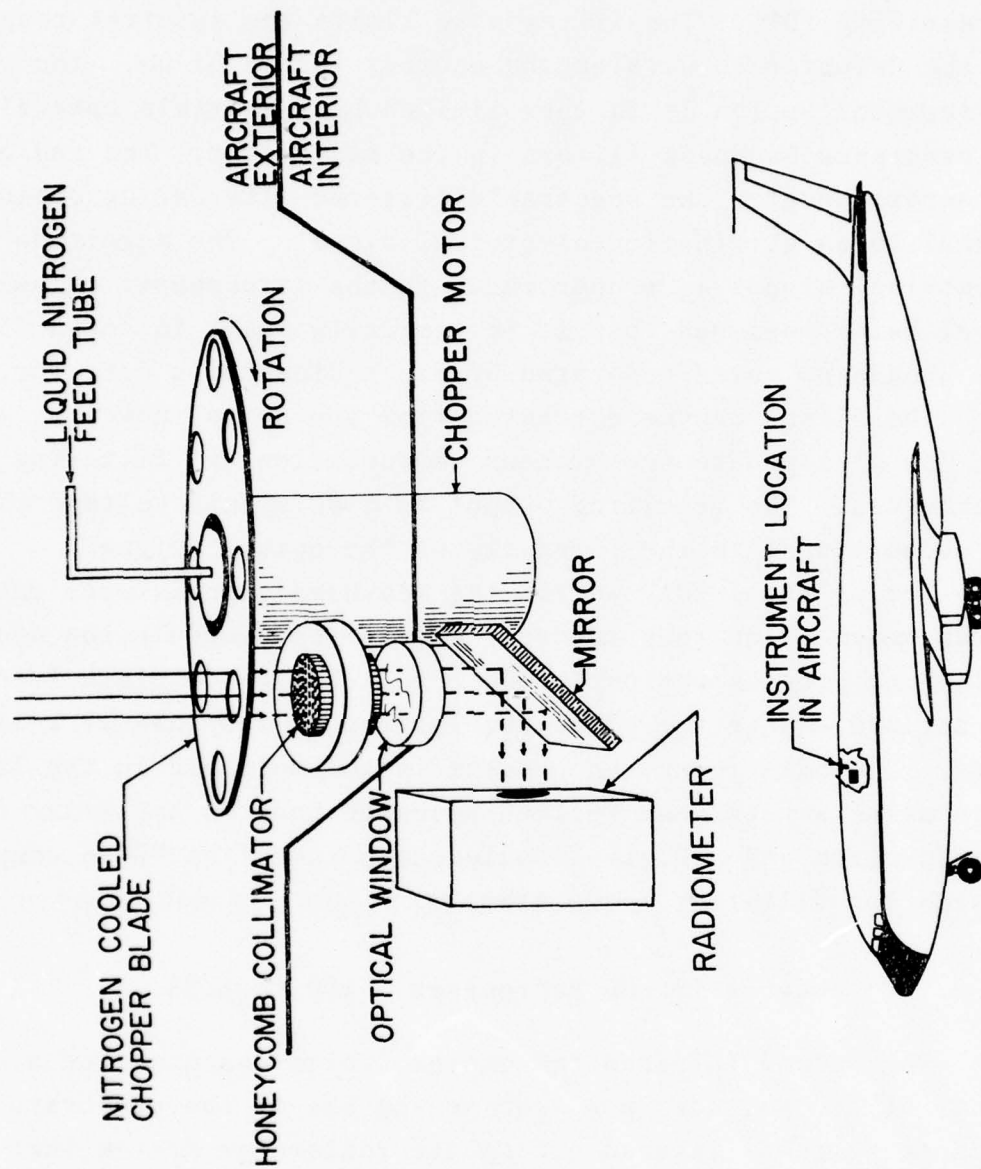


Figure A.2. Liquid nitrogen cooled chopper and radiometer system.

The radiometer collects the optical signal and focuses it onto a cold-filtered InSb detector. The cold filter reduces the background photon noise seen by the detector which improves its detectivity (D^*). The filter also limits the spectral response of the detector to wavelengths shorter than $3.04\text{ }\mu\text{m}$. The spectral measurement region is further limited by selectable optical interference bandpass filters in the radiometer. The radiometer's detector converts the spectrally filtered alternating optical signal to an alternating electrical signal. The magnitude of this electrical signal is proportional to the atmospheric emission level being measured, but it is typically small in comparison to the broadband noise generated by the radiometer's detector.

The signal can be extracted from the noise, however, through the use of standard synchronous demodulation and filtering techniques. The resulting output is a dc signal voltage which is proportional to the intensity of the optical signal.

During the ICECAP series the measured signals were recorded on an Ampex CP100 tape recorder before the demodulation and filtering process was performed. This leaves complete freedom to set and change the effective instrument response at a later date. The data reduction process is accomplished in the laboratory using a Princeton Applied Research Lock-In Amplifier for the demodulation and a Digital Equipment Corporation PDP-8 computer system for filtering, data storage, processing and plotting.

Near Infrared Radiometer, 1.0 to $1.75\text{ }\mu\text{m}$

The second infrared radiometer, which was used for measurements at $1.7\text{ }\mu\text{m}$, does not require the use of the elaborate cold chopper system. Instead a complete radiometer system that operates at ambient temperatures, except for the detector, has been developed by *Huppi* [1977]. The optical layout of this system is shown in Figure A.3.

The basic lens system consists of a 2-inch diameter, $f/2.5$ objective lens followed by a 1-inch diameter $f/.7$ field lens. In addition, the detector is immersed (deposited) on a third lens of

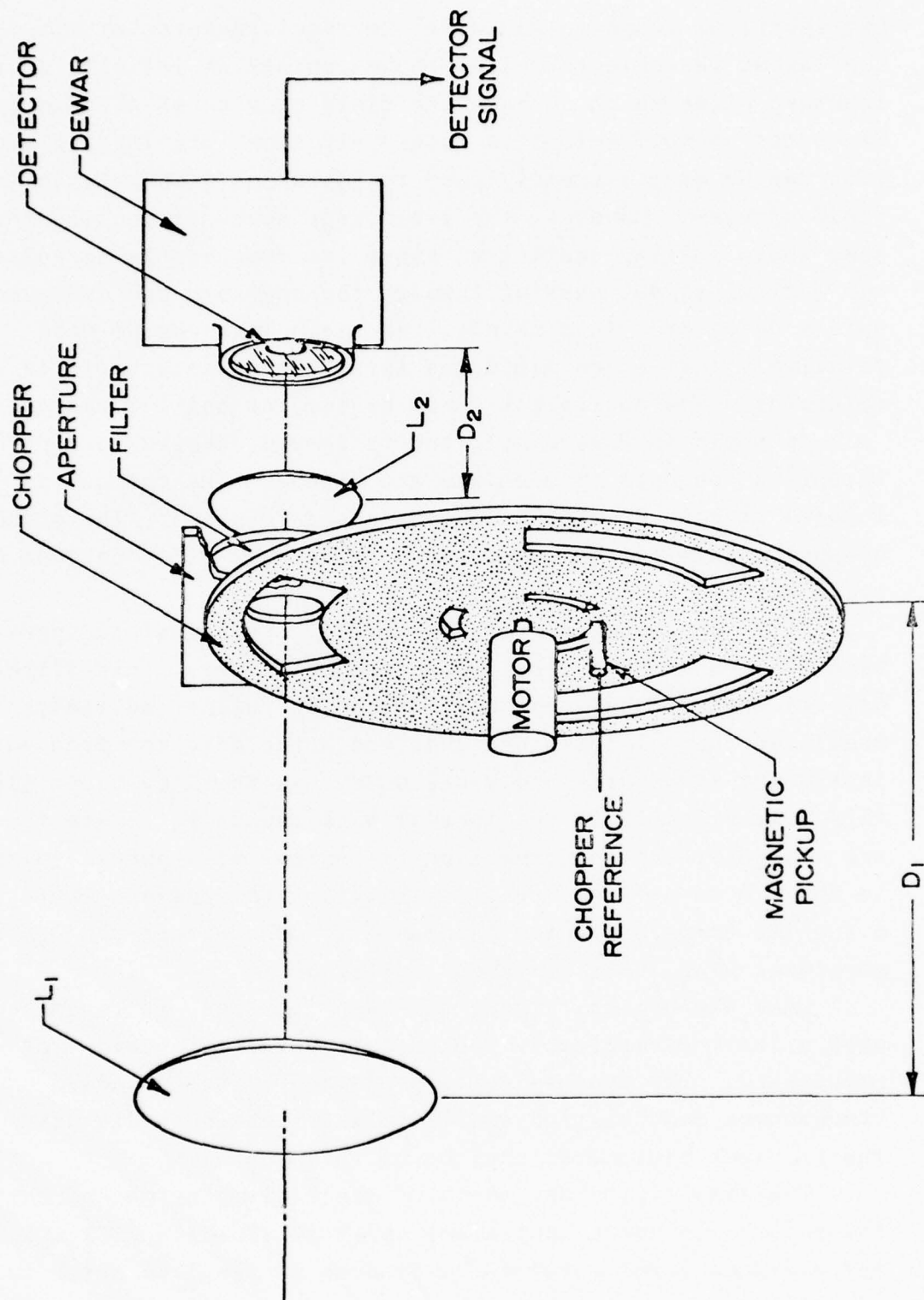


Figure A.3 Optical layout of 1.0 to 1.75 μm radiometer.

hemispherical shape to minimize the required detector size. In the layout the objective lens images points at infinity on the aperture plane which defines the field of view of the radiometer. Since the objective lens is relatively slow, its imaging properties can be made extremely good to guarantee a sharply defined field of view. However, the field lens does not require these same sharp imaging qualities, since its function is to collect the optical signal passing through the aperture and condense it onto a detector. As a result, the field lens can be made relatively fast which minimizes the required detector size and maintains a low equivalent f number for the optical system.

As shown in Figure A.3, the radiometer design incorporates an optical chopper to modulate the signal. The chopper is located within .025 inches of the aperture plane. The standard chopper modulates the complete aperture on a fifty percent duty cycle basis.

After the modulation is performed, the signal is spectral-band limited by an optical interference filter. This filter defines the spectral response of the instrument and limits the modulated thermal emissions that reach the detector from the instrument structures and background. As shown by *Huppi* [1977], this filter can limit the thermal backgrounds to levels that are insignificant in comparison to typical atmospheric emissions in the 1.0 to 1.75 μm region. This is also apparent in Figure A.4 which compares typical atmospheric OH overtone and $\text{O}_2(^1\Delta_g)(0,0)$ emissions with 300⁰K blackbody emissions.

Once the optical signal has been filtered, it is collected onto a thermoelectrically cooled detector and is ready for processing. The processing is performed by the standard synchronous demodulation and filtering techniques discussed in the previous radiometer section of this appendix.

The sensitivity and noise of the radiometer can be characterized by its noise equivalent spectral radiance NESR which is the radiance level required to produce a signal to noise ratio of one. The actual NESR for the radiometer has been measured at $9.3 \times 10^{-12} \text{ W/cm}^2 \text{ sr } \mu\text{m}$ for a .05 μm optical bandwidth, a 10⁰

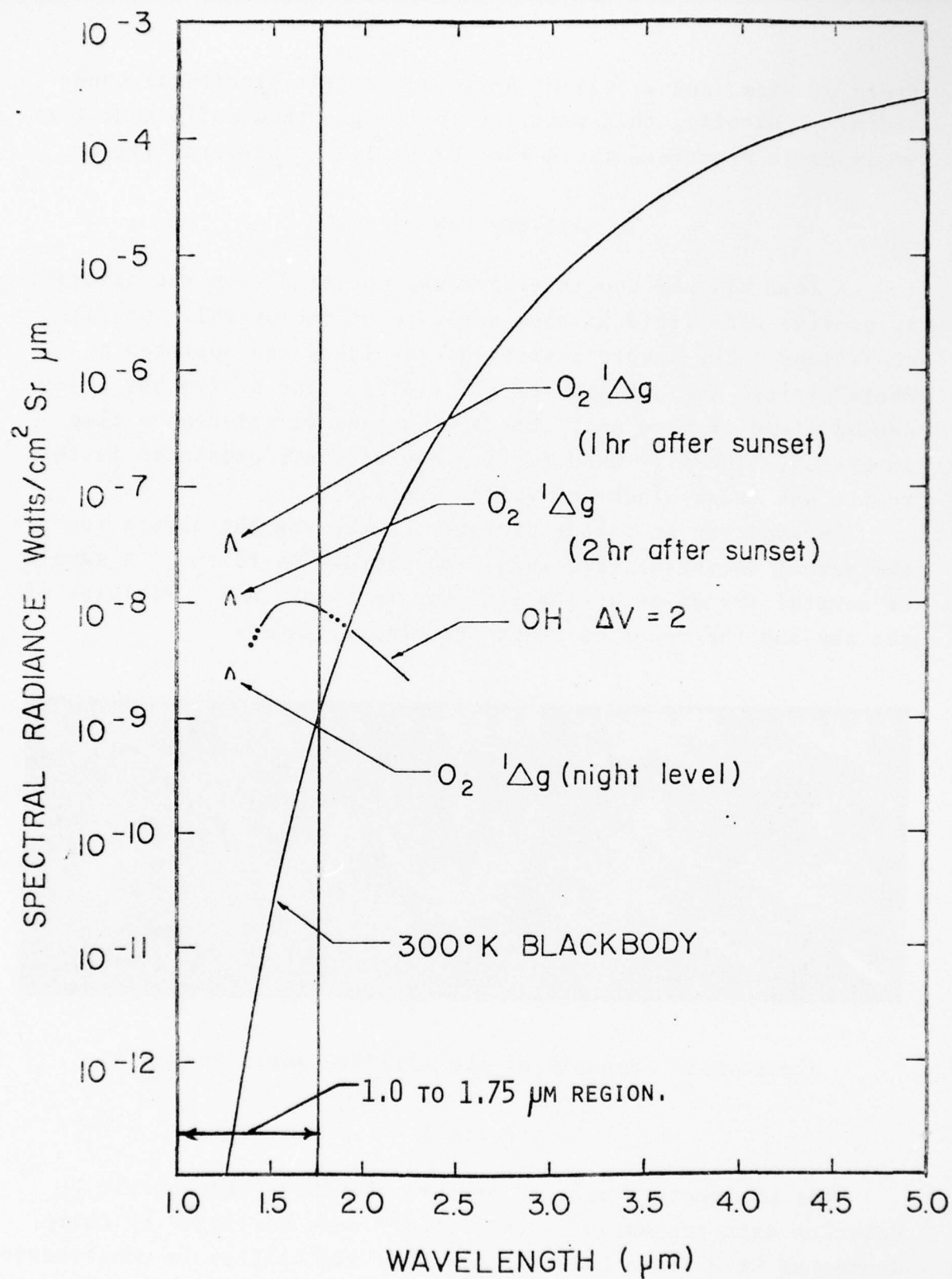


Figure A.4. Some typical upper atmospheric night airglow emission intensities compared with emissions from a 300°K blackbody.

field of view, and a .025 HZ noise equivalent electrical bandwidth. Typically, this sensitivity is more than sufficient for atmospheric measurements in the 1.2 to 1.7 μm spectral region.

All-Sky Camera

A 16mm all-sky camera system was operated from the aircraft to provide wide field of view coverage of the overall auroral conditions. The camera system was developed and operated by PhotoMetrics, Inc., *Kofsky et al.* [1975]. The system has a 160 degree field of view and takes photographs at selectable time intervals. The film used for the measurements presented in this report was Kodak black and white, Type 2475.

In addition to taking pictures of the sky the camera records the actual universal time when each picture is taken. A sample of several frames of a film is shown in Figure A.5. Pictures of the sky and the recorded times are clearly shown.

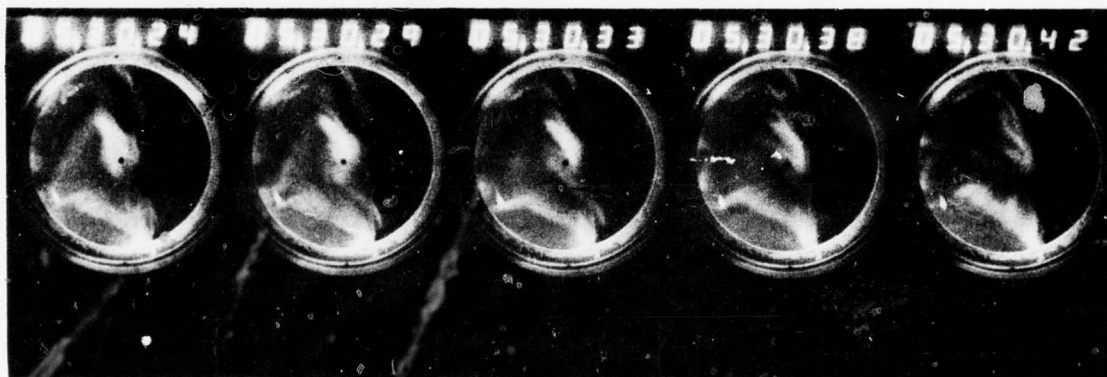


Figure A.5 Example of the All-Sky Camera Format.

Photometers

The photometers used to measure the 3914A atmospheric emission data presented in this report were developed by Larry Jensen of Utah State University. They are similar in construction to the type used for the ICECAP Rocket-borne Measurement Program.

A basic optical and electrical layout which is representative of the photometers is shown in Figure A.6. Basically the system consists of a filter to define the spectral bandwidth, a lens to condense the optical signal, an aperture to define the field of view, a photomultiplier to convert the optical signal to an electrical signal, and electronics to amplify and process the electrical signal. The complete optical head, consisting of the optics, the photomultiplier, the preamplifier, and the log amplifier, is contained in a 7-inch x 1.5 inch x 2.0 inch aluminum box. This small size made the photometers ideal for use in the aircraft, since they were easily mounted to the 1.7 μm radiometer.

Only one photometer was used during the 1975 measurements. It was operated with a 10° field of view, a 14A spectral bandwidth centered at 3914A, and a 40 HZ response time. The minimum detectable signal was limited by the dark current of the photomultiplier, the lower limit being 7 Rayleighs.

During the 1976 measurements, two additional photometers were added. They used the same design and had the same characteristics except one had a 5° field of view and the other had a 2° field of view. They were included to give increased spatial resolution. They were specifically selected to match the additional field of view options of the 2.75 to 3.04 μm radiometer.

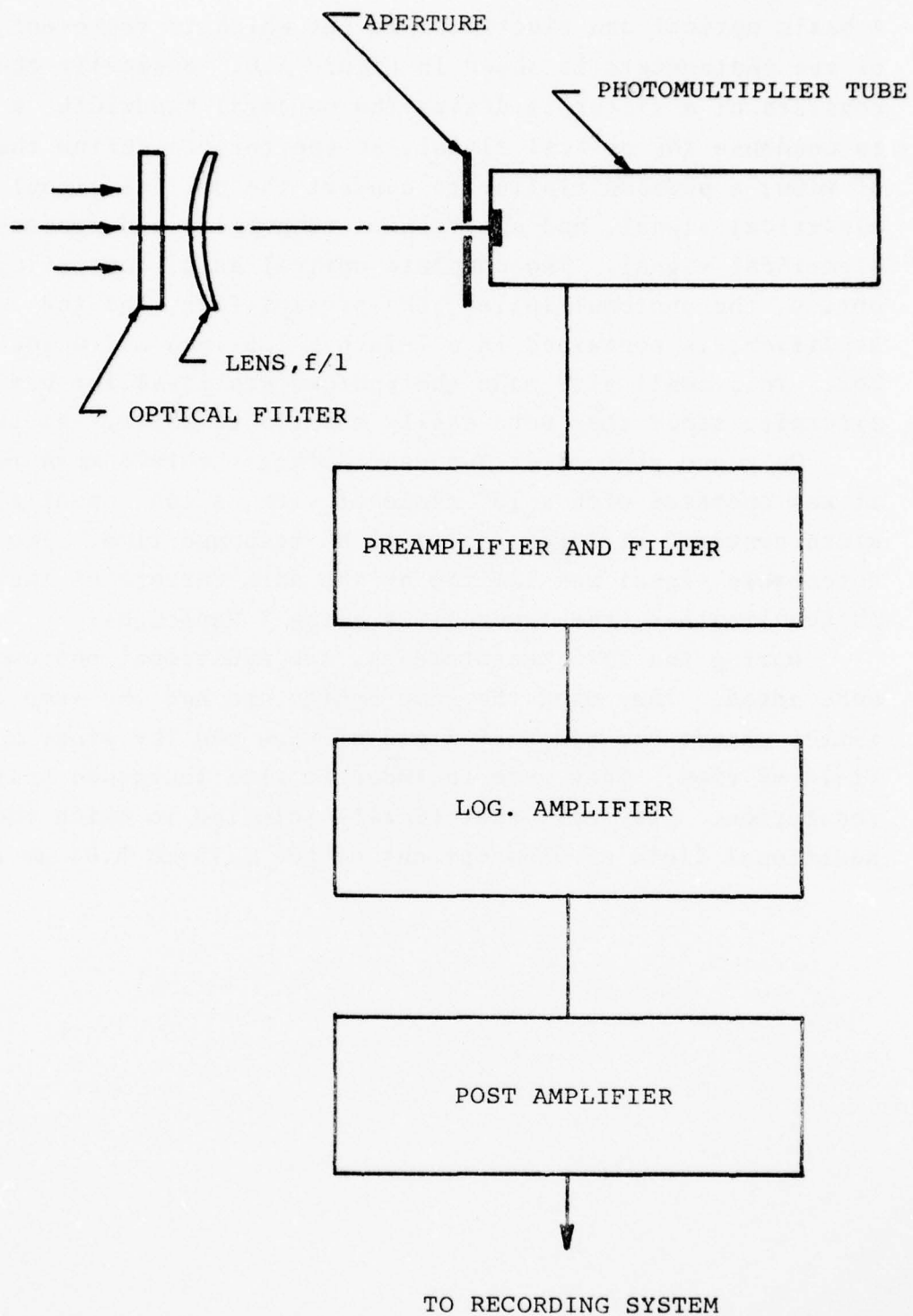


Figure A.6 Optical and Electrical Layout of 3914A Photometer.

APPENDIX B

COORDINATION OF AIRCRAFT MEASUREMENTS AND CHATANIKA RADAR MEASUREMENTS

The Chatanika incoherent scatter radar system, operated by Stanford Research Institute, provides altitude information and densities of the charged particles creating an aurora. Since it is desirable to study the altitude dependencies of the enhanced infrared emissions, an attempt was made to coordinate some scans of the radar system with the aircraft flight plans. The coordination was only attempted in the 1976 measurement series; and since the radar system was also supporting the rocket launches, only a limited amount of coordination was possible. Table B.1 summarizes the type and quality of the coverage provided by the radar system for the various aircraft flights as reported by *Kořsky et al.* [1977]. This summary along with the aircraft data presented in this report should provide a starting place for the altitude dependence analysis of the infrared emissions.

TABLE B.1. SUMMARY OF MEASUREMENT MODES OF THE DNA 617 BACKSCATTER RADAR FOR THE NIGHTS OF THE 1976 AIRCRAFT MEASUREMENTS.

DATE	RADAR MODE	TIME	OVERLAP ON AIRCRAFT
28 FEB	PRE-PLANNED MERIDIAN SCANS*	0801-0940	VERY GOOD
	TRUNCATED ** MERIDIAN SCANS	0943-1001	FAIR
	3-POSITION ⁺	1001-1220	POOR
29 FEB	TRUNCATED MERIDIAN SCANS	0720-0929	FAIR. A/C 60 n.m. W
	3-POSITION	0931-1210	POOR W
01 MAR	3-POSITION	0551-0942	POOR
	TRUNCATED MERIDIAN SCANS	0943-1103	FAIR. A/C W
	3-POSITION	1103-1250	POOR
03 MAR	TRUNCATED MERIDIAN SCANS	0510-0720	MAY BE GOOD
	3-POSITION	0723-	A/C LANDING
07 MAR	3-POSITION	0624-0910	A/C TAKEOFF
	TRUNCATED MERIDIAN SCANS	0912-1049	MAY BE GOOD
	3-POSITION	1049-	
08 MAR	3-POSITION	0630-0927	POOR
	TRUNCATED MERIDIAN SCANS AZ 044 ⁰ T after 0938	0927-1211	MAY BE GOOD
26 MAR	8-POSITION ⁺⁺	0644-0911	FAIR
	TRUNCATED MERIDIAN SCANS	0917-1017	FAIR
	AZ 044 ⁰ T, 36 ⁰ to 90 ⁰ El		
	3-POSITION, NOT AS ABOVE ⁺⁺⁺	1017-1140	FAIR
	TRUNCATED MERIDIAN SCANS AZ 044 ⁰ T, 36 ⁰ TO 90 ⁰ El	1140-1208	FAIR

* SCANS DESIGNED TO OVERLAP THE AIRCRAFT FLIGHT PROFILE.

** GENERALLY FROM $\sim 100^{\circ}$ TO $\sim 30^{\circ}$ El (MEASURED FROM N HORIZON) ON 029⁰T AZIMUTH.

+ 67⁰ ELEVATION(MEASURED FROM N HORIZON), 029⁰, 154⁰, 264⁰T. THE ANTENNA IS MOVED EACH 3 MIN, AND THE A/C FIELD MAY FORTUITOUSLY INTERCEPT THE REGION IT MEASURED.

++ 76.5⁰, 209⁰; 62⁰, 272⁰; 52⁰, 280⁰; 76.5⁰, 209⁰; 62⁰, 145⁰; 52⁰, 137⁰; 76.5⁰, 209⁰; 62⁰, 209⁰, with 2 min dwell.

+++ 63.2⁰, 044⁰; 62⁰, 270⁰; 62⁰, 148⁰, with ~ 3 min dwell.

APPENDIX C

ADDITIONAL INFRARED ENHANCEMENT DATA

Additional data measured during the 1975 and 1976 ICECAP aircraft-borne measurements are cataloged in this section. A significant amount of data showing auroral enhancements is given. For completeness, data are also given for cases where the auroral enhancements were minimal.

Brief descriptions of the data are itemized in Table C.1. Significant or peculiar features of each piece of data are mentioned.

TABLE C.1. TABLE OF FIGURE DESCRIPTIONS

<u>Figure No.</u>	<u>Description</u>
C.1	March 1, 1976. From top to bottom the figure gives the aircraft latitude, the aircraft longitude, the data at 3914A, 2.8 μm , and 1.70 μm . Noteable enhancements were seen in the 2.8 μm region which appear to be directly correlated with 3914A(N_2^+) enhancements. This data is of significance because the F.O.V. of the photometer and the 2.8 μm radiometer were decreased from 10° to 5° . This provides a higher spatial resolution measurement. However, it should be noted that the spectral bandwidth of the 2.8 μm channel was increased to give additional signal to compensate for the signal decrease which resulted from the decreased field of view.
C.2	The data measured March 1, 1976 from 0930 to 1000 is plotted on an expanded time scale. A direct correlation between the 3914A(N_2^+) emissions and the 2.8 μm emissions during the enhancement at 0945 UT is apparent.

- C.3 The data measured March 1, 1976 from 1015 to 1115 UT is plotted on an expanded time scale. Direct correlations between the 3914A enhancements and the $2.8 \mu\text{m}$ enhancements at 1029 UT and 1150 UT are apparent. Also there appear to be enhancements in the $1.70 \mu\text{m}$ OH data, but they do not appear to be directly correlated with the visible aurora as monitored by the 3914A photometer.
- C.4 The presented data was measured March 3, 1976 with the instrumentation viewing vertically with a 10° FOV. The data was measured through a sunset transition period, and as a result the $1.70 \mu\text{m}$ and 3914A data were dominated by solar scatter at early times. At later times, from 0500 to 0525, large enhancements of the $2.94 \mu\text{m}$ emissions were seen. These enhancements are directly correlated with enhancements in the 3914A emissions. Also at 0508 an enhancement occurred in the $1.7 \mu\text{m}$ channel. It is probable that these emissions are due to the Meinel system of $\text{N}_2^+(\text{A}^2_{\pi_u} \rightarrow \text{X}^2_{\Sigma_g^+})$ and the first positive bands of $\text{N}_2(\text{B}^3_{\Pi_g} \rightarrow \text{A}^3_{\Sigma_u^+})$ which slightly contaminate the selected $1.7 \mu\text{m}$ hydroxyl band.
- C.5 The data measured March 3, 1976 from 0450 to 0530 is plotted on an expanded time scale. Significant directly correlated enhancements are seen in the 3914A (N_2^+) data and the $2.94 \mu\text{m}$ data at 0503, 0508, and 0520. Some variations are also apparent in the $1.7 \mu\text{m}$ (OH) channel. A $1.7 \mu\text{m}$ enhancement at 0508 appears to be somewhat correlated with the visible aurora, but the enhancement lasts slightly longer than the $2.94 \mu\text{m}$ and 3914A enhancement. Perhaps the $1.7 \mu\text{m}$ enhancement can be explained by enhancements of the Meinel system of $\text{N}_2^+(\text{A}^2_{\pi_u} \rightarrow \text{X}^2_{\Sigma_g^+})$ and the first positive bands of $\text{N}_2(\text{B}^3_{\Pi_g} \rightarrow \text{A}^3_{\Sigma_u^+})$ which

slightly contaminate the selected $1.7\text{ }\mu\text{m}$ hydroxyl band.

C.6 Data measured March 3 under sunlit conditions and through a sunset transition are presented. In addition to the standard data format, the solar elevation angle is given as in Fig. C.4 for various positions and times. From the figure, it should be noted that the levels of the 3914A data and the $1.7\text{ }\mu\text{m}$ data are dominated by solar scatter at early times. However the $2.94\text{ }\mu\text{m}$ channel is not dominated nearly as much by the solar scatter. For example at 0310 the solar elevation angle is about minus 1 degree and the $2.94\text{ }\mu\text{m}$ signal level is not significantly larger than the value measured under night sky conditions. It should be remembered that sunset at a 100 km altitude occurs at minus 11.5 degrees solar elevation angle. Thus, it appears that one could readily measure $2.9\text{ }\mu\text{m}$ enhancements under sunlit conditions from the NKC-135 aircraft during a period when the solar elevation angle is between 0 degrees and minus 11.5 degrees. In fact, significant enhancements similar to those shown in Figure C.5 should be detectable even at larger solar elevation angles. For example, on March 3 a 200 kR enhancement would have increased the signal about 25% at a time of 0226 which corresponds to 7 degrees solar elevation.

C.7 Data measured March 8, 1976 are presented. The data has many directly correlated enhancements between the $2.94\text{ }\mu\text{m}$ data and the 3914A (N_2^+) data. Several small increases occur in the $1.7\text{ }\mu\text{m}$ (OH) channel. Some of the OH increases result from increased optical viewing depth of the OH layer which occurs during aircraft turns. The other small increases probably result from enhancements of the Meinel N_2^+

system and the N_2 first positive bands which slightly contaminate the selected OH bands.

C.8 The presented data was measured March 2, 1975. Only small enhancements of the 3914A (N_2^+) emissions were seen. No significant enhancements in the 2.83 μm emissions were observed above the OH background. The general behaviors of the 2.83 μm emissions and the 1.7 μm emissions are similar. Therefore, the 2.83 μm emissions are mainly a measurement of the OH fundamental sequence.

C.9 Data measured on March 11, 1975 are presented. Some enhancements in the 3914A (N_2^+) emissions are apparent. Enhancements in the 2.83 μm data, which are correlated with the 3914A data, are detectable but are not large in comparison to the OH background at 2.83 μm . The 1.7 μm OH data has an interesting increase which is centered at 0825 UT. This increase does not appear in the 2.83 μm data as one might expect.

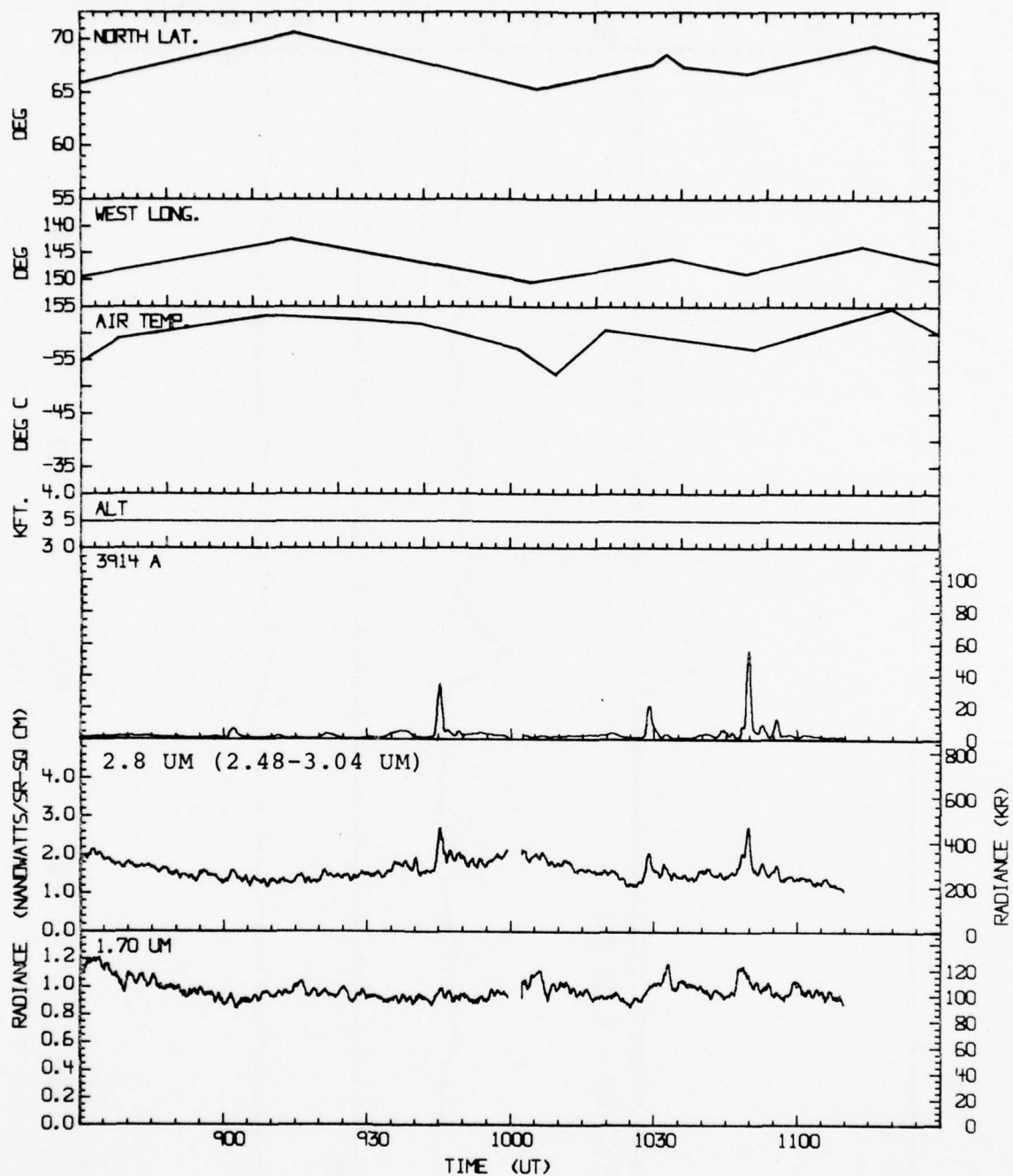


Figure C.1 Measured data for March 1, 1976 showing significant infrared enhancements which are correlated with aurora.

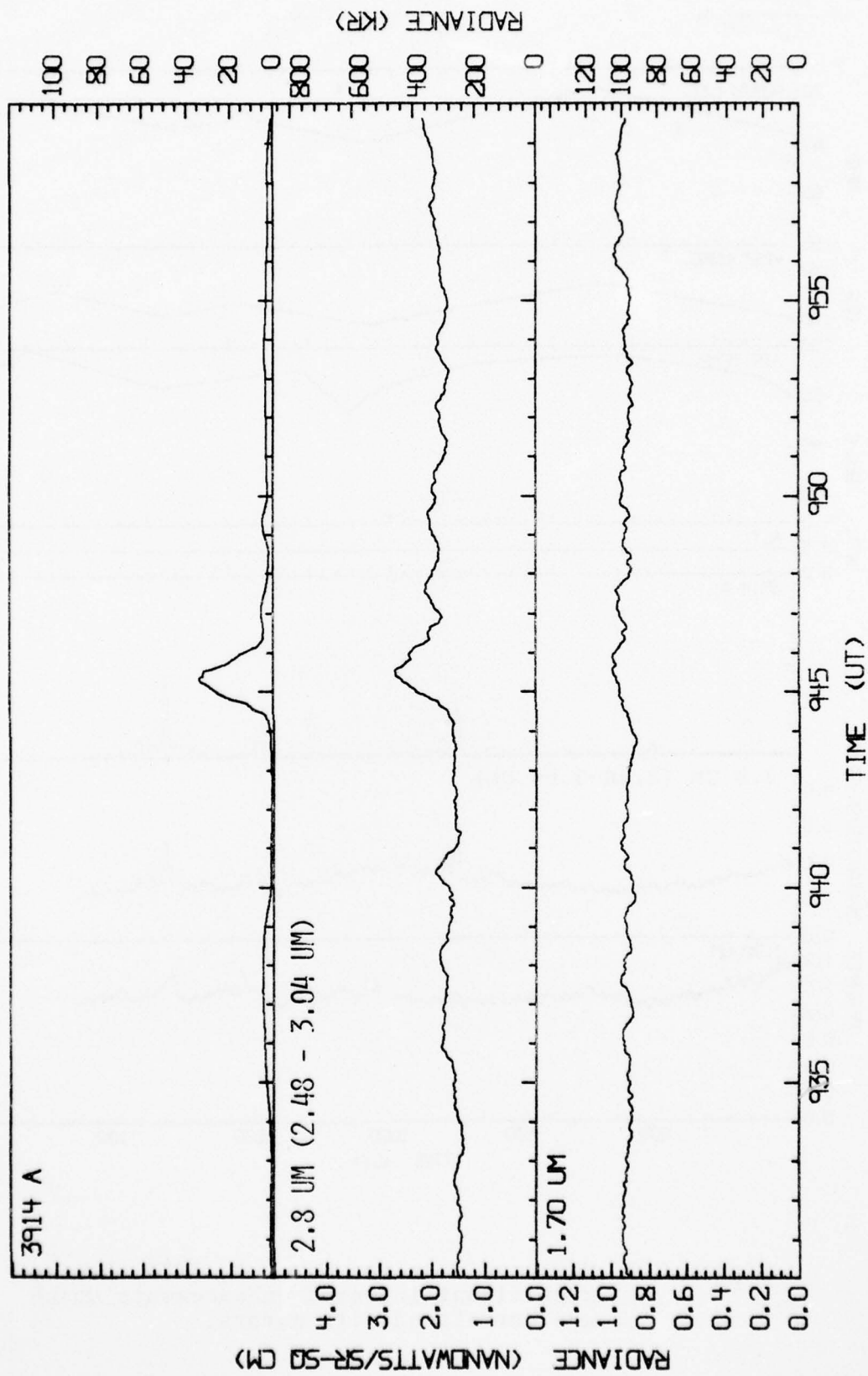


Figure C.2 Measured data for March 1, 1976 from 0930 to 1000 UT plotted on an expanded time scale to illustrate the temporal and spatial correlation between the emissions.

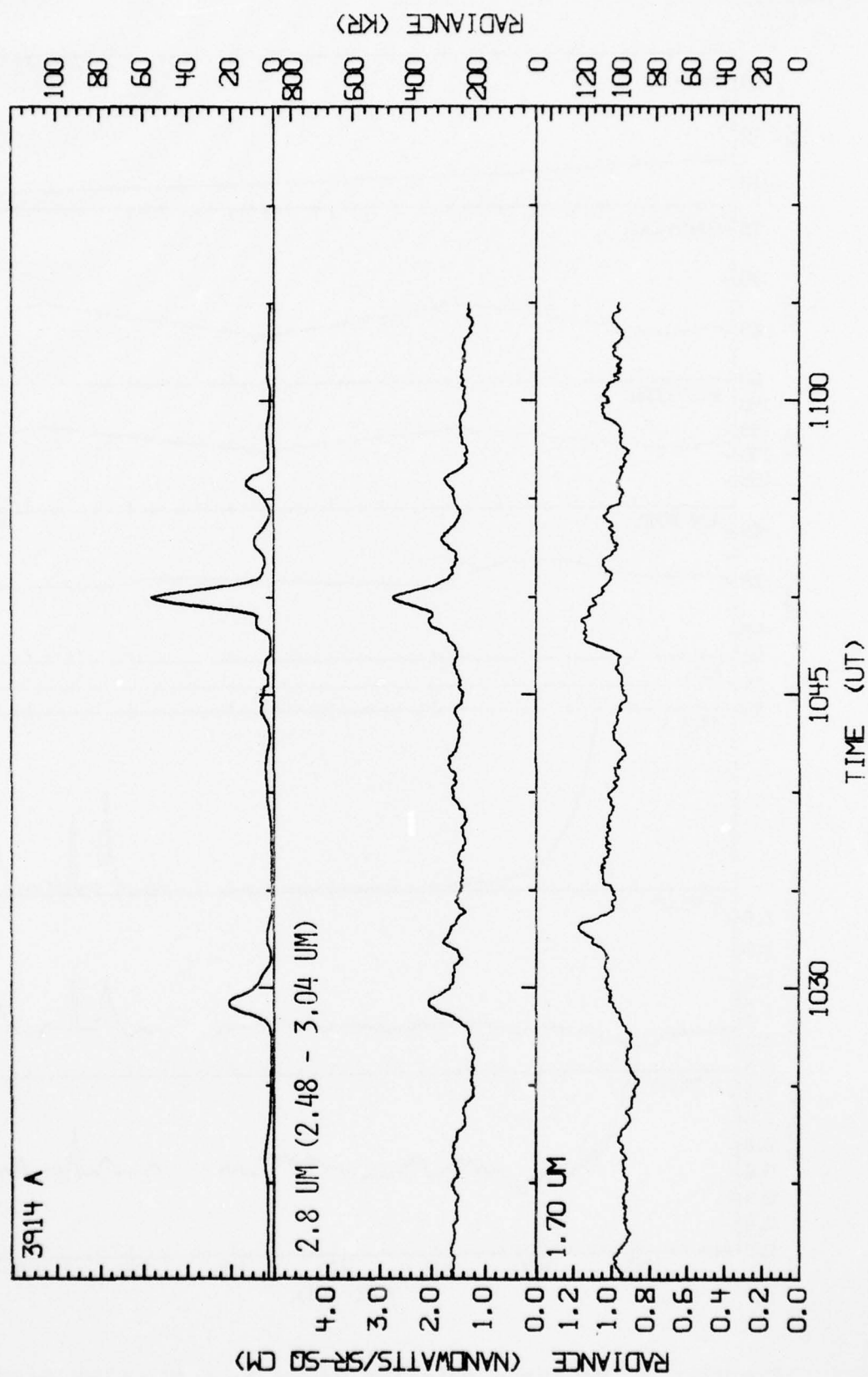


Figure C.3 Measured data for March 1, 1976 from 1015 to 1115 UT plotted on an expanded time scale to illustrate the temporal and spatial correlation between the emissions.

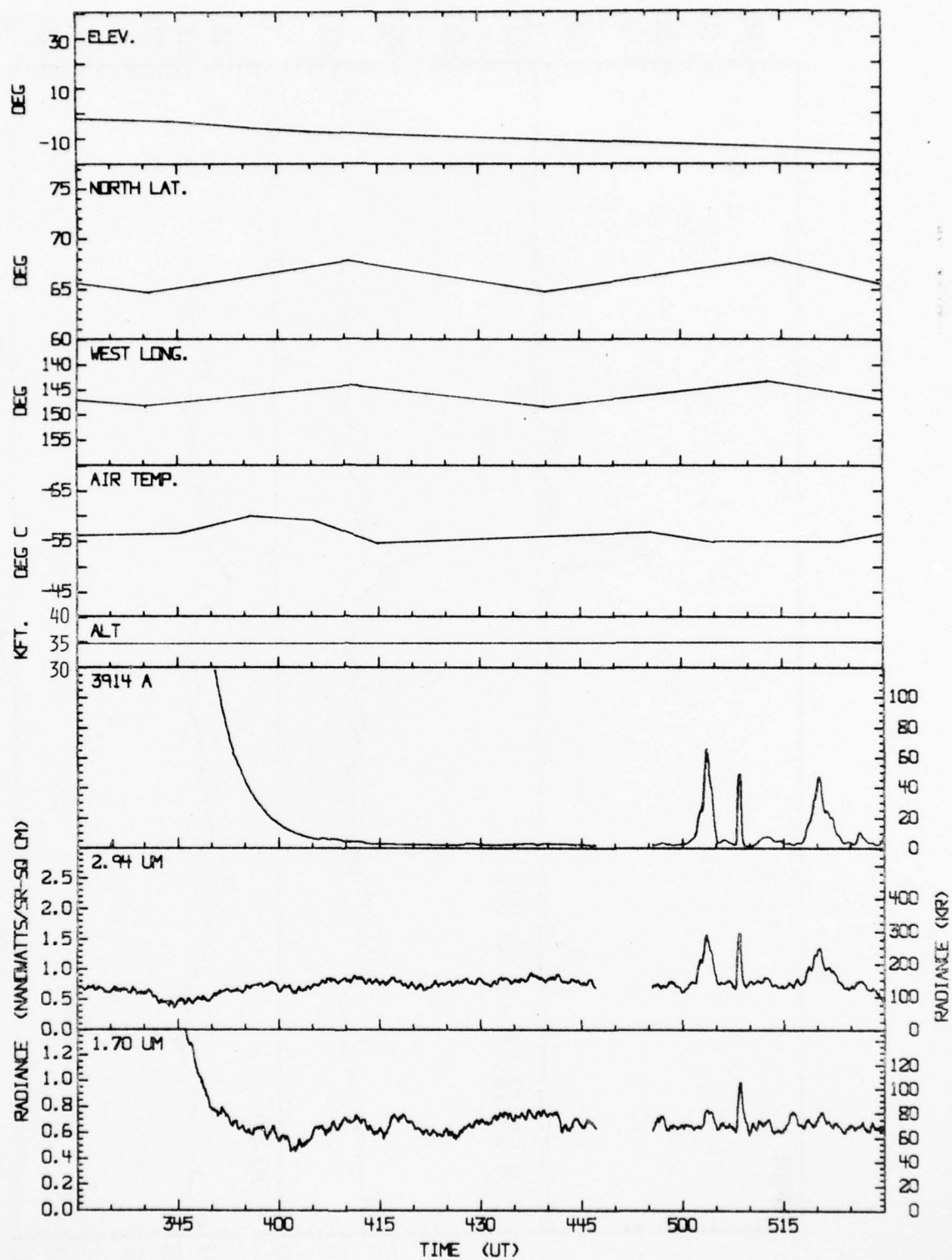


Figure C.4 Measured data for March 3, 1976 which includes significant auroral enhancements and a sunset transition.

3 MAR 76 IC76-6

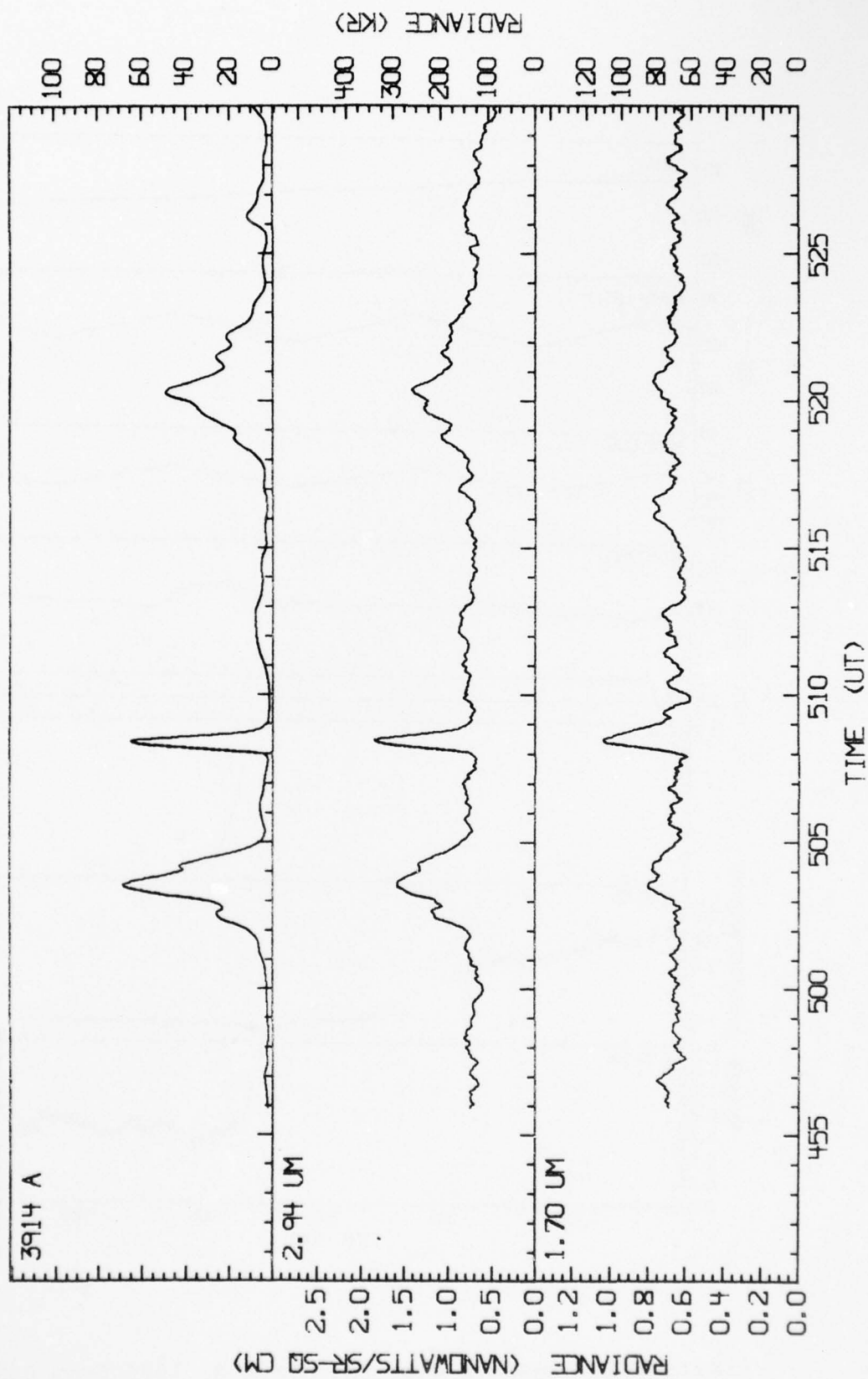


Figure C.5 Measured data for March 3, 1976 from 0450 to 0530 plotted on an expanded time scale to illustrate the temporal and spatial correlation between the emissions.

AD-A051 454

UTAH STATE UNIV LOGAN ELECTRO-DYNAMICS LAB
AIRCRAFT BORNE MEASUREMENTS OF INFRARED ENHANCEMENTS DURING ICE--ETC(U)
SEP 77 R J HUPPI, J W REED

F/G 4/1

F19628-74-C-0190

UNCLASSIFIED

EDL-SRL-77-2

AFGL-TR-77-0232

NL

2 OF 2

AD
A051454



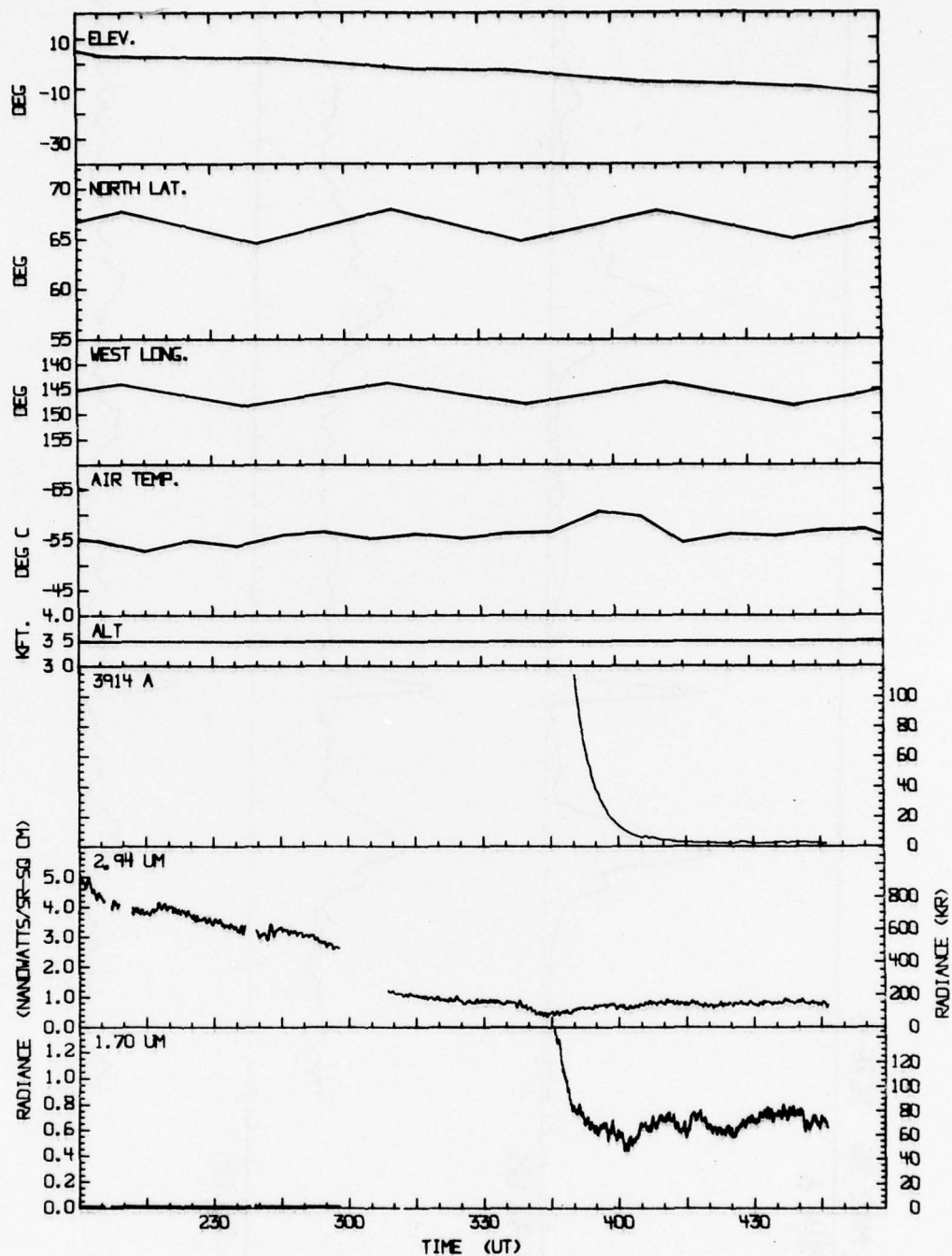


Figure C.6 Measured data for March 3, 1976 from 0200 to 0500 showing intensities during daylight and sunset transition conditions.

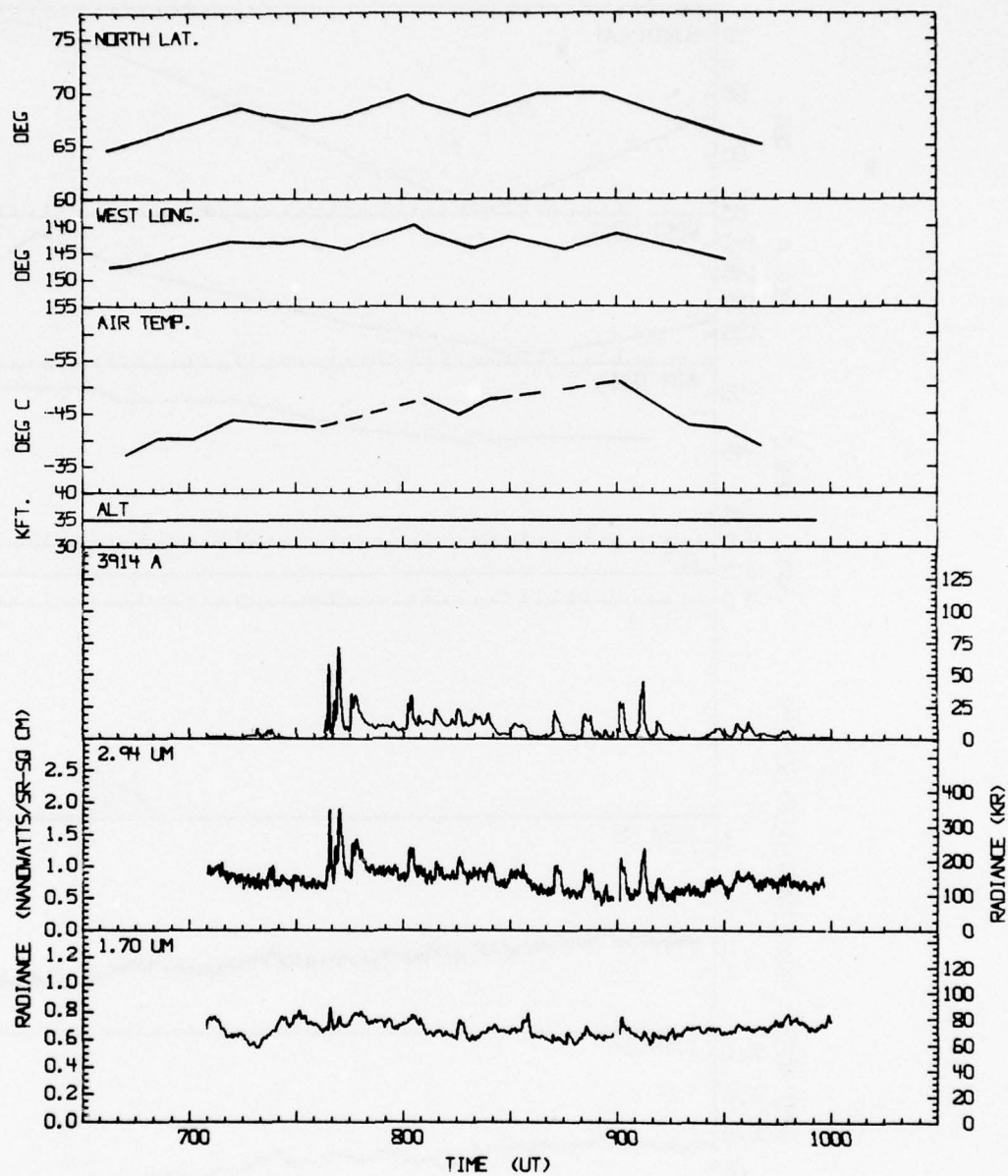


Figure C.7 Measured data for March 8, 1976 showing significant infrared enhancements which are correlated with the aurora.

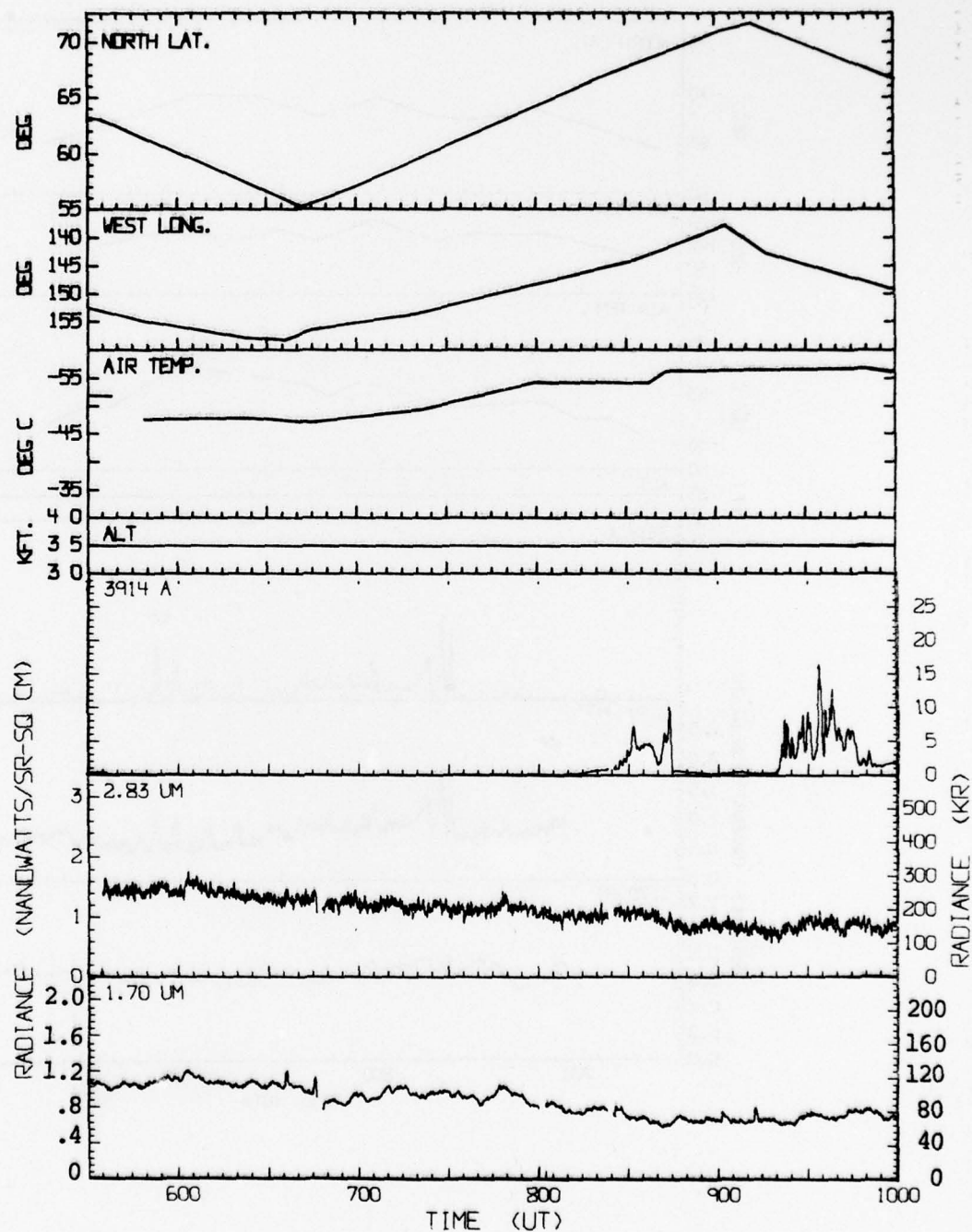


Figure C.8 Measured data for March 2, 1975 showing correlation between the 2.83 μm emissions and the 1.7 μm (OH) emissions during a period when the auroral activity was minimal.

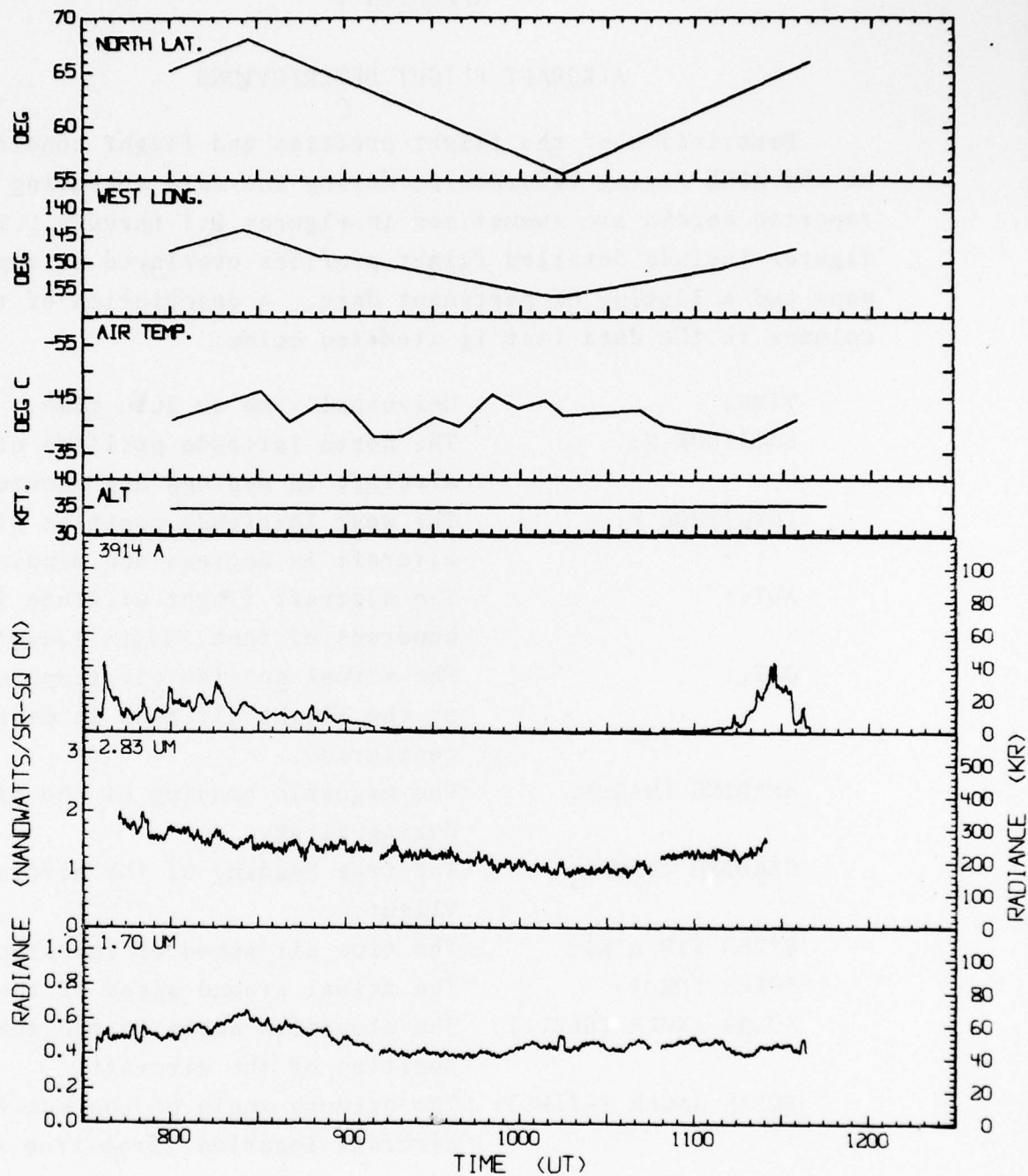


Figure C.9 Measured data for March 11, 1975 showing small enhancements in the 3914A and 2.83 μm emissions.

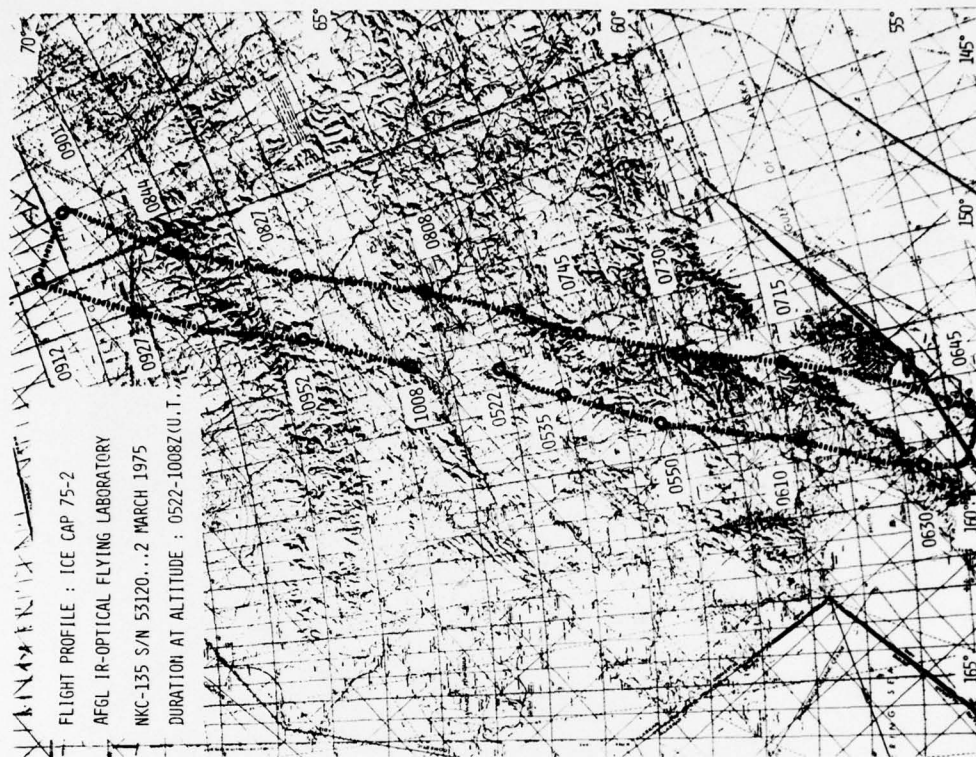
APPENDIX D

AIRCRAFT FLIGHT DESCRIPTIONS

Description of the flight profiles and flight conditions of the AFGL Flying Laboratory, during the data measuring periods reported herein are summarized in Figures D.1 through D.9. The figures include detailed flight profiles overlayed on topographical maps and a listing of pertinent data. A description of the various columns in the data list is itemized below:

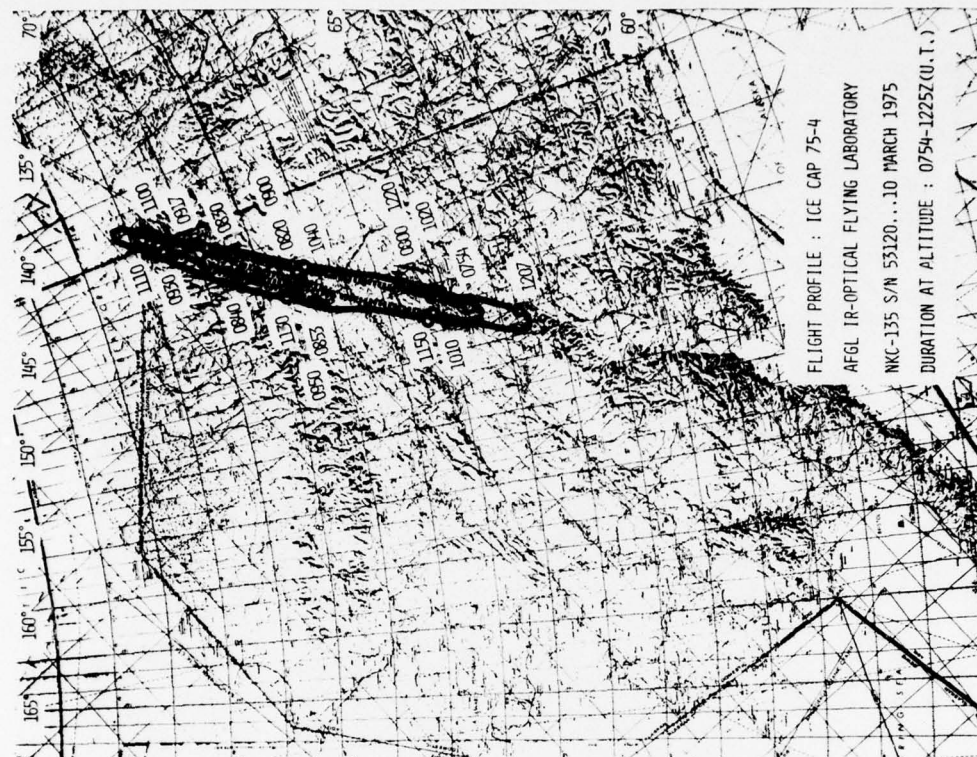
TIME:	Universal time or Zulu time.
LATITUDE N:	The north latitude position of the aircraft in degrees and minutes.
LONGITUDE W:	The west longitude position of the aircraft in degrees and minutes.
ALT.:	The aircraft flight altitude in hundreds of feet (Flight Level).
OAT.:	The actual <u>outside air temperature</u> at the flight altitude in degrees centigrade.
HEADING (MAG.):	The magnetic heading of the aircraft during flight.
HEADING (TRUE):	The true heading of the aircraft during flight.
SPEED (TR.AIR):	The true air speed of the aircraft.
SPEED (GRD):	The actual ground speed of the aircraft.
SOLAR ANGLE (ELEV.):	The elevation angle of the sun at the position of the aircraft.
SOLAR ANGLE (AZIM.):	The azimuth angle of the sun from the aircraft location (from true north).

The data presented in the figures were derived from the actual flight logs taken by the aircraft navigator during the flights. It is presented as an additional aid for understanding the data presented herein.



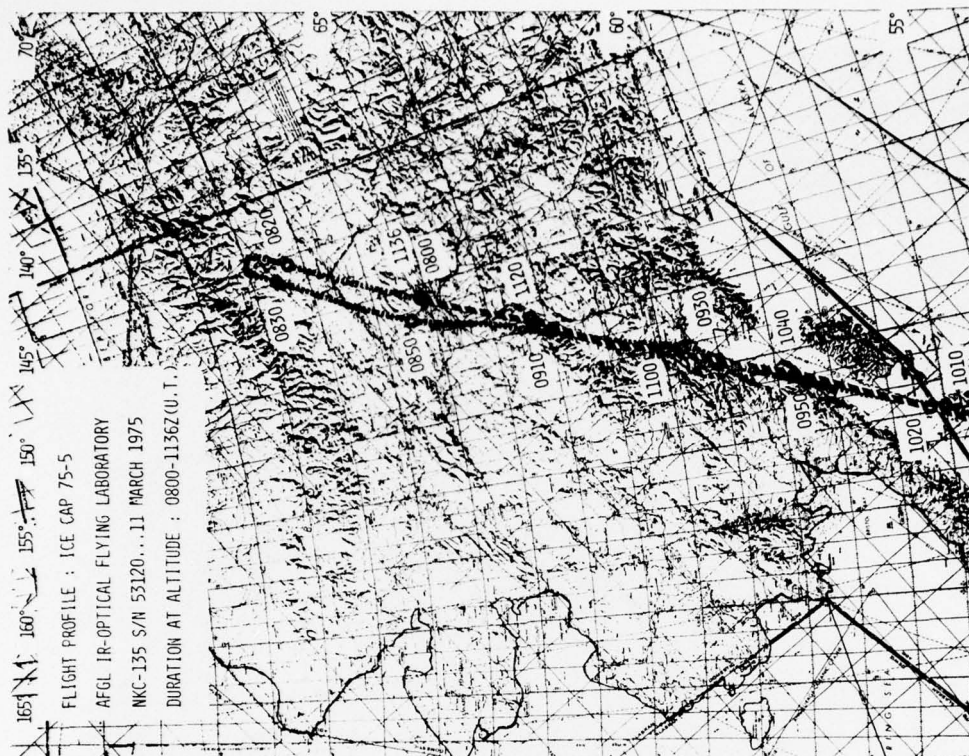
MISSION: ICECAP 75-2				EIL/EIL				DATE: 2 March 1975			
TIME	LATITUDE	LONGITUDE	ALTITUDE	QAT	HEADING	SPEED	SOLAR ANGLE	TIME	HEADING	SPEED	SOLAR ANGLE
Z	N	W	FL	°C	°	KTS	°	Z	°	KTS	°
1 0459	64 40	147 06	170	-	289	317	380	0912	289	317	380
2 0511	64 58	148 54	247	-44.0	200	226	400	0927	200	226	400
3 0522	64 04	151 13	350	-54.0	200	225	450	0949	200	225	450
4 0527	63 39	152 10	350	-52.0	178	202	450	0952	178	202	450
5 0535	63 00	152 50	350	-53	-	-	420	0953	-	-	420
6 0539	62 26	153 33	350	-52.0	178	202	450	0954	178	202	450
7 0550	61 20	154 41	350	-47.5	179	202	450	0955	179	202	450
8 0600	60 02	155 29	350	-48.0	176	198	450	0956	176	198	450
9 0610	58 51	156 15	350	-48.0	176	197	450	0957	176	197	450
10 0625	57 13	157 32	350	-48.0	180	200	450	0958	180	200	450
11 0630	56 36	157 47	350	-47	-	202	445	0959	-	202	445
12 0635	55 59	157 57	350	-47.5	180	200	450	0960	180	200	450
13 0645	55 35	156 17	350	-46.5	000	022	450	0961	000	022	450
14 0650	55 56	155 49	350	-48.0	000	022	445	0962	000	022	445
15 0700	57 04	154 41	350	-48.5	358	019	480	0963	358	019	480
16 0715	58 54	153 25	350	-49.0	352	014	485	0964	352	014	485
17 0730	60 42	152 12	350	-51.0	352	015	476	0965	352	015	476
18 0738	61 41	151 20	350	-52	-	-	460	0966	-	-	460
19 0745	62 28	150 34	350	-52.0	358	024	476	0967	358	024	476
20 0800	64 08	148 20	350	-54.5	359	026	475	0968	359	026	475
21 0808	65 02	147 21	350	-53.5	351	019	474	0969	351	019	474
22 0827	67 14	144 54	350	-54.0	351	022	475	0970	351	022	475
23 0838	68 23	143 10	350	-54	-	032	-	0971	-	032	-
24 0844	69 04	142 00	350	-56.0	360	034	470	0972	360	034	470
25 0851	69 46	140 27	350	-56.5	002	038	473	0973	002	038	473
26 0901	70 45	137 56	350	-56.5	268	306	473	0974	268	306	473
27 0908	71 14	139 30	350	-57	-	-	450	0975	-	-	450
28 0912	71 35	140 39	350	-56.5	268	306	475	0976	268	306	475
29 0927	70 10	144 00	350	-56.5	168	202	474	0977	168	202	474
30 0938	68 59	146 05	350	-55	-	-	455	0978	-	-	455
31 0939	68 52	146 14	350	-56.5	173	205	474	0979	173	205	474
32 0952	67 26	147 47	350	-56.5	173	203	474	0980	173	203	474
33 1006	-	-	-	-	-	-	-	0981	-	-	-
34 1008	65 40	150 11	350	-55	178	206	474	0982	178	206	474
35 1110	64 40	147 06	LAND	-	-	-	-	0983	-	-	-

Figure D.1. Flight description for measurements performed 2 Mar 75.



MISSION: ICECAP 75-4				DATE: 10 MARCH 1975			
				EIL/FILE			
TIME	LATITUDE	LONGITUDE	ALT.	TRUE	HEADING	SPEED	SOLAR ANGLE
Z	O	N	FL.	O	O	KTS	O
1 0716	64 40	147 06	170	-	-	-	-23.1 315.1
2 0728	64 36	149 05	170	-	-	-	-23.4 316.2
3 0754	64 30	148 22	350	45.5	031	430	-25.5 323.7
4 0800	65 09	147 30	350	47.5	002	030	-25.5 326.4
5 0810	66 12	146 03	350	50.5	002	031	-25.5 331.0
6 0820	67 21	144 37	350	57.5	002	033	-25.1 335.4
7 0830	68 24	142 58	350	59.5	002	031	-24.8 340.1
8 0832	68 37	142 33	350	59.0	175	207	-24.6 341.1
9 0840	68 25	143 58	350	58.5	175	207	-24.9 341.8
10 0850	67 28	145 41	350	57.5	176	208	-25.9 342.4
11 0853	67 13	146 09	350	57.0	007	036	-26.2 342.7
12 0900	67 24	145 00	350	57.5	007	030	-26.3 346.2
13 0910	68 25	143 04	350	59.5	008	040	-25.6 351.1
14 0917	69 05	141 32	350	59.5	008	042	-25.1 354.6
15 0922	69 36	140 14	350	59.5	000	035	-24.7 357.6
16 0930	69 31	141 33	350	59.5	177	211	-24.8 358.2
17 0940	69 30	143 33	350	59.5	176	210	-25.8 358.8
18 0950	67 26	145 13	350	58.5	172	204	-26.8 359.6
19 1000	66 22	146 46	350	54.0	172	202	-27.9 000.8
20 1010	65 14	148 12	350	54.5	172	200	-29.0 002.1
21 1020	65 00	147 24	350	50.5	005	033	-29.2 005.7
22 1030	66 07	145 47	350	50.5	358	027	-27.8 010.4
23 1040	67 14	144 38	350	51.5	356	027	-26.4 014.4
24 1050	68 22	143 11	350	58.0	000	032	-24.9 018.4
25 1100	69 19	141 05	450	-	006	041	-23.4 023.3
26 1110	69 42	141 15	350	59.5	175	210	-27.7 025.8
27 1120	68 46	143 43	350	58.0	175	209	-23.6 025.9
28 1130	67 42	145 30	350	58.5	171	203	-24.8 027.0
29 1140	66 30	147 02	350	51.5	168	198	-25.3 028.3
30 1150	65 17	148 18	350	52.0	168	196	-26.1 029.8
31 1200	64 10	149 23	350	49	170	197	-26.7 031.7
32 1207	63 40	149 02	350	49	002	029	-26.6 034.2
33 1210	63 56	148 39	350	-	356	025	-26.1 035.3
34 1216	64 30	147 55	350	-	349	017	-25.1 037.5
35 1220	65 08	147 32	350	-	342	011	-24.3 038.7
36 1225	65 42	146 50	350	---	150	179	-23.3 040.7
37 1245	64 36	147 10	250	37.5	285	313	-22.8 045.8
38 1312	64 40	147 06	AND	---	---	---	---

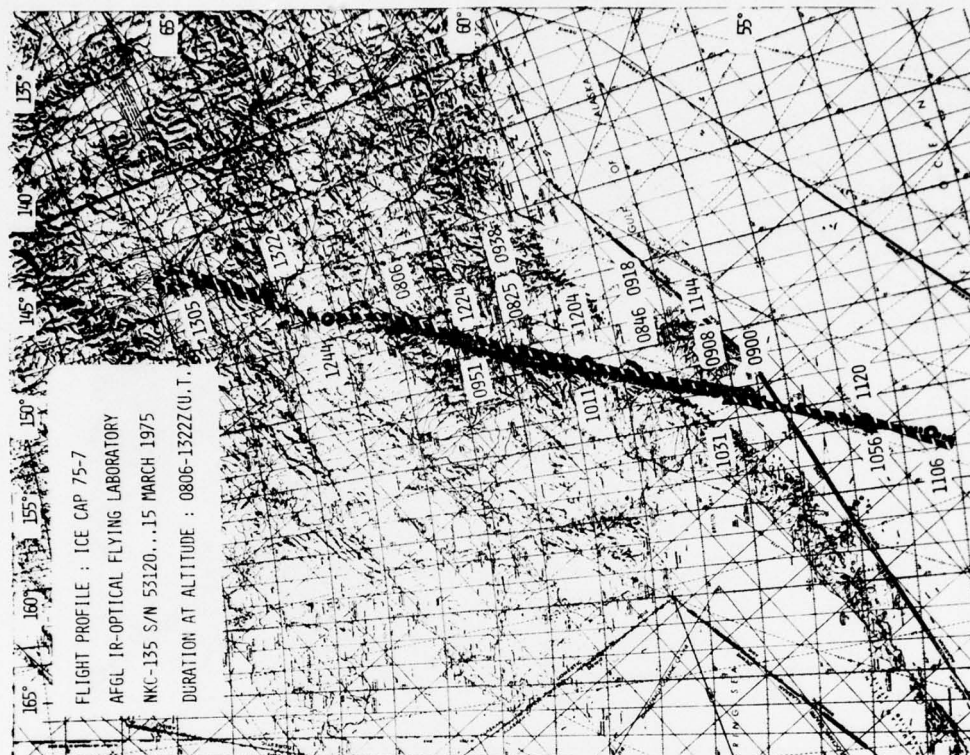
Figure D.2. Flight description for measurements performed 10 Mar 75.



FLIGHT PROFILE : ICE CAP 75-5
 AFGL IR-OPTICAL FLYING LABORATORY
 NKC-135 S/N 53120...11 MARCH 1975
 DURATION AT ALTITUDE : 0800-1136Z (U.T.)

MISSION: ICECAP 75-5										DATE: 11 MARCH 1975									
TIME		LATITUDE		LONGITUDE		ALT.		EIL/EIL		HEADING		SPEED		SOLAR ANGLE		GRD		ELEV. AZIM.	
Z	O	N	O	N	O	FL	FL	TRUE	Q	MAG	TRUE	TR. AIR	GRD	ELEV.	AZIM.	KTS	KTS	KTS	O
1	0718	64	40	147	06	1/0	-	-	-	002	030	442	450	-22.8	315.7				
2	0800	65	08	147	31	350	-41	-41	-41	000	029	440	445	-25.1	326.5				
3	0810	66	14	146	02	350	-43	-43	-43	000	031	435	450	-25.1	331.1				
4	0820	67	17	144	25	350	-45	-45	-45	000	031	435	450	-24.8	335.6				
5	0830	67	33	144	59	350	-47	-47	-47	178	209	430	430	-24.9	337.9				
6	0840	66	30	146	47	350	-41	-41	-41	180	210	485	450	-26.0	338.5				
7	0850	65	23	148	23	350	-44	-44	-44	177	205	500	455	-27.1	339.2				
8	0900	64	10	149	15	350	-44	-44	-44	155	183	500	440	-28.5	340.8				
9	0910	63	00	150	20	350	-38	-38	-38	170	196	490	442	-29.8	342.3				
10	0920	61	49	151	18	350	-38	-38	-38	168	193	490	440	-31.1	343.7				
11	0930	60	38	152	04	350	-42	-42	-42	182	206	490	445	-32.5	345.6				
12	0940	59	36	153	15	350	-40	-40	-40	185	208	495	444	-33.7	347.1				
13	0950	58	29	154	13	350	-46	-46	-46	180	202	500	450	-34.9	348.6				
14	1000	57	13	155	12	350	-43	-43	-43	174	195	500	450	-36.3	350.4				
15	1010	56	01	155	51	350	-45	-45	-45	174	194	500	455	-37.6	352.6				
16	1013	55	41	156	10	350	-	-	-	174	194	500	455	-38.0	353.1				
17	1016	55	49	156	13	350	-42	-42	-42	002	022	450	450	-37.9	354.0				
18	1020	56	17	155	46	350	-42	-42	-42	002	023	440	440	-37.5	355.8				
19	1030	57	27	154	56	350	-43.0	-43.0	-43.0	358	019	444	446	-36.4	000.0				
20	1040	58	42	153	55	350	-43.0	-43.0	-43.0	358	020	445	450	-35.1	004.4				
21	1050	59	51	153	05	350	-40.0	-40.0	-40.0	358	021	444	452	-33.8	008.2				
22	1100	60	58	151	58	350	-39.0	-39.0	-39.0	000	024	444	450	-32.3	012.4				
23	1110	62	03	151	17	350	-38.5	-38.5	-38.5	000	025	440	446	-30.9	016.0				
24	1120	63	16	149	41	350	-37.0	-37.0	-37.0	000	026	440	450	-29.2	020.4				
25	1130	64	28	148	21	350	-40.5	-40.5	-40.5	000	028	450	460	-27.4	024.4				
26	1136	65	08	147	32	350	-40.5	-40.5	-40.5	003	031	440	-	-26.4	026.8				
27	1136	-	-	-	-	-	-	-	-	-	-	-	-	-	-				
28	1147	-	-	-	-	-	-	-	-	-	-	-	-	-	-				
29	1213	64	40	147	06	LAND	-	-	-	-	-	-	-	-	-				
30																			
31																			
32																			
33																			
34																			
35																			

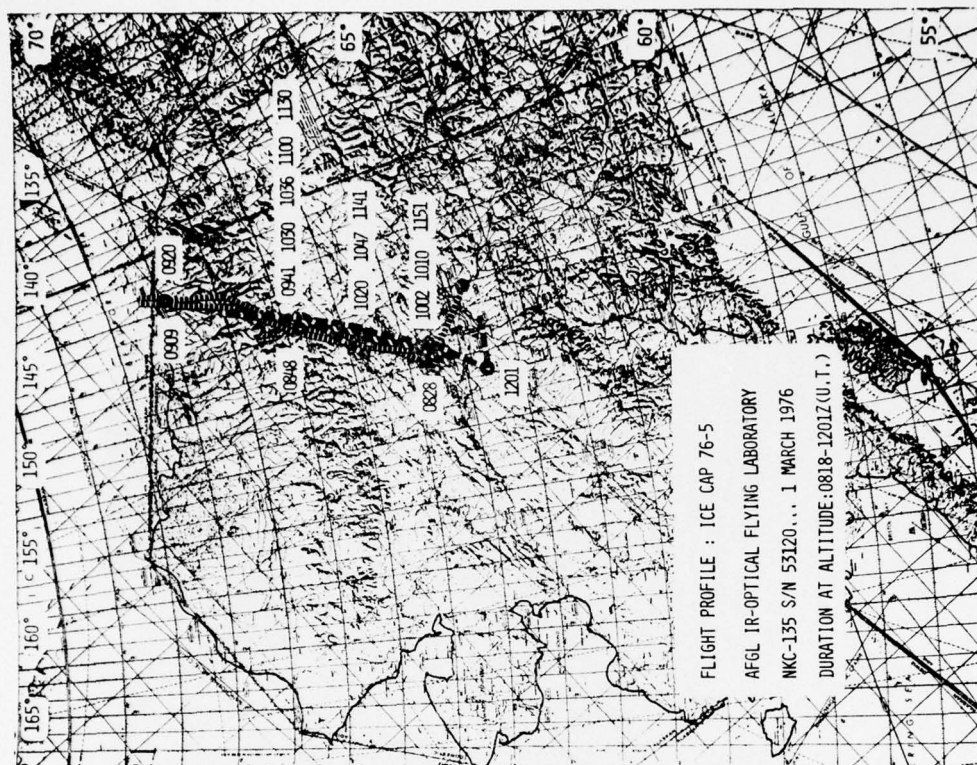
Figure D.3. Flight description for measurements performed 11 Mar 75.



MISSION: ICECAP 75-7 EIL/EIL DATE: 15 March 1975

TIME	Z	LATITUDE	LONG	TRUO	ALT.	QAT	HEADING	SPEED	SOLAR ANGLE
1	0743	64	40	147	06	710	---	---	---
2	0806	63	02	150	11	350	43.5	---	---
3	0816	61	53	151	16	350	43.5	176	202
4	0825	60	45	152	15	350	43.5	176	201
5	0835	59	38	153	08	350	40.0	177	200
6	0845	58	29	154	02	350	41.5	179	202
7	0856	57	16	154	56	350	41.5	182	204
8	0900	56	44	155	15	350	41.5	182	203
9	0904	56	53	155	26	350	41.0	---	TURN
10	0908	57	21	154	58	350	43.0	356	018
11	0918	58	30	154	07	350	42.0	356	018
12	0928	59	38	153	12	350	41.5	354	017
13	0938	60	45	152	17	350	41.5	357	021
14	0948	61	50	151	04	350	41.5	358	023
15	0951	61	56	151	20	350	41.5	---	TURN
16	1001	60	46	152	40	350	41.5	180	204
17	1011	59	40	153	18	350	41.5	170	193
18	1021	58	29	153	59	350	40.5	175	198
19	1031	57	20	154	58	350	42.5	185	207
20	1041	56	13	155	51	350	41.0	189	210
21	1046	55	40	156	13	350	44.5	186	207
22	1056	54	35	156	59	350	44.5	188	208
23	1106	53	26	157	31	350	44.5	185	205
24	1110	53	40	157	34	350	54.5	---	TURN
25	1120	54	38	156	47	350	56.0	353	013
26	1129	55	39	156	07	350	45.0	350	010
27	1134	56	14	155	46	350	43.5	350	013
28	1144	57	23	155	05	350	42.0	354	015
29	1154	58	31	154	08	350	42.0	359	021
30	1204	59	38	153	12	350	41.5	355	018
31	1214	60	45	152	12	350	41.0	354	017
32	1224	61	55	151	04	350	41.0	359	023
33	1234	63	03	149	41	350	40.0	357	023
34	1244	64	09	149	10	350	42.5	354	021
35	1254	65	06	147	44	350	46.5	005	033
36	1305	66	12	146	05	350	45.0	000	029
37	1321	65	08	147	29	350	45.0	180	210
38	1346	64	40	147	06	---	---	---	---

Figure D.4. Flight description for measurements performed 15 Mar 75.



MISSION: ICECAP 76-5										DATE: 1 MARCH 76									
TIME		LATITUDE		LONGITUDE		EIL/EIL		HEADING		SPEED		SOLAR ANGLE							
Z	0	N	W	M	S	FL	OC	MAG	TRUE	KTS	MPH	ELEV.	AZIM.						
1	0753	64	40	147	06	170	00	00	00	00	00	-28.6	323.4						
2	0818	0811				350	--	000	000	440	--	--	--						
3	0828	65	41	149	50	350	-53.0	004	032	390	420	-29.1	330.4						
4	0838	66	42	148	12	350	-59.0	359	029	390	420	-28.9	335.2						
5	0848	67	45	146	45	350	-60.5	359	030	385	420	-28.6	339.9						
6	0858	68	49	144	55	350	-61.5	357	030	405	420	-28.0	344.9						
7	0909	69	56	143	31	350	-63.5	357	030	405	420	-27.2	349.6						
8	0920	69	57	143	20	350	-63.5	177	210	470	420	-27.4	352.9						
9	0930	68	56	144	05	350	-62.5	175	207	495	440	-28.5	354.8						
10	0941	67	49	146	50	350	-61.5	172	203	497	470	-29.6	354.7						
11	0952	66	43	148	21	350	-58.5	175	203	497	422	-30.7	356.2						
12	1002	65	36	149	23	350	-57.0	180	208	500	420	-31.8	357.7						
13	1010	65	35	149	23	350	-52.5	359	027	395	440	-31.9	000.2						
14	1020	66	42	148	05	350	-60.5	352	022	395	440	-30.7	004.5						
15	1030	67	48	146	45	350	-59.0	356	027	400	435	-29.4	008.8						
16	1032	68	03	146	29	350	--	--	--	--	--	-29.1	009.6						
17	1034	67	57	146	21	350	--	178	208	450	400	-29.2	010.5						
18	1036	67	45	146	45	350	-63.0	176	206	500	435	-29.4	010.5						
19	1047	66	42	148	27	350	-57.5	--	--	500	--	-30.3	011.8						
20	1050	66	44	148	47	350	--	030	060	450	480	-30.2	012.3						
21	1054	67	02	147	51	350	--	002	032	450	500	-29.8	014.5						
22	1100	67	45	146	33	350	-59.0	356	027	400	440	-28.8	017.5						
23	1110	68	44	145	13	350	-62.0	359	027	410	440	-27.4	021.7						
24	1120	68	49	145	06	350	-64.5	187	218	497	439	-27.0	024.4						
25	1130	67	50	146	50	350	-61.0	173	203	500	425	-27.7	025.6						
26	1141	66	42	148	20	350	-55.0	175	203	500	425	-28.5	027.2						
27	1151	65	37	149	34	350	-50.0	174	201	500	430	-29.2	028.9						
28	1201	64	35	150	51	350	-46.5	079	201	450	460	-29.9	030.6						
29	1245	64	40	147	06	LAND													
30																			
31																			
32																			
33																			
34																			
35																			

Figure D.5. Flight description for measurements performed 1 Mar 76.

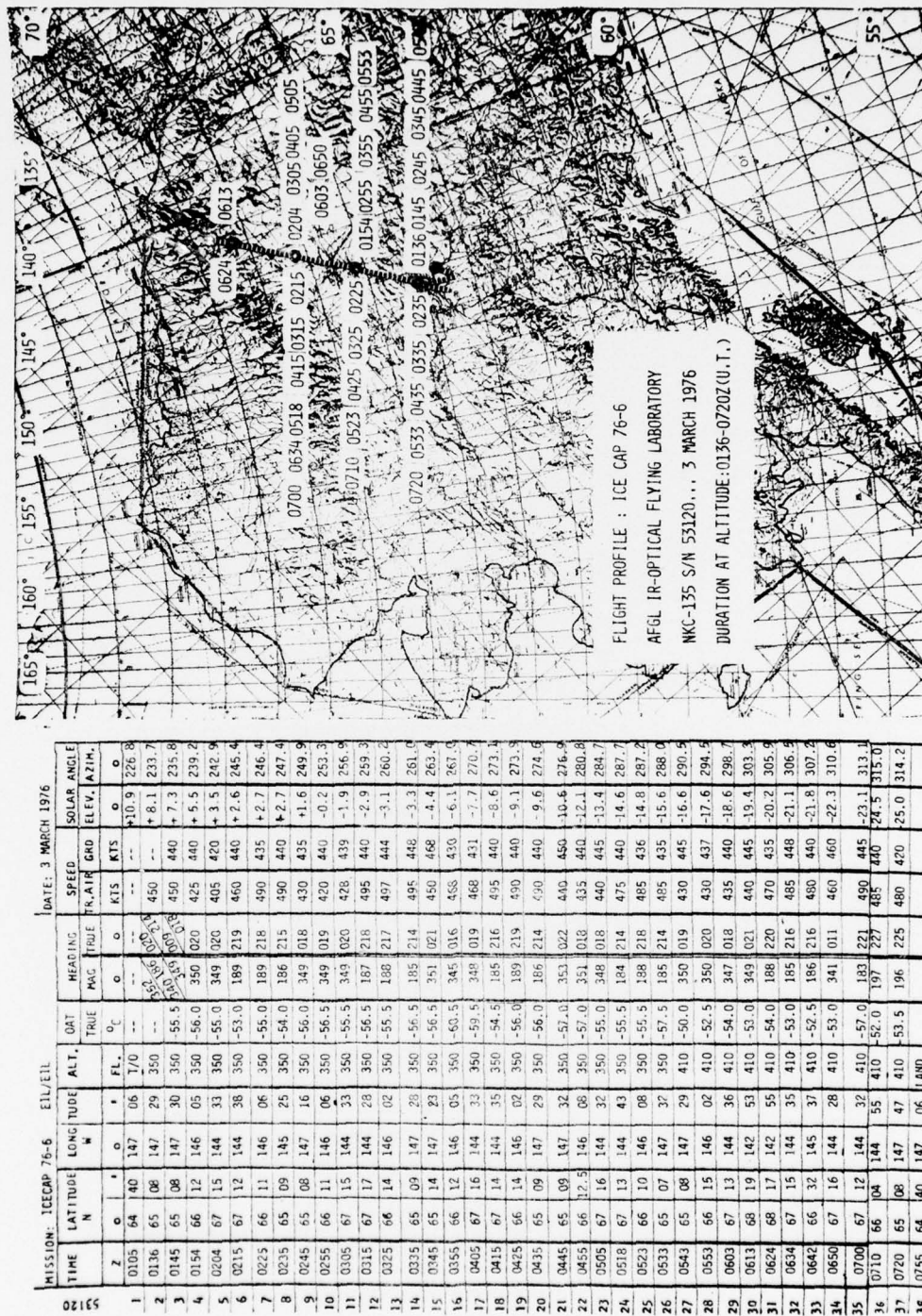
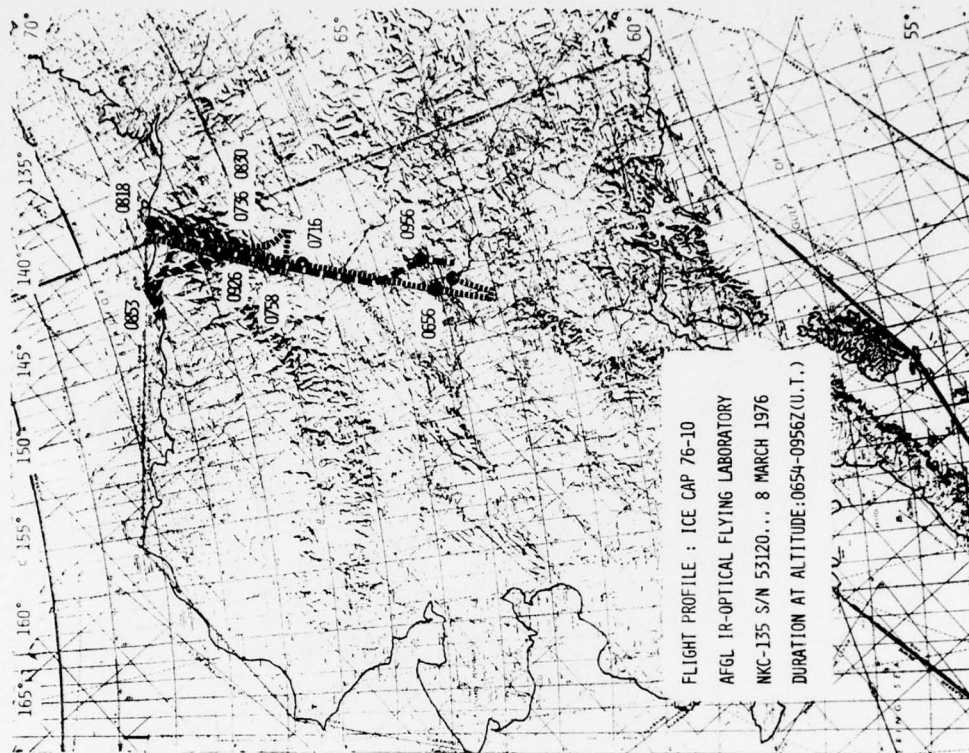


Figure D.6. Flight description for measurements performed 3 Mar 76.



MISSION: ICECAP 76-10 EIL/EIL										DATE: 8 MARCH 1976									
TIME	Z	O	N	LATITUDE	LONGITUDE	ALT.	OR	TRUE	HEADING	MAG	TRUE	TRAIL	SPEED	TRAIL	GRD	ELEV.	AZIM.	SOLAR	ANGLE
1	0630	64	40	147	06	170	--	--	--	--	--	--	--	--	--	--	--	--	--
2	0654	64	47	147	45	350	--	--	360	029	420	440	440	440	440	440	440	440	440
3	0656	65	02	147	24	350	-37.5	360	029	420	440	440	440	440	440	440	440	440	440
4	0706	66	10	146	00	350	-41.0	354	025	425	440	440	440	440	440	440	440	440	440
5	0716	67	18	144	29	350	-40.5	357	029	430	440	440	440	440	440	440	440	440	440
6	0726	68	16	142	55	350	-44.5	358	030	435	450	450	450	450	450	450	450	450	450
7	0736	68	16	142	55	350	--	164	196	480	450	450	450	450	450	450	450	450	450
8	0741	67	47	143	07	350	--	099	142	390	385	385	385	385	385	385	385	385	385
9	0750	67	22	143	10	350	-43.0	263	296	402	385	385	385	385	385	385	385	385	385
10	0758	67	50	144	18	350	--	014	047	430	440	440	440	440	440	440	440	440	440
11	0813	69	27	141	19	350	--	357	032	435	430	430	430	430	430	430	430	430	430
12	0818	69	36	140	08	350	--	184	218	475	440	440	440	440	440	440	440	440	440
13	0821	69	10	141	10	350	-48.0	186	210	475	440	440	440	440	440	440	440	440	440
14	0830	68	17	143	00	350	-45.0	188	211	465	430	430	430	430	430	430	430	430	430
15	0838	68	22	143	21	350	-48.0	001	032	500	490	490	490	490	490	490	490	490	490
16	0850	69	36	142	57	350	--	345	023	432	430	430	430	430	430	430	430	430	430
17	0853	69	59	143	26	350	--	239	272	390	370	370	370	370	370	370	370	370	370
18	0905	69	56	143	24	350	--	089	124	450	450	450	450	450	450	450	450	450	450
19	0915	69	26	141	25	350	-51.5	187	210	470	440	440	440	440	440	440	440	440	440
20	0926	68	19	143	10	350	-45.5	189	211	470	450	450	450	450	450	450	450	450	450
21	0936	67	15	144	36	350	-43.0	181	212	465	440	440	440	440	440	440	440	440	440
22	0946	66	10	146	16	350	-42.5	181	211	470	440	440	440	440	440	440	440	440	440
23	0956	65	10	146	00	350	-39.5	118	146	470	450	450	450	450	450	450	450	450	450
24	1037	64	40	147	06	LAND													
25																			
26																			
27																			
28																			
29																			
30																			
31																			
32																			
33																			
34																			
35																			

Figure D.8. Flight description for measurements performed 8 Mar 76.

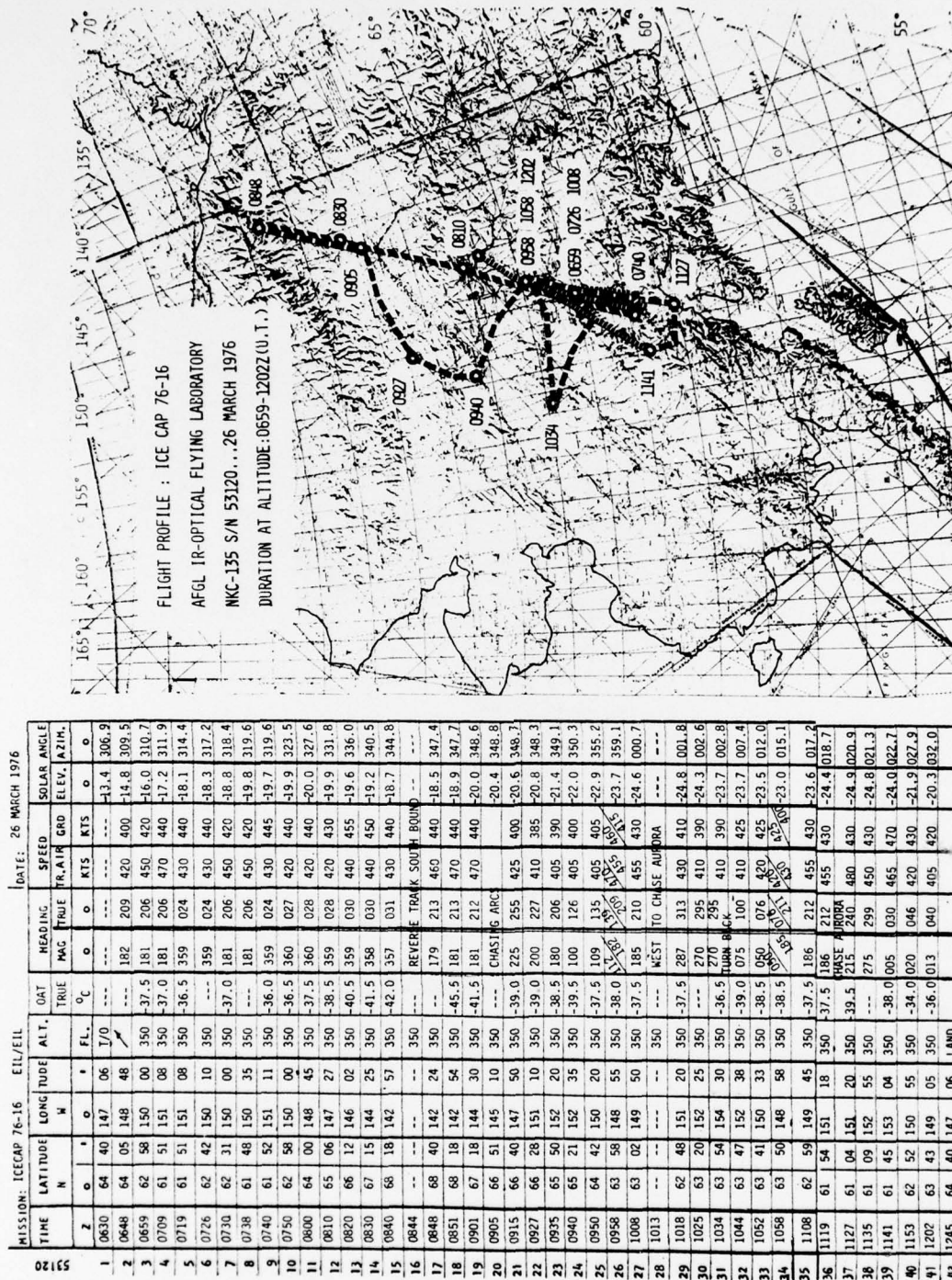


Figure D.9. Flight description for measurements performed 26 Mar 76.

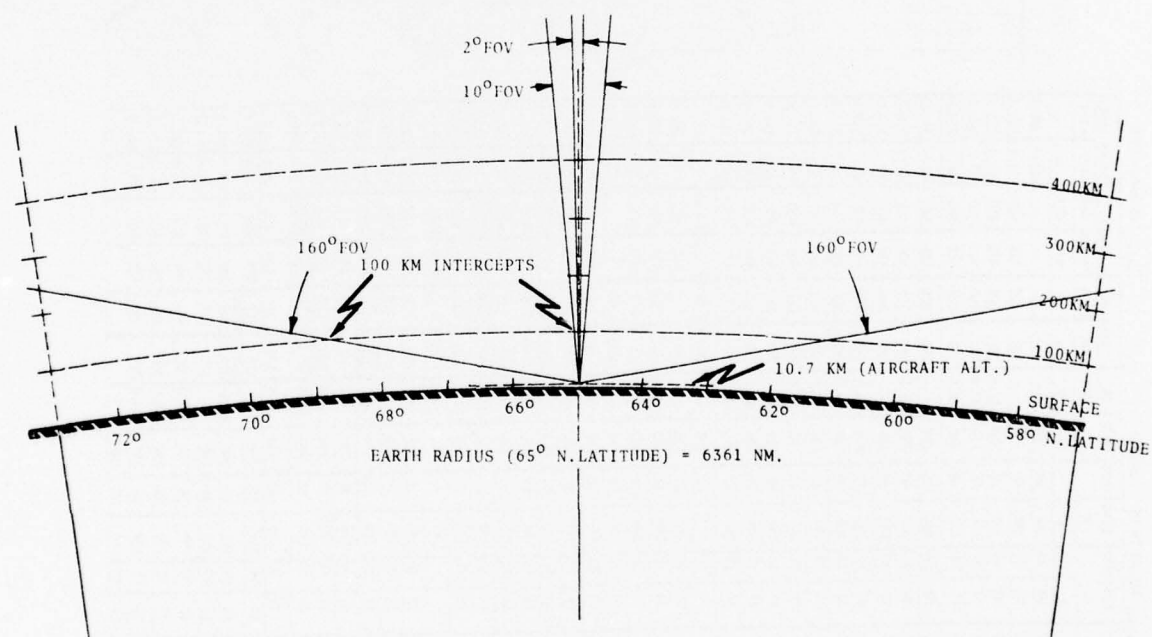
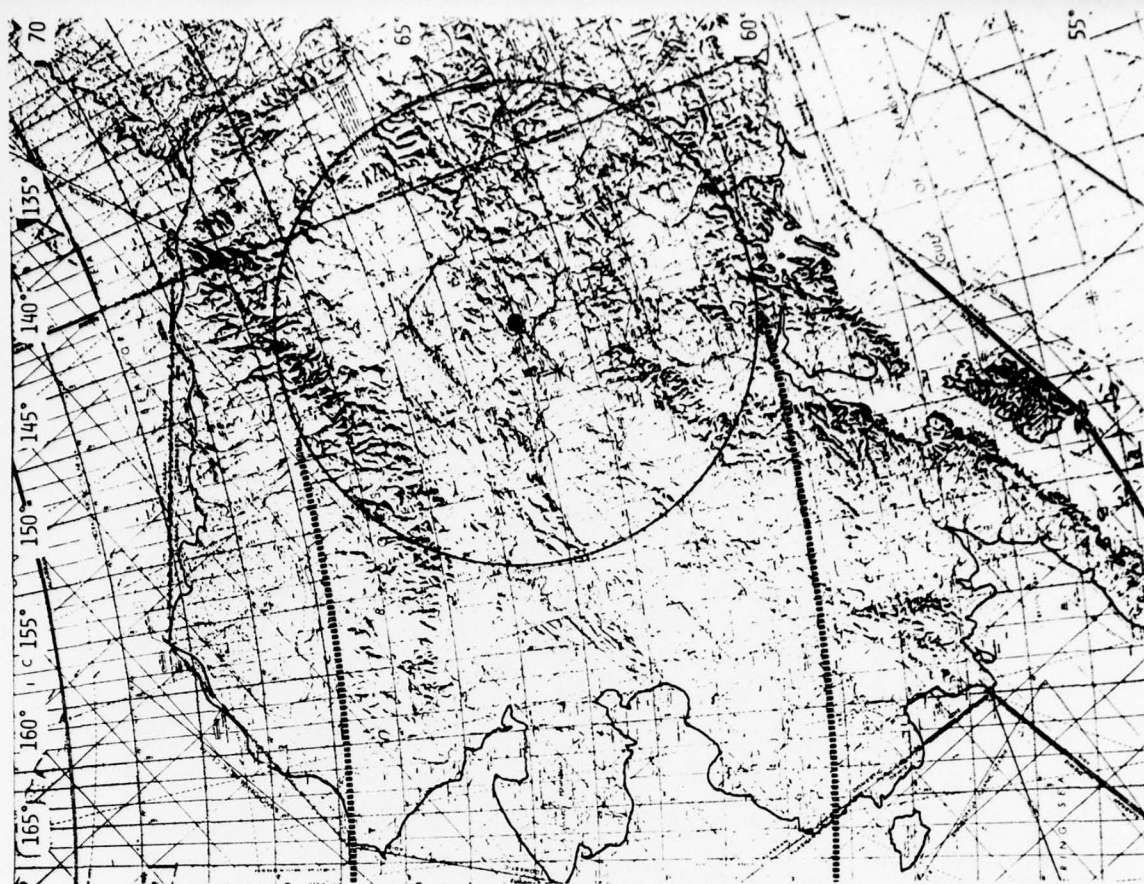


Figure D.10 Cross Section of Alaska Showing Footprint of 100km Intercept with 2°, 10° and 160° Airborne Instrument Fields of View.

REFERENCES

1. Huppi, R.J. [1977] "A Versatile Radiometer for Infrared Emission Measurements of the Atmosphere and Targets", Op. Engrg., Vol. 16, No. 5. October 1977, p. 485.
2. Huppi, E.R., Rogers, J.W., and Stair, A.T., Jr., [1974] "Aircraft Observations of the Infrared Emission of the Atmosphere in the 700-2800 cm^{-1} Region", Applied Optics, Vol. 13, No. 6, June 1974, p. 1466.
3. Kofsky, I.L., Sluder, R.B., and Trobridge, C.A., [1975] "Data Reduction and Auroral Characterization for ICECAP II, HAES Report No. 27", DNA 3789F, Final Report Contract DNA 001-75-C-0085, Oct 25, 1975, p. 59.
4. Kofsky, I.L., Villanucci, D.P., and Sluder, R.B., "Data Reduction and Auroral Characterization for ICECAP III," HAES Report 59, DNA No. 4220F, 31 Jan 1977, p. 161.

DIRECTOR
DEFENSE ADVANCED RSCH PROJ AGENCY
ARCHITECT BUILDING
1400 WILSON BLVD.
ARLINGTON, VA 22209
ATTN LTC W A WHITAKER

DIRECTOR
DEFENSE ADVANCED RSCH PROJ AGENCY
ARCHITECT BUILDING
1400 WILSON BLVD.
ARLINGTON, VA 22209
ATTN MAJOR GREGORY CANAVAN

DEFENSE DOCUMENTATION CENTER
CAMERON STATION
ALEXANDRIA, VA 22314
ATTN TC

DEFENSE DOCUMENTATION CENTER
CAMERON STATION
ALEXANDRIA, VA 22314
ATTN TC

DIRECTOR
DEFENSE NUCLEAR AGENCY
WASHINGTON, DC 20305
ATTN RAE CHARLES A BLANK

DIRECTOR
DEFENSE NUCLEAR AGENCY
WASHINGTON, DC 20305
ATTN TITL TECH LIBRARY

DIRECTOR
DEFENSE NUCLEAR AGENCY
WASHINGTON, DC 20305
ATTN TITL TECH LIBRARY

DIRECTOR
DEFENSE NUCLEAR AGENCY
WASHINGTON, DC 20305
ATTN TISI ARCHIVES

DIRECTOR
DEFENSE NUCLEAR AGENCY
WASHINGTON, DC 20305
ATTN RAEV HAROLD C FITZ, JR

DIRECTOR
DEFENSE NUCLEAR AGENCY
WASHINGTON, DC 20305
ATTN RAE MAJ. J. MAYO

DIRECTOR
DEFENSE NUCLEAR AGENCY
WASHINGTON, DC 20305
ATTN RAE G. SOPER

DIRECTOR
DEFENSE NUCLEAR AGENCY
WASHINGTON, DC 20305
ATTN MAJOR R. BIGONI

DIR OF DEFENSE RSCH & ENGINEERING
DEPARTMENT OF DEFENSE
WASHINGTON DC 20301
ATTN DD/S&S (OS) DANIEL BROCKWAY

DIR OF DEFENSE RSCH & ENGINEERING
DEPARTMENT OF DEFENSE
WASHINGTON, DC 20301
ATTN DD/S&S DANIEL BROCKWAY

COMMANDER
FIELD COMMAND
OFFENSE NUCLEAR AGENCY
KIRTLAND AFB, NM 87115
ATTN FCPR

DIRECTOR
BMD ADVANCED TECH CTP
HUNTSVILLE, AL 35807
ATTN ATC-O, W. DAVIES

CHIEF LIVERMORE DIVISION
FLD COMMAND DNA
LAWRENCE LIVERMORE LABORATORY
P.O. BOX 818
LIVERMORE, CA 94550
ATTN FCPR

DEP. CHIEF OF STAFF FOR RSCH, DEV&ACQ
DEPARTMENT OF THE ARMY
WASHINGTON DC 20310
ATTN MCB DIVISION

COMMANDER/DIRECTOR
ATMOSPHERIC SCIENCES LABORATORY
U S ARMY ELECTRONICS COMMAND
WHITE SANDS MISSILE RANGE, NM 88002
ATTN DRSFL-BL-SY-A F. NTLES

DEP. CHIEF OF STAFF FOR RSCH, DEV&ACQ
DEPARTMENT OF THE ARMY
WASHINGTON, DC 20310
ATTN DAMA-CS Z-C

(3 copies)

DEP. CHIEF OF STAFF FOR RSCH, DEV&ACQ
DEPARTMENT OF THE ARMY
WASHINGTON DC 20310
ATTN DAMA-WS ZC

COMMANDER/DIRECTOR
ATMOSPHERIC SCIENCES LABORATORY
U S ARMY ELECTRONICS COMMAND
WHITE SANDS MISSILE RANGE, NM 88002
ATTN H. BALLARD (3 copies)

DIRECTOR
US ARMY BALLISTIC RESEARCH LABS
ABERDEEN PROVING GROUNDS, MD 21005
ATTN DRXBR-AM, G. KELLER

COMMANDER
HARRY DIAMOND LABORATORIES
2800 POWDER MILL RD
ADELPHI MD 20783
ATTN DRXDO-NP, F.H. WIMINETZ

DIRECTOR
US ARMY BALLISTIC RESEARCH LABS
ABERDEEN PROVING GROUNDS, MD 21005
ATTN DRXRD-RSP, J. HEIMEPL

COMMANDER
U S ARMY NUCLEAR AGENCY
FORT BLISS, TX 79916
ATTN MONA-WE

DIRECTOR
US ARMY BALLISTIC RESEARCH LABS
ABERDEEN PROVING GROUNDS, MD 21005
ATTN JOHN MESTER

DIRECTOR
BMD ADVANCED TECH CTP
HUNTSVILLE, AL 35807
ATTN ATC-T, M CAPPS

DIRECTOR
US ARMY BALLISTIC RESEARCH LABS
ABERDEEN PROVING GROUNDS, MD 21005
ATTN TECH LIBRARY

COMMANDER
US ARMY ELECTRONICS COMMAND
FORT MONMOUTH, N.J. 37703
ATTN INST FOR EXPL RESEARCH

COMMANDER
NAVAL OCEANS SYSTEMS CENTER
SAN DIEGO, CA 92152
ATTN CODE 2200 HERBERT HUGHES

COMMANDER
US ARMY ELECTRONICS COMMAND
FORT MONMOUTH, N.J. 37703
ATT ORSEL
(5 copies)

COMMANDER
NAVAL OCEANS SYSTEMS CENTER
SAN DIEGO, CA 92152
ATTN CODE 2200 RICHARD PAPPERT

COMMANDER
US ARMY ELECTRONICS COMMAND
FORT MONMOUTH, N.J. 37703
ATTN STANLEY KRONENBERGER

COMMANDER
NAVAL OCEANS SYSTEMS CENTER
SAN DIEGO, CA 92152
ATTN CODE 2200 JURGEN R RICHTER

COMMANDER
US ARMY ELECTRONICS COMMAND
FORT MONMOUTH, N.J. 37703
ATTN WEAPONS EFFECTS SECTION

DIRECTOR
NAVAL RESEARCH LABORATORY
WASHINGTON, DC 20375
ATTN CODE 7712 DOUGLAS P MCNITT

COMMANDER
US ARMY FOREIGN SCIENCE & TECH CTR
220 7TH STREET, NE
CHARLOTTESVILLE VA 22901
ATTN ROBERT JONES

DIRECTOR
NAVAL RESEARCH LABORATORY
WASHINGTON, DC 20375
ATTN CODE 7701 JACK D BROWN

CHIEF
US ARMY RESEARCH OFFICE
P.O. BOX 12211
TRIANGLE PARK, N.C. 27709
ATT ROBERT MACE

DIRECTOR
NAVAL RESEARCH LABORATORY
WASHINGTON, DC 20375
ATTN CODE 2600 TECH LIB

COMMANDER
NAVAL OCEANS SYSTEMS CENTER
SAN DIEGO, CA 92152
ATTN CODE 2200 ILAN ROTHMULLER

DIRECTOR
NAVAL RESEARCH LABORATORY
WASHINGTON, DC 20375
ATTN CODE 7127 CHARLES Y JOHNSON

COMMANDER
NAVAL OCEANS SYSTEMS CENTER
SAN DIEGO, CA 92152
ATTN CODE 2200 WILLIAM MOLER

DIRECTOR
NAVAL RESEARCH LABORATORY
WASHINGTON, DC 20375
ATTN CODE 7700 TIMOTHY P COFFEY

DIRECTOR
NAVAL RESEARCH LABORATORY
WASHINGTON, DC 20375
ATTN CODE 7709 WAHAR ALI

SUPER INTENDENT
NAVAL POST GRADUATE SCHOOL
MONTEREY, CA 93940
ATTN TECH REPORTS LIBRARIAN

DIRECTOR
NAVAL RESEARCH LABORATORY
WASHINGTON, DC 20375
ATTN CODE 7750 DARRELL F STROBEL

COMMANDER
NAVAL ELECTRONICS SYSTEMS COMMAND
NAVAL ELECTRONICS SYSTEMS COMMAND HQS
ATTN PME 117

DIRECTOR
NAVAL RESEARCH LABORATORY
WASHINGTON, DC 20375
ATTN CODE 7750 PAUL JULUFENNE

COMMANDER
NAVAL INTELLIGENCE SUPPORT CTR
4301 SUITLAND RD. BLDG 5
WASHINGTON, DC 20390
ATTN DOCUMENT CONTROL

DIRECTOR
NAVAL RESEARCH LABORATORY
WASHINGTON, DC 20375
ATTN CODE 7750 J. FEDDER

AF GEOPHYSICS LABORATORY, AFSC
HANSCOM AFB, MA 01731
ATTN LKB KENNETH S W CHAMPION

DIRECTOR
NAVAL RESEARCH LABORATORY
WASHINGTON, DC 20375
ATTN CODE 7750 S. OSSAKOW

AF GEOPHYSICS LABORATORY, AFSC
HANSCOM AFB, MA 01731
ATTN OPR ALVA T STAIR

(5 copies)

DIRECTOR
NAVAL RESEARCH LABORATORY
WASHINGTON, DC 20375
ATTN CODE 7751 J. DAVIS

AF GEOPHYSICS LABORATORY, AFSC
HANSCOM AFB, MA 01731
ATTN OPR J. ULWICK

COMMANDER
NAVAL SURFACE WEAPONS CENTER
WHITE OAK, SILVER SPRING, MD 20910
ATTN CODE WA501 NAVY NUC PRGMS OFF

AF GEOPHYSICS LABORATORY, AFSC
HANSCOM AFB, MA 01731
ATTN OPR R. MURPHY

COMMANDER
NAVAL SURFACE WEAPONS CENTER
WHITE OAKS, SILVER SPRING, MD 20910
ATTN TECHNICAL LIBRARY

AF GEOPHYSICS LABORATORY, AFSC
HANSCOM AFB, MA 01731
ATTN OPR J. KENNEALY

AF GEOPHYSICS LABORATORY, AFSC
HANSKOM AFB, MA 01731
ATTN PHG JC MCCLAY

AF GEOPHYSICS LABORATORY, AFSC
HANSKOM AFB, MA 01731
ATTN LKO ROCCO NARCISI

AF GEOPHYSICS LABORATORY, AFSC
HANSKOM AFB, MA 01731
ATTN LKO, R. HUFFMAN

AF WEAPONS LABORATORY, AFSC
KIRTLAND AFB, NM 87117
ATTN MAJ. GARY GANONG, DYM

COMMANDER
ASD
WPAFB, OH 45433
ATTN ASD-YH-EX LTC ROBERT LEVEPETTE

SAMSO/AW
POST OFFICE BOX 92960
WORLDWAY POSTAL CENTER
LOS ANGELES, CA 90009
ATTNS7J MAJOR LAWRENCE DOAN

SAMSO/SW
P.O. BOX 92960
WORLDWAY POSTAL CENTER
LOS ANGELES, CA 90009
ATTN AW

AFTAC
PATRICK AFB, FL 32925
ATTN TECH LIBRARY

AFTAC
PATRICK AFB, FL 32925
ATTN TD

HQ
AIR FORCE SYSTEMS COMMAND
ANDREWS AFB
WASHINGTON, DC 20331
ATTN DLS

HQ
AIR FORCE SYSTEMS COMMAND
ANDREWS AFB
WASHINGTON, DC 20331
ATTN TECH LIBRARY

HQ
AIR FORCE SYSTEMS COMMAND
ANDREWS AFB
WASHINGTON, DC 20331
ATTN DLCAE

HQ
AIR FORCE SYSTEMS COMMAND
ANDREWS AFB
WASHINGTON, DC 20331
ATTN DLTH

HQ
AIR FORCE SYSTEMS COMMAND
ANDREWS AFB
WASHINGTON, DC 20331
ATTN DLXP

HQ
AIR FORCE SYSTEMS COMMAND
ANDREWS AFB
WASHINGTON, DC 20331
ATTNSDP

HQ USAF/RD
WASHINGTON, DC 20330
ATTN RDQ

COMMANDER
ROME AIR DEVELOPMENT CTR
GRIFFISS AFB, NY 13440
ATTN JJ. SIMONS DCSO

LOS ALAMOS SCIENTIFIC LABORATORY
P.O. BOX 1663
LOS, ALAMOS, NM 87545
ATTN DOC CON FOR JOHN ZINN

DIVISION OF MILITARY APPLICATION
U S ENERGY RSCH & DEV ADMIN
WASHINGTON, DC 20545
ATTN DOC CON

LOS ALAMOS SCIENTIFIC LABORATORY
P.O. BOX 1663
LOS, ALAMOS, NM 87545
ATTN DOC CON FOR REFERENCE LIBRARY
ANN BEYER

LOS ALAMOS SCIENTIFIC LABORATORY
P.O. BOX 1663
LOS, ALAMOS, NM 87545
ATTN DOC CON FOR R A JEFFRIES

SANDIA LABORATORIES
LIVERMORE LABORATORY
P.O. BOX 965
LIVERMORE, CA 94556
ATTN DOC CONTROL FOR
THOMAS COOK ORG 8001

LOS ALAMOS SCIENTIFIC LABORATORY
P.O. BOX 1663
LOS, ALAMOS, NM 87545
ATTN DOC CON FOR CR MEHL ORG 5230

SANDIA LABORATORIES
P.O. BOX 5800
ALBUQUERQUE, NM 87115
ATT DOC CONT. FOR
W.D. BROWN ORG 1353

LOS ALAMOS SCIENTIFIC LABORATORY
P.O. BOX 1663
LOS, ALAMOS, NM 87545
ATTN DOC CON FOR H V ARGO

SANDIA LABORATORIES
P.O. BOX 5800
ALBUQUERQUE, NM 87115
ATT DOC CONT. FOR
L. ANDERSON ORG 1247

LOS ALAMOS SCIENTIFIC LABORATORY
P.O. BOX 1663
LOS, ALAMOS, NM 87545
ATTN DOC CON FOR M. TIERNEY J-10

SANDIA LABORATORIES
P.O. BOX 5800
ALBUQUERQUE, NM 87115
ATT DOC CONT.
FOR MORGAN KRAMMA ORG 5720

LOS ALAMOS SCIENTIFIC LABORATORY
P.O. BOX 1663
LOS, ALAMOS, NM 87545
ATTN DOC CON FOR ROBERT BROWNLEE

SANDIA LABORATORIES
P.O. BOX 5800
ALBUQUERQUE, NM 87115
ATT DOC CONT.
FOR FRANK HUDSON ORG 1722

LOS ALAMOS SCIENTIFIC LABORATORY
P.O. BOX 1663
LOS, ALAMOS, NM 87545
ATTN DOC CON FOR WILLIAM MAIER

SANDIA LABORATORIES
P.O. BOX 5800
ALBUQUERQUE, NM 87115
ATT DOC CONT.
FOR ORG 3422-1 SANDIA REPTS COLL.

UNIVERSITY OF CALIFORNIA
LAWRENCE LIVERMORE LABORATORY
P.O. BOX 808
LIVERMORE CA 94550
ATTN JULIUS CHANG L-71

ARGONNE NATIONAL LABORATORY
RECORDS CONTROL
9700 SOUTH CASS AVENUE
ARGONNE, IL 60439
ATTN DOC CON FOR A C WAHL

UNIVERSITY OF CALIFORNIA
LAWRENCE LIVERMORE LABORATORY
P.O. BOX 808
LIVERMORE CA 94550
G.P. HAUGEN L-404

ARGONNE NATIONAL LABORATORY
RECORDS CONTROL
9700 SOUTH CASS AVENUE
ARGONNE, IL 60439
ATTN DOC CON FOR DAVID W GREEN

UNIVERSITY OF CALIFORNIA
LAWRENCE LIVERMORE LABORATORY
P.O. BOX 808
LIVERMORE CA 94550
ATTN D.J. WJERPLES L-142

ARGONNE NATIONAL LABORATORY
RECORDS CONTROL
9700 SOUTH CASS AVENUE
ARGONNE, IL 60439
ATTN DOC CON FOR LIR SVCS REPTS SEC

CALIFORNIA, STATE OF
AIR RESOURCE BOARD
9528 TELSTA AVE
AL MONTE, CA 91731
ATTN LEO ZAFONTE

ARGONNE NATIONAL LABORATORY
RECORDS CONTROL
9700 SOUTH CASS AVENUE
ARGONNE, IL 60439
ATTN DOC CON FOR S GARELNICK

CALIFORNIA INSTITUTE OF TECHNOLOGY
JET PROPULSION LABORATORY
4800 OAK GROVE DRIVE
PASADENA, CA 91103
ATTN JOSEPH A JELLO

ARGONNE NATIONAL LABORATORY
RECORDS CONTROL
9700 SOUTH CASS AVENUE
ARGONNE, IL 60439
ATTN DOC CON FOR GERALD T REEDY

U S ENERGY RSCH & DEV ADMIN
DIVISION OF HEADQUARTERS SERVICES
LIBRARY BRANCH G-043
WASHINGTON, DC 20545
ATTN DOC CON FOR CLASS TECH LIR

UNIVERSITY OF CALIFORNIA
LAWRENCE LIVERMORE LABORATORY
P.O. BOX 808
LIVERMORE CA 94550
ATTN W.H. DUEWER GEN L-404

DEPARTMENT OF TRANSPORTATION
OFFICE OF THE SECRETARY
TAD-44,1, ROOM 10402-R
400 7TH STREET S.W.
WASHINGTON, DC 20590
ATTN SAMUEL C CORONITI

NASA
GODDARD SPACE FLIGHT CENTER
GREENBELT, MD 20771
ATTN A C AIKEN

NASA
600 INDEPENDENCE AVENUE S W
WASHINGTON, DC 20546
ATTN R FELLOWS

NASA
GODDARD SPACE FLIGHT CENTER
GREENBELT, MD 20771
ATTN A TEMPKIN

NASA
600 INDEPENDENCE AVENUE S W
WASHINGTON, DC 20546
ATTN A SCHARDT

NASA
GODDARD SPACE FLIGHT CENTER
GREENBELT, MD 20771
ATTN A J RAJER

NASA
600 INDEPENDENCE AVENUE S W
WASHINGTON, DC 20546
ATTN M TEPPER

NASA
GODDARD SPACE FLIGHT CENTER
GREENBELT, MD 20771
ATTN TECHNICAL LIBRARY

NASA
LANGLEY RESEARCH CENTER
LANGLEY STATION
HAMPTON, VA 23365
ATTN CHARLES SCHENKAYDER MS-168

NASA
GODDARD SPACE FLIGHT CENTER
GREENBELT, MD 20771
ATTN J. SIRE

NASA
AMES RESEARCH CENTER
MOFFETT FIELD, CA 94035
ATTN N-254-4 WALTER L. STARR

NASA
600 INDEPENDENCE AVENUE S W
WASHINGTON, DC 20546
ATTN A GESSOW

NASA
AMES RESEARCH CENTER
MOFFETT FIELD, CA 94035
ATTN N-254-4 R WHITTEN

NASA
600 INDEPENDENCE AVENUE S W
WASHINGTON, DC 20546
ATTN D P CAUFFMAN

NASA
AMES RESEARCH CENTER
MOFFETT FIELD, CA 94035
ATTN N-254-4 ILIA G POPPOFF

NASA
600 INDEPENDENCE AVENUE S W
WASHINGTON, DC 20546
ATTN LTC D R HALLENBECK CODE SC

NASA
AMES RESEARCH CENTER
MOFFETT FIELD, CA 94036
ATTN N-254-3 NEIL H FARLOW

NASA
GEORGE C MARSHALL SPACE FLIGHT CENTER
HUNTSVILLE, AL 35812
ATTN C R BALCHER

CENTRAL INTELLIGENCE AGENCY
ATTN RO/SI RM 5G48 HQ BLDG
WASHINGTON DC 20505
ATTN NEO/OSI-2G4R HQS

NASA
GEORGE C MARSHALL SPACE FLIGHT CENTER
HUNTSVILLE, AL 35812
ATT N H STONE

DEPARTMENT OF COMMERCE
NATIONAL BUREAU OF STANDARDS
WASHINGTON, DC 20234
ATTN SEC OFFICER FOR
ATTN JAMES DEVOE

NASA
GEORGE C MARSHALL SPACE FLIGHT CENTER
HUNTSVILLE, AL 35812
ATT W A ORAN

DEPARTMENT OF COMMERCE
NATIONAL BUREAU OF STANDARDS
WASHINGTON, DC 20234
ATTN SEC OFFICER
STANLEY ARAMOWITZ

NASA
GEORGE C MARSHALL SPACE FLIGHT CENTER
HUNTSVILLE, AL 35812
ATT CODE ES22JOHN WATTS

DEPARTMENT OF COMMERCE
NATIONAL BUREAU OF STANDARDS
WASHINGTON, DC 20234
ATTN SEC OFFICER FOR
ATTN J COOPER

NASA
GEORGE C MARSHALL SPACE FLIGHT CENTER
HUNTSVILLE, AL 35812
ATTN W T ROBERTS

DEPARTMENT OF COMMERCE
NATIONAL BUREAU OF STANDARDS
WASHINGTON, DC 20234
ATTN SEC OFFICER FOR
ATTN GEORGE A SINNATT

NASA
GEORGE C MARSHALL SPACE FLIGHT CENTER
HUNTSVILLE, AL 35812
ATTN R D HUDSON

DEPARTMENT OF COMMERCE
NATIONAL BUREAU OF STANDARDS
WASHINGTON, DC 20234
ATTN SEC OFFICER FOR
ATTN K KESSLER

ALBANY METALLURGY RESEARCH CENTER
U S BUREAU OF MINES
P.O. BOX 70
ALBANY, OR 97321
ATTN ELEANOR ARSHIRE

DEPARTMENT OF COMMERCE
NATIONAL BUREAU OF STANDARDS
WASHINGTON, DC 20234
ATTN SEC OFFICER FOR
ATTN M KRAUSS

DEPARTMENT OF COMMERCE
NATIONAL BUREAU OF STANDARDS
WASHINGTON, DC 20234
ATTN SEC OFFICER FOR
ATTN LEWIS H GEVANTMAN

AERODYNE RESEARCH, INC.
BEDFORD RESEARCH PARK
CROSBY DRIVE
BEDFORD, MA 01731 ATTN M CAMAG

NATIONAL OCEANIC & ATMOSPHERIC ADMIN
ENVIRONMENTAL RESEARCH LABORATORIES
DEPARTMENT OF COMMERCE
BOULDER, CO 80302
ATTN GEORGE C REID AERONOMY LAB

AERONOMY CORPORATION
217 S NEIL STREET
CHAMPAIGN, IL 61820
ATTN A BOWHILL

NATIONAL OCEANIC & ATMOSPHERIC ADMIN
ENVIRONMENTAL RESEARCH LABORATORIES
DEPARTMENT OF COMMERCE
BOULDER, CO 80302
ATTN ELDON FERGUSON

AEROSPACE CORPORATION
P.O. BOX 92957
LOS ANGELES, CA 90009
ATTN N COHEN

NATIONAL OCEANIC & ATMOSPHERIC ADMIN
ENVIRONMENTAL RESEARCH LABORATORIES
DEPARTMENT OF COMMERCE
BOULDER, CO 80302
ATTN FRED FEHSENFELD

AEROSPACE CORPORATION
P.O. BOX 92957
LOS ANGELES, CA 90009
ATTN HARRIS MAYER

AERO-CHEM RESEARCH LABORATORIES, INC
P.O. BOX 12
PRINCETON, NJ 08540
ATTN A FONTIJN

AEROSPACE CORPORATION
P.O. BOX 92957
LOS ANGELES, CA 90009
ATTN SIDNEY W KASH

AERO-CHEM RESEARCH LABORATORIES, IN
P.O. BOX 12
PRINCETON, NJ 08540
ATTN H PERGAMENT

AEROSPACE CORPORATION
P.O. BOX 92957
LOS ANGELES, CA 90009
ATTN T WIDHOPF

AERODYNE RESEARCH, INC.
BEDFORD RESEARCH PARK
CROSBY DRIVE
BEDFORD, MA 01731 ATTN F BIEN

AEROSPACE CORPORATION
P.O. BOX 92957
LOS ANGELES, CA 90009
ATTN R J MCNEAL

AEROSPACE CORPORATION
P.O. BOX 92957
LOS ANGELES, CA 90009
ATTN R GROVE

AEROSPACE CORPORATION
P.O. BOX 92957
LOS ANGELES, CA 90009
ATTN IRVING M GARFUNKEL

BATTELLE MEMORIAL INSTITUTE
505 KING AVENUE
COLUMBUS, OH 43201
ATTN DONALD J HAMMAN

AEROSPACE CORPORATION
P.O. BOX 92957
LOS, ANGELES, CA 90009
ATTN THOMAS D TAYLOR

BATTELLE MEMORIAL INSTITUTE
505 KING AVENUE
COLUMBUS, OH 43201
ATTN DONALD J HAM

AEROSPACE CORPORATION
P.O. BOX 92957
LOS, ANGELES, CA 90009
ATTN V JOSEPHSON

BATTELLE MEMORIAL INSTITUTE
505 KING AVENUE
COLUMBUS, OH 43201
ATTN STOIAO

AEROSPACE CORPORATION
P.O. BOX 92957
LOS, ANGELES, CA 90009
ATTN JULIAN REINHEIMER

BATTELLE MEMORIAL INSTITUTE
505 KING AVENUE
COLUMBUS, OH 43201
ATTN RICHARD K THATCHER

AEROSPACE CORPORATION
P.O. BOX 92957
LOS, ANGELES, CA 90009
ATTN R D RAWCLIFFE

BROWN ENGINEERING COMPANY, INC
CUMMINGS RESEARCH PARK
HUNTSVILLE, AL 35807
ATTN N PASSINO

AVCO-EVERETT RESEARCH LABORATORY INC THE TRUSTEES OF BOSTON COLLEGE
2385 REVERE BEACH PARKWAY
EVERETT, MA 02149
ATTN TECHNICAL LIBRARY

CHESTNUT HILL CAMPUS
CHESTNUT HILL, MA 02167
ATTN CHAIRMAN DEPT OF CHEM

AVCO-EVERETT RESEARCH LABORATORY INC BROWN ENGINEERING COMPANY, INC
2385 REVERE BEACH PARKWAY
EVERETT, MA 02149
ATTN GEORGE SUTTON

CUMMINGS RESEARCH PARK
HUNTSVILLE, AL 35807
ATTN RONALD PATRICK

AVCO-EVERETT RESEARCH LABORATORY INC CALIFORNIA AT RIVERSIDE, UNIV OF
2385 REVERE BEACH PARKWAY
EVERETT, MA 02149
ATTN C W VON ROSENBERG JR

RIVERSIDE, CA 92502
ATTN ALAN C LLOYD

CALIFORNIA AT RIVERSIDE, UNIV OF
RIVERSIDE, CA 92502
ATTN JAMES N PITTS JR

CALSPAN CORPORATION
P.O. BOX 235
BUFFALO, NY 14221
ATTN G C VALLEY

CALIFORNIA AT SAN DIEGO, UNIV OF
3175 MIRAMAR ROAD
LA JOLLA, CA 92037
ATTN S C LIN

CALSPAN CORPORATION
P.O. BOX 235
BUFFALO, NY 14221
ATTN M G DUNN

CALIFORNIA UNIVERSITY OF
BERKELEY CAMPUS ROOM 318
SPROUL HALL
BERKELEY, CA 94720
ATTN SEC OFFICER FOR
HAROLD JOHNSTON

CALSPAN CORPORATION
P.O. BOX 235
BUFFALO, NY 14221
ATTN W WURSTER

CALIFORNIA UNIVERSITY OF
BERKELEY CAMPUS ROOM 318
SPROUL HALL
BERKELEY, CA 94720
ATTN SEC OFFICER FOR F MOZER

COLORADO, UNIVERSITY OF
OFFICE OF CONTRACTS AND GRANTS
380 ADMINISTRATIVE ANNEX BOULDER,
ATTN A PHELPS JILA CO 80302

CALIFORNIA UNIVERSITY OF
BERKELEY CAMPUS ROOM 318
SPROUL HALL
BERKELEY, CA 94720
ATTN SEC OFFICER FOR DEPT OF CHAM
W H MILLER

COLORADO, UNIVERSITY OF
OFFICE OF CONTRACTS AND GRANTS
380 ADMINISTRATIVE ANNEX
BOULDER, CO 80302
ATTN JEFFREY B PEARCE LASP

CALIFORNIA, STATE OF
AIR RESOURCES BOARD
9528 TELSTAR AVENUE
EL MONTE, CA 91731
ATTN LEO ZAFONTE

COLORADO, UNIVERSITY OF
OFFICE OF CONTRACTS AND GRANTS
380 ADMINISTRATIVE ANNEX
BOULDER, CO 80302
ATTN C BEATY JILA

CALSPAN CORPORATION
P.O. BOX 235
BUFFALO, NY 14224
ATTN C E TREANOR

COLORADO, UNIVERSITY OF
OFFICE OF CONTRACTS AND GRANTS
380 ADMINISTRATIVE ANNEX
BOULDER, CO 80302
ATTN C LINEBERGER JILA

COLORADO, UNIVERSITY OF
OFFICE OF CONTRACTS AND GRANTS
380 ADMINISTRATIVE ANNEX
BOULDER, CO 80302
ATTN CHARLES A BARTH LADD

GENERAL ELECTRIC COMPANY
TEMPO-CENTER FOR ADVANCED STUDIES
816 STATE STREET (P.O. DRAWER 00)
SANTA BARBARA, CA 93102
ATTN NASAIC

COLUMBIA UNIVERSITY, THE TRUSTEES
IN THE CITY OF NEW YORK
LA MONT DOHERTY GEOLOGICAL
OBSERVATORY-TORREY CLIFF
PALISADES, NY 19064
ATTN B PHELAN

GENERAL ELECTRIC COMPANY
TEMPO-CENTER FOR ADVANCED STUDIES
816 STATE STREET (P.O. DRAWER 00)
SANTA BARBARA, CA 93102
ATTN WARREN S KNAFF

COLUMBIA UNIVERSITY, THE TRUSTEES OF
CITY OF NEW YORK
116TH STREET & BROADWAY
NEW YORK, NY 10027
ATTN RICHARD N ZARE

GENERAL ELECTRIC COMPANY
TEMPO-CENTER FOR ADVANCED STUDIES
816 STATE STREET (P.O. DRAWER)
SANTA BARBARA, CA 93102
ATTN TIM STEPHENS

COLUMBIA UNIVERSITY, THE TRUSTEES OF
CITY OF NEW YORK
116TH & BROADWAY
NEW YORK, NY 10027
ATTN SEC OFFICER H M FOLEY

GENERAL ELECTRIC COMPANY
TEMPO-CENTER FOR ADVANCED STUDIES
816 STATE STREET (P.O. DRAWER 00)
SANTA BARBARA, CA 93102
ATTN DON CHANDLER

CONCORD SCIENCES
P.O. BOX 119
CONCORD, MA 01742
ATTN EMMETT A SUTTON

GENERAL ELECTRIC COMPANY
TEMPO-CENTER FOR ADVANCED STUDIES
816 STATE STREET (P.O. DRAWER 00)
SANTA BARBARA, CA 93102
ATTN B CAMBILL

DENVER, UNIVERSITY OF
COLORADO SEMINARY
DENVER RESEARCH INSTITUTE
P.O. BOX 10127 DENVER, CO 80210
ATTN SEC OFFICER FOR MR VAN ZYL

GENERAL ELEC. CO.
SPACE DIVISION
VALLEY FORGE SPACE CTR
GODDARD BLVD
KING OF PRUSSIA
P.O. BOX 8555
PHILADELPHIA, PA 19101
ATTN M H BORTNER, SPACE SCIENCE LAB

DENVER, UNIVERSITY OF
COLORADO SEMINARY
DENVER RESEARCH INSTITUTE
P.O. BOX 10127 DENVER, CO 80210
ATTN SEC OFFICER FOR DAVID MURCRAE

GENERAL ELECTRIC COMPANY
SPACE DIVISION
VALLEY FORGE SPACE CENTER
GODDARD BLVD KING OF PRUSSIA
P.O. BOX 8555
PHILADELPHIA, PA 19101
ATTN J BURNS

GENERAL ELECTRIC COMPANY
SPACE DIVISION
VALLEY FORGE SPACE CENTER
GODDARD BLVD KING OF PRUSSIA
P.O. BOX 8555
PHILADELPHIA, PA 19101
ATTN F ALYEA

GENERAL ELECTRIC COMPANY
SPACE DIVISION
VALLEY FORGE SPACE CENTER
GODDARD BLVD KING OF PRUSSIA
P.O. BOX 8555
PHILADELPHIA, PA 19101
ATTN P ZAVITSANDS

GENERAL ELECTRIC COMPANY
SPACE DIVISION
VALLEY FORGE SPACE CENTER
GODDARD BLVD KING OF PRUSSIA
P.O. BOX 8555
PHILADELPHIA, PA 19101
ATTN R H FOSALL

GENERAL ELECTRIC COMPANY
SPACE DIVISION
VALLEY FORGE SPACE CENTER
GODDARD BLVD KING OF PRUSSIA
P.O. BOX 8555
PHILADELPHIA, PA 19101
ATTN T BAURER

GENERAL RESEARCH CORPORATION
P.O. BOX 3587
SANTA BARBARA, CA 93105
ATTN JOHN ISE JR

GEOPHYSICAL INSTITUTE
UNIVERSITY OF ALASKA
FAIRBANKS, AK 99701
ATTN D HENDERSON

GEOPHYSICAL INSTITUTE
UNIVERSITY OF ALASKA
FAIRBANKS, AK 99701
ATTN J S WAGNER PHYSICS DEPT

GEOPHYSICAL INSTITUTE
UNIVERSITY OF ALASKA
FAIRBANKS, AK 99701
ATTN R J WATKINS

GEOPHYSICAL INSTITUTE
UNIVERSITY OF ALASKA
FAIRBANKS, AK 99701
ATTN T N DAVIS

GEOPHYSICAL INSTITUTE
UNIVERSITY OF ALASKA
FAIRBANKS, AK 99701
ATTN R PARTHASARATHY

GEOPHYSICAL INSTITUTE
UNIVERSITY OF ALASKA
FAIRBANKS, AK 99701
ATTN NEAL BROWN

LOWELL, UNIVERSITY OF
CENTER FOR ATMOSPHERIC RESEARCH
450 AIKEN STREET
LOWELL, MA 01854
ATTN G T BEST

LOCKHEED MISSILES AND SPACE COMPANY
3251 HANOVER STREET
PALO ALTO, CA 94394
ATTN JOHN KUMER DEPT 52-54

LOCKHEED MISSILES AND SPACE COMPANY
3251 HANOVER STREET
PALO,ALTO,CA 94304
ATTNJOHN B CLADIS DEPT 52-12

INSTITUTE FOR DEFENSE ANALYSIS
400 ARMY-NAVY DRIVE
ARLINGTON,VA 22202
ATTN ERNEST BAUER

LOCKHEED MISSILES AND SPACE COMPANY
3251 HANOVER STREET
PALO,ALTO,CA 94304
ATTNBILLY M MCCORMAC DEPT 52-54

INSTITUTE FOR DEFENSE ANALYSIS
400 ARMY-NAVY DRIVE
ARLINGTON VA 22202
ATTN HANS WOLFHARD

LOCKHEED MISSILES AND SPACE COMPANY
3251 HANOVER STREET
PALO,ALTO,CA 94304
ATTNTOM JAMES DEPT 52-54

MISSION RESEARCH CORPORATION
735 STATE STREET
SANTA BARBARA,CA 93101
ATTN D ARCHER

LOCKHEED MISSILES AND SPACE COMPANY
3251 HANOVER STREET
PALO,ALTO,CA 94304
ATTNJ R REAGAN D/52-12

MISSION RESEARCH CORPORATION
735 STATE STREET
SANTA BARBARA,CA 93101
ATTN D FISCHER

LOCKHEED MISSILES AND SPACE COMPANY
3251 HANOVER STREET
PALO,ALTO,CA 94304
ATTNMARTIN WALT DEPT 52-10

MISSION RESEARCH CORPORATION
735 STATE STREET
SANTA BARBARA,CA 93101
ATTN M SCHEIBE

LOCKHEED MISSILES AND SPACE COMPANY
3251 HANOVER STREET
PALO,ALTO,CA 94304
ATTNRICHARD G JOHNSON DEPT 52-12

MISSION RESEARCH CORPORATION
735 STATE STREET
SANTA BARBARA,CA 93101
ATTN D SAPPENFIELD

LOCKHEED MISSILES AND SPACE COMPANY
3251 HANOVER STREET
PALO,ALTO,CA 94304
ATTNROBERT D SEARS DEPT 52-14

MISSION RESEARCH CORPORATION
735 STATE STREET
SANTA BARBARA,CA 93101
ATTN D SOWLE

LOCKHEED MISSILES AND SPACE COMPANY
3251 HANOVER STREET
PALO,ALTO,CA 94304
ATTNJ R WINKLER

PHOTOMETRIC, INC.
442 MARRETT ROAD
LEXINGTON,MA 02173
ATTN IRVING L KOFSKY

PHYSICAL DYNAMICS INC.
P.O. BOX 1069
BERKELEY, CA 94701
ATTN J B WORKMAN

PITTSBURGH, UNIVERSITY OF
OF THE COMWLTH SYS OF HIGHER EDUC
CATHEDRAL OF LEARNING
PITTSBURGH, PA 15213
ATTN FREDERICK KAUFMAN

PHYSICAL DYNAMICS INC.
P.O. BOX 1069
BERKELEY, CA 94701
ATTN A THOMPSON

PITTSBURGH, UNIVERSITY OF
OF THE COMWLTH SYS OF HIGHER EDUC
CATHEDRAL OF LEARNING
PITTSBURGH, PA 15213
ATTN EDWARD GERJUOY

PHYSICAL SCIENCES, INC.
30 COMMERCE WAY
WOBURN, MA 01801
ATTN KURT WRAY

PRINCETON UNIV, THE TRUSTEES OF
FORRESTAL CAMPUS LIBRARY
BOX 710
PRINCETON UNIVERSITY
PRINCETON, NJ 08540
ATTN ARNOLD J KELLY

PHYSICAL SCIENCES, INC.
30 COMMERCE WAY
WOBURN, MA 01801
ATTN R L TAYLOR

R & D ASSOCIATES
P.O. BOX 9695
MARINA DEL REY, CA 90291
ATTN RICHARD LATTEP

PHYSICAL SCIENCES, INC.
30 COMMERCE WAY
WOBURN, MA 01801
ATTN G CALEDONIA

R & D ASSOCIATES
P.O. BOX 9695
MARINA DEL REY, CA 90291
ATTN R G LINDGREN

PHYSICS INTERNATIONAL COMPANY
2700 MERCED STREET
SAN LEANDRO, CA 94577
ATTN DOC CON FOR TECH LIB

R & D ASSOCIATES
P.O. BOX 9695
MARINA DEL REY, CA 90291
ATTN BRYAN GABBARO

PITTSBURGH, UNIVERSITY OF
OF THE COMWLTH SYS OF HIGHER EDUC
CATHEDRAL OF LEARNING
PITTSBURGH, PA 15213
ATTN WADE L FITE

R & D ASSOCIATES
P.O. BOX 9695
MARINA DEL REY, CA 90291
ATTN H A DRY

PITTSBURGH, UNIVERSITY OF
OF THE COMWLTH SYS OF HIGHER EDUC
CATHEDRAL OF LEARNING
PITTSBURGH, PA 15213
ATTN MANFRED A BIONDI

R & D ASSOCIATES
P.O. BOX 9695
MARINA DEL REY, CA 90291
ATTN ROBERT E LELEVIER

SCIENCE APPLICATIONS, INC.
P.O. BOX 2351
LA JOLLA, CA 92038
ATTN DANIEL A HAMLIN

R & D ASSOCIATES
P.O. BOX 9695
MARINA DEL REY, CA 90291
ATTN R P TURCO

SCIENCE APPLICATIONS, INC.
P.O. BOX 2351
LA JOLLA, CA 92038
ATTN DAVID SACHS

R & D ASSOCIATES
P.O. BOX 9695
MARINA DEL REY, CA 90291
ATTN ALBERT L LATTER

SPACE DATA CORPORATION
1331 SOUTH 26TH STREET
PHOENIX, AZ 85034
ATTN EDWARD F ALLEN

R & D ASSOCIATES
P.O. BOX 9695
MARINA DEL REY, CA 90291
ATTN FORREST GILMORE

STANFORD RSCH INSTITUTE INTERNATIONAL
333 RAVENSWOOD AVENUE
MENLO PARK, CA 94025
ATTN M BARON

R & D ASSOCIATES
P.O. BOX 9695
MARINA DEL REY, CA 90291
ATTN D DEE

STANFORD RSCH INSTITUTE INTERNATIONAL
333 RAVENSWOOD AVENUE
MENLO PARK, CA 94025
ATTN L LEADABRAND

R & D ASSOCIATES
1815 N. FT. MYER DRIVE
11TH FLOOR
ARLINGTON, VA 22209
ATTN HERBERT J MITCHELL

STANFORD RSCH INSTITUTE INTERNATIONAL
333 RAVENSWOOD AVENUE
MENLO PARK, CA 94025
ATTN WALTER G CHESTNUT

R & D ASSOCIATES
1815 N. FT. MYER DRIVE
11TH FLOOR
ARLINGTON, VA 22209
ATTN J W ROSENGREN

STANFORD RSCH INSTITUTE INTERNATIONAL
1611 NORTH KENT STREET
ARLINGTON, VA 22209
ATTN WARREN W BERNING

RAND CORPORATION
1700 MAIN STREET
SANTA MONICA, CA 90406
ATTN CULLEN CRAIN

STANFORD RSCH INSTITUTE INTERNATIONAL
1611 NORTH KENT STREET
ARLINGTON, VA 22209
ATTN CHARLES HULBERT

STEWART RADIANCE LABORATORY
1 DE ANGELO DRIVE
BEDFORD, MA 01730
ATTN: R.J. HUPPI (25 copies)

VISIDYNE, INC.
19 THIRD AVENUE
NORTHWEST INDUSTRIAL PARK
BURLINGTON, MA 01803
ATTN J W CARPENTER

TECHNOLOGY INTERNATIONAL CORPORATION
75 WIGGINS AVENUE
BEDFORD, MA 01730
ATTN W P ROQUIST

VISIDYNE, INC.
19 THIRD AVENUE
NORTHWEST INDUSTRIAL PARK
BURLINGTON, MA 01803
ATTN WILLIAM REIDY

UNITED TECHNOLOGIES CORPORATION
755 MAIN STREET
HARTFORD, CT 06103
ATTN H MICHELS

VISIDYNE, INC.
19 THIRD AVENUE
NORTHWEST INDUSTRIAL PARK
BURLINGTON, MA 01803
ATTN T C DEGGES

UNITED TECHNOLOGIES CORPORATION
755 MAIN STREET
HARTFORD, CT 06103
ATTN ROBERT MBULLIS

VISIDYNE, INC.
19 THIRD AVENUE
NORTHWEST INDUSTRIAL PARK
BURLINGTON, MA 01803
ATTN CHARLES HUMPHREY

UTAH STATE UNIVERSITY
LOGAN, UT 84321
ATTN DORAN BAKER

VISIDYNE, INC.
19 THIRD AVENUE
NORTHWEST INDUSTRIAL PARK
BURLINGTON, MA 01803
ATTN: J. REED (10 copies)

UTAH STATE UNIVERSITY
LOGAN, UT 84321
ATTN KAY BAKER

WAYNE STATE UNIVERSITY
1064 MACKENZIE HALL
DETROIT, MI 48202
ATTN PIETER K ROL
CHAM ENGRG & MAT SCI

UTAH STATE UNIVERSITY
LOGAN, UT 84321
ATTN C WYATT

UTAH STATE UNIVERSITY
LOGAN, UT 84321
ATTN D BURT

WAYNE STATE UNIVERSITY
1064 MACKENZIE HALL
DETROIT, MI 48202
ATTN R H KUMMLER

VISIDYNE, INC.
19 THIRD AVENUE
NORTHWEST INDUSTRIAL PARK
BURLINGTON, MA 01803
ATTN HENRY J SMITH

WAYNE STATE UNIVERSITY
DEPT. OF PHYSICS
DETROIT, MI 48202
ATTN WALTER E KAUFFLA

YALE UNIVERSITY
NEW HAVEN, CT 06520
ATTN ENGINEERING DEPARTMENT.

AF GEOPHYSICS LABORATORY, AFSC
HANSCOM AFB, MA 01731
ATTN: OPR B.SANDFORD

(10 copies)

DIRECTOR
DEFENSE ADVANCED RSCH PROJ AGENCY
ARCHITECT BUILDING
1400 WILSON BLVD.
ARLINGTON, VA 22209
ATTN S. ZAKANYCZ